Universität Bremen

Mechanobiological Control of Circular Dorsal Ruffle Dynamics

Julia Lange

Dissertation zur Erlangung des akademischen Grades
Doktor der Naturwissenschaften
(Dr. rer. nat)

Erstgutachter: Prof. Dr. Hans-Günther Döbereiner
Zweitgutachterin: Prof. Dr. Olivia Masseck

Eingereicht am 19.07.2019

Abstract

Dynamic structures of polymerized actin play a crucial role in different cellular processes. These include different kinds of actin waves in a multitude of cell types, like *Dictyostelium*, neutrophiles, macrophages and fibroblasts. These actin waves are connected to a remodeling of the cytoskeleton, cell protrusion and migration as well as the uptake of extracellular fluids, but their specific functions are still debated. One type of them are circular dorsal ruffles (CDRs), actin-based ring-like membrane undulations on the dorsal cell side of fibroblasts, which emerge after growth factor stimulation. A large number of macromolecules were shown to be localized in CDRs and to be crucial for CDR formation. However, to date, the detailed signaling pathway and the underlying mechanism of CDR formation including their molecular main players remain unknown. Different studies on CDRs described them as actin waves in an excitable system or as wavefronts in a bistable regime between two stable states of actin. However, other studies focused on the interaction between actin polymerization and the cell membrane via the interplay of curved membrane protein complexes.

This thesis further investigates the mechanism underlying CDR formation. For this study, the morphology of cells is an essential effector for the dynamics of actin waves. Their complexity and dynamical remodeling pose a challenge to the comparability of data. Therefore, in this work, fibroblasts are shaped into well-defined morphologies by seeding them on disk-like adhesion patterns made of fibronectin. This enables to identify long-range interactions between different CDRs combined with the influence of stochastic perturbations and thus uncovers the important role of the membrane tension in CDR dynamics. In combination with microfluidics, the response of the actin wave machinery to biochemical interference with drugs that target different parts of the actin machinery is investigated. The system allows systematical measurements of CDR velocities, periodicities and lifetimes that are performed to carry out a before/after comparison of the treated cells for examining the influence of actin, PIP_3 and N-WASP. It is observed a dependence of CDR velocities, periodicities and lifetimes on the total amount of actin leading to the conclusion of a direct regulating role of actin in CDR formation and propagation. Furthermore, it is found that the actin nucleator N-WASP plays a fundamental role in CDR formation but not in CDR propagation. Numerical solutions of wavefronts in a bistable regime of a model system on an annulus domain resemble experimentally gained data and further uncover a dependence of the stimulation threshold for propagating wavefronts on the total actin concentration. The results underline the hypothesis that CDRs can be considered as wavefronts in a bistable regime between two stable states of actin.

Contents

Acknowledgements

First, I would like to thank **Prof. Dr. Hans-Günther Döbereiner** for supervising this PhD project, in particular for the interest and enthusiasm, the discussions and the untiring perseverance. During this time, I learned a lot! Further, I would like to thank **Prof. Dr. Olivia Masseck** for the interest in this study and for beeing the second examiner of this thesis.

A special thank goes to my colleagues from the **Döbereiner lab**, especially to **Christina Oettmeier** and **Dr. Erik Bernitt**. Thank you so much for all the skills and knowledge you shared with me. You taught me so much and I benefited a lot from your experiences.

Furthermore, I am very grateful to **Anja Bammann**. The excellent lab work and the reliable support over the last years were crucial for this work.

Anna Piorecka-Ecken, **Merthe Schwachenwald**, **Malte Ohmstede**, **Jonghyun Lee** and **Dr. Adrian Fessel**, thank you so much for all the discussions and the proofreading of specific parts of this thesis.

Last but not least, I am deeply grateful for all the support from **my family**.

List of Figures

List of Tables

List of Abbreviations

In the following a list of the most frequently used abbreviations is presented. The list does not contain all abbreviations, that are used in this work, but includes the acronyms, that are important to know in the context of this study.

Arp2/3	actin-related protein 2/3
CDR	circular dorsal ruffle
DMEM	Dulbecco's modified Eagle's medium
FBS	fetal bovine serum
GAP	GTPase-activating protein
GDI	guanine nucleotide dissociation inhibitor
GEF	guanine nucleotide exchange factor
N-WASP	neural Wiskott-Aldrich syndrome protein
PBS	phosphate buffered saline
PDGF	platelet-derived growth factor
PDMS	polydimethylsiloxane
PI3K	phosphatidylinositol 3-kinase
PIP_2	phosphatidylinositol 4,5-bisphosphate
PIP_3	phosphatidylinositol 3,4,5-trisphosphate
PLL-g-PEG	Poly(L-lysine)-graft-poly(ethylene glycol)
RTK	receptor tyrosine kinase
SE	standard error

1 Introduction

Eukaryotic cells are built up of a cytoskeleton that consists of the structure protein actin. Polymerization of globular actin into filaments and depolymerization induce dynamic changes of the actin cytoskeleton that lead to protrusions and provide the basis for cell motility. Moreover, in various cell types spatiotemporal actin patterns in form of self-organized protein density waves are observed and coupled to a remodeling of the actin cytoskeleton, cell protrusion and migration [Allard and Mogilner, 2013].

Among actin waves in *Dictyostelium* cells, neutrophiles or macrophages, one specific type of actin waves are membrane ruffles and more specifically circular dorsal ruffles (CDRs), that have been observed, inter alia, in fibroblasts [Vicker, 2000, Weiner et al., 2007, Masters et al., 2016, Bernitt et al., 2015]. These are transient actin-based vertical undulations of the cell membrane on the dorsal cell side, differing from peripheral ruffles due to their ring-shaped morphology [Itoh and Hasegawa, 2012]. Ruffles appear after stimulation of receptor tyrosine kinases (RTKs) with growth factors like platelet-derived growth factor (PDGF), epidermal growth factor (EGF) and hepatocyte growth factor (HGF) in cells like fibroblasts or differentiated epithelial cell types after initiating a downstream signaling cascade that involves many molecules, among others, phosphoinositides, small GTPases, actin and actin associated proteins [Buccione et al., 2004].

Within a few minutes after stimulation, phase densed actin structures appear due to a rapid polymerization of branched actin filaments. These structures organize into circular arrays, followed by a collapse after 5 to 20 minutes while forming endocytotic vesicles (see Fig. 1.1 A) [Buccione et al., 2004]. The internalization of these macropinosomes leads to an undirected uptake of receptors and external fluids from the near extracellular environment [Swanson, 2008, Bloomfield and Kay, 2016]. Because of the prompt uptake of extracellular fluids through this process, it seems evident that it is used by cancer cells to gain nutrients for a lasting propagation in the tumor environment [Ha et al., 2016]. Furthermore, it is exploited by pathogenes like Ebola viruses, human immunodeficiency viruses and Zika viruses as a gate opener to enter the cell and infect it. Additionally, some bacteria or viruses are able to induce membrane ruffles independent of growth factor stimulation to be taken up by the cells within macropinosomes [Mercer and Helenius, 2009, Stow and Condon, 2016]. However, macropinocytosis can also be used as an important tool to infiltrate engineered cytotoxic exosomes into cells in order to medicate diseases, for example to medicate cancer [Mercer and Helenius, 2009, Reyes-Reyes et al., 2010]. Moreover, CDRs are not only studied on the biological and molecular level, but, as introduced above, they are also considered as wave phe-

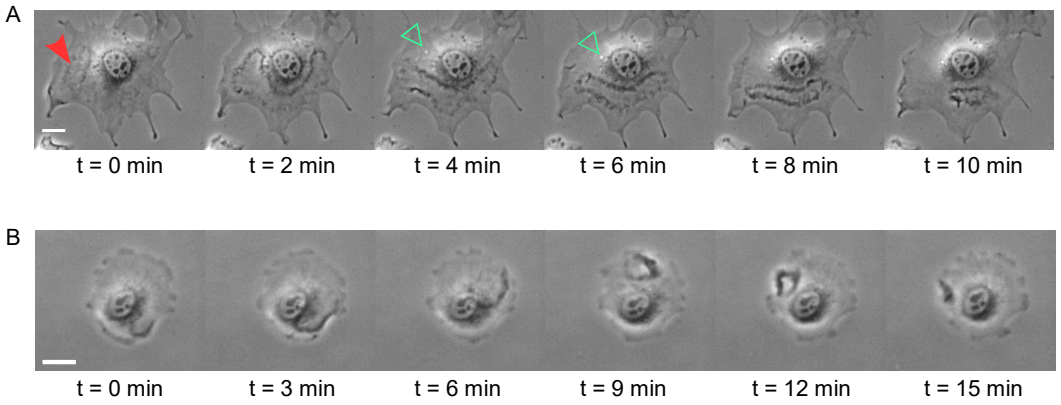

Figure 1.1: Circular dorsal ruffles. A: Time-lapse sequence of micrographs of a randomly shaped fibroblast after stimulation with PDGF. Red filled arrowhead indicates the beginning of CDR formation, whereas the green unfilled arrowhead highlights a newly formed vesicle. B: Time-lapse sequence of micrographs of a disk-shaped fibroblast without external growth factor stimulation. A CDR is formed without external growth factor stimulation at t=0 min and collapsed 15 minutes later at t=15 min. (Scale bars: 20 µm).

nomena based on an activator-inhibitor coupling, that leads to wave propagation over the cell membrane [Allard and Mogilner, 2013].

1.1 State of the art in actin wave and CDR research

The finding of membrane ruffles can at least be dated back to 1958, when Abercrombie described the observation of membrane protrusions at the leading edge of locomotive fibroblasts [Abercrombie and Ambrose, 1958]. In the following decades, different studies documented the influence of growth factors like PDGF and EGF on the formation of ruffles [Mellström et al., 1983, Chinkers et al., 1979]. Experiments with these growth factors provided insights into the molecular nature of the triggering event and signaling cascade [Mellström et al., 1988]. As time went by, more and more macromolecules were identified, which are localized to membrane ruffles, especially to CDRs, and take part in its initiation process. Over the years, a huge number of involved macromolecules have been uncovered, that comprises of, among others, actin associated proteins, membrane deforming proteins, signaling molecules like GTPases and phosphoinositides. However, their detailed signaling pathway and underlying wave machinery are still unclear [Buccione et al., 2004, Orth and McNiven, 2006, Itoh and Hasegawa, 2012, Hoon et al., 2012].

This study mainly focuses on the description of CDRs as actin waves and the investigation of the mechanism of the actin wave machinery underlying CDRs. Apart from fibroblasts there are different kinds of actin waves in various cell types like *Dictyostelium*,

neutrophiles and macrophages with similar appearences and features to CDRs [Vicker, 2000, Weiner et al., 2007, Masters et al., 2016]. The recent boom in studying traveling actin waves started around 20 years ago. Various studies investigated wave propagation in the model organism *Dictyostelium*, that was usually utilized, among others, for examining cell locomotion. Vicker and coworkers uncovered actin waves as self-organized reaction-diffusion waves of f-actin and detected a link between actin waves and cell locomotion [Vicker, 2000, Vicker, 2002]. Subsequently, the dependence of traveling actin waves on important macromolecules, like the actin nucleator actin-related protein 2/3 (Arp2/3), phosphatidylinositol 3,4,5-trisphosphate (PIP_3) and their kinase phosphatidylinositol 3-kinase (PI3K) and phosphatase PTEN as well as the role of these macromolecules in the underlying wave machinery were attempted to be understood in *Dictyostelium* [Bretschneider et al., 2004, Gerisch et al., 2009, Gerisch et al., 2012].

In macrophages, similar molecular main players interact and lead to traveling actin waves to in *Dictyostelium* and fibroblasts. Phosphoinositides, that regulate actin dynamics and recruit actin polymerizing complexes like neural Wiskott-Aldrich syndrome protein (N-WASP), were assumed to play a central role [Masters et al., 2016]. However, in neutrophiles, actin waves were discovered to depend on interactions between the Hem-1 component of the SCAR/WAVE-complex and f-actin itself [Weiner et al., 2007].

To date, it is not clear whether the different types of actin waves in various cell types have the same underlying wave machinery with the same molecular main players. In this regard, Allard and Mogilner argued on basis of various proposed models that different types of actin waves, despite a different molecular nature, may all result from activation-inhibition feedback mechanisms in actin dynamics in the concept of excitable systems [Allard and Mogilner, 2013]. This concept was widely used to study the underlying wave machinery by using reaction-diffusion models. However, individual models are based on the concept of bistability or mechanical interactions [Beta, 2010, Peleg et al., 2011].

In the context of CDRs, a reaction-diffusion system was proposed by Zeng et al. [Zeng et al., 2011]. They suggested an antagonistic model between the molecular main players of small GTPases Rac and Rho and considered CDRs as waves in an excitable system. However, other studies focused on mechanical interactions between protrusion forces of actin polymerization and the membrane shape that induced traveling waves [Gov and Gopinathan, 2006, Shlomovitz and Gov, 2007, Peleg et al., 2011]. It was shown that these different types of mechanisms led to wave propagation with similar features to CDRs, but the overall question remains what mechanism the CDR formation and dynamics underlies and what the molecular main players in this process are [Zeng et al., 2011, Peleg et al., 2011].

Great advances in uncovering the mechanism underlying CDRs were obtained by

Bernitt, Döbereiner and coworkers. By using fibroblasts that were shaped into well-defined morphologies via microcontact printed adhesion patterns (see Fig. 1.1 B), they systematically studied a periodic CDR appearence and propagation without external stimulation with growth factors. Based on their experimental results, they discussed CDRs as waves in an active medium and studied the dynamics via the FithHugh-Nagumo model, a prototype of an excitable system [Bernitt et al., 2015, Bernitt, 2015]. In this context, a noisy environment was taken into account that led to stochastic perturbations which generate the periodic CDR reappearence [Bernitt and Döbereiner, 2017]. A pioneering work followed that focused on CDRs as wavefronts in a bistable regime between two stable states of actin [Bernitt et al., 2017]. This is in contrast to former studies which focused on actin waves as waves in an excitable system with one steady state, but provides an interesting new approach for studying CDR dynamics, which is in line with the model for actin waves in macrophages, that also based on the concept of bistability [Masters et al., 2016].

1.2 Aim of this work

As introduced above, it is controversially discussed, which mechanisms underly CDR propagation and which molecular main players are involved in the process. The hypothesis in this work is that CDRs propagate as wavefronts in a bistable regime between two different steady states of actin. This is based on an activator-inhibitor coupling involving actin and its nucleator N-WASP and an inhibitor of actin polymerization, which is conjectured to be PIP_3. This hypothesis is followed by a recently proposed model of Bernitt et al. presupposing a model with a bistable regime due to different observed states of actin in the exterior and the interior of CDRs [Bernitt et al., 2017], which contradicted to further studies that considered CDRs as waves in an excitable medium [Zeng et al., 2011, Bernitt et al., 2015, Bernitt, 2015]. Moreover, while also studying other types of actin waves, the concept of bistability has only been marginally widespread, although it may not seem extraordinary in the framework of an actin cytoskeleton [Beta, 2010, Masters et al., 2016].

To examine this hypothesis and to understand the molecular nature of the wave machinery of CDRs, this work focuses on a systematic experimental investigation of CDR formation, dynamics and interactions in fibroblasts of type NIH WT 3T3 on well-defined cell morphologies. To avoid the impact of cellular boundary conditions and to confine CDR propagation on a one-dimensional trajectory, microcontact printed substrates made of fibronectin are used, in combination with a microfluidic perfusion system that is utilized to change systematically biochemical conditions by using biochemical compounds like Jasplakinolide, Wortmannin and Wiskostatin. These cell drugs interfere with specific proteins like Jasplakinolide with f-actin, Wortmannin with PI3K, an enzyme that catalyzes phosphatidylinositol 4,5-bisphosphate (PIP_2) to PIP_3, and Wiskostatin with the actin nucleator N-WASP. These drugs have been also utilized in previous

studies on randomly shaped cells to study which proteins are localized in different types of actin waves and affect its formation [Masters et al., 2016, Weiner et al., 2007, Legg et al., 2007, Wennström et al., 1994]. In contrast to former studies, in this work a quantitative analysis of CDR lifetimes, velocities and periodicities is presented that was not possible in randomly shaped cells due to the variability of the cell geometry and the impact of the cellular boundaries [Bernitt, 2015]. This leads to an identification of the role of actin, PIP_3 and N-WASP in CDR formation and propagation. Furthermore, a so far hidden role of the membrane tension is revealed.

To increase the understanding if CDRs behave as waves in an excitable or as wavefronts in a bistable regime, numerical solutions of wavefront propagation within the bistable regime of a model system [Bernitt et al., 2017] on an annulus domain are carried out. The idea is to check if known features from excitable regimes, like coherently propagating wave pulses that annihilate each other and periodically reappear, are also able to generate in a bistable regime.

1.3 Outline of this work

The structure of this work is outlined hereafter. Following this introduction, the main part of this thesis begins with an overview of the theoretical background. Within this part, the molecular components which are localized in CDRs and are known to be involved in its formation are introduced (Chapter 2). They are subdivided into actin, actin assembly factors, Rho GTPases, phosphoinositides, growth factors and receptor tyrosine kinases as well as membrane deforming proteins. This chapter is essential to the understanding of the subsequent chapter (Chapter 3) about the mechanisms underlying the actin wave machinery. It describes the general concepts of reaction-diffusion models and different proposed models of actin waves with various molecular main players. Furthermore, it details specific models of CDR formation in the context of excitability and bistability. This chapter provides the basis on which this work is built up.

The materials and methods used in this work are presented in Chapter 4. This includes, among others, cell culture and the microcontact printing technique used to study cells under constant geometrical und physiological conditions as well as the setup of a microfluidic perfusion system and the biochemical compounds utilized to interfere with specific proteins within fibroblasts to investigate the role of actin, PIP_3 and N-WASP in CDR dynamics. Moreover, techniques of data analysis and numerical simulations are presented.

Core of this work are the experimental results, which are described in Chapter 5, 6, 7 and 8. Each of them are subdivided into a short introduction, a main part and a short summary of the results. First of them (Chapter 5) investigates CDR formation and dynamics in disk-shaped fibroblasts under physiological conditions. In contrast

to previous studies, it provides a detailed analysis of observables like CDR velocities, periodicities, lifetimes and traveling distances to obtain a complete picture of CDR propagation. Additionally, it focuses on the interaction of different CDRs and uncover the influence of long-range interactions between CDRs. Thus, the results lead to the conclusion that the membrane tension and actin play a governing role in CDR dynamics.

In the subsequent chapters, the role of different macromolecules, namely actin (Chapter 6), PIP_3 (Chapter 7) and N-WASP (Chapter 8), in CDR formation and dynamics is examined by means of biochemical compounds. A detailed qualitative and quantitative investigation allows for conclusions regarding the role of the studied macromolecules, demonstrating which molecules mainly govern CDR dynamics or are only important in CDR formation without regulating CDR dynamics. It emphasizes the important role of actin in CDR formation and propagation, revealing fundamental insights into the actin wave machinery and leads to a new discussion of existing models.

Furthermore, theoretical experiments of wavefront propagations on an annulus domain within a bistable regime of an existing model under variation of specific parameters are integrated in Chapter 5 & 6 to verify the hypothesis that CDRs are captured as wavefronts in a bistable regime of two different actin states. It attempts to demonstrate that a system with such a bistable regime is also able to generate coherently propagating wavefronts with similar features as CDRs in disk-shaped fibroblasts. These theoretical experiments are in line with experimental results and further underpin the important role of actin itself in CDR formation and propagation.

Finally, to complete this work, a conclusion and outlook are given in the last chapter (Chapter 9).

2 Molecular Components in CDRs

CDRs are actin-based ring-shaped membrane undulations appearing after stimulation with growth factors. In this process, a large number of molecules is involved that faclilitate the formation of CDRs. To date, the detailed molecular pathway has not been fully elucidated. In the following, a rough outline of the molecular interactions according to Hoon et al. is presented (see Fig. 2.1) [Hoon et al., 2012]. At the beginning of the process, growth factor stimulation activates RTKs, initiating a downstream signaling cascade, which includes the two main players PI3K and the small GTPases Rac. Activation of RTKs leads to an accumulation of PIP_2 at the cell membrane, which is converted from PIP_2 to PIP_3 via PI3K. Rac activation follows due to a signaling cascade downstream of PIP_3. Furthermore, aggregation of curved membrane protein complexes with Bin/Amphiphysin/Rvs (BAR) and Fes/CIP4 homology BAR (F-BAR) domains as well as the activation of actin nucleators like Arp2/3 lead to bundling and branching of actin filaments to create ring-shaped membrane undulations, namely CDRs. The required actin is provided by a depletion of stress fibers in the cell cortex [Hoon et al., 2012].

This chapter introduces the main components in CDR formation required to understand the mechanism underlying CDR dynamics. The chapter commences with the protein actin itself (Section 2.1), and with actin assembly factors participating in the formation of actin filaments and branched networks (Section 2.2). These proteins are known to be involved in CDR formation and are assumed to play a fundamental role in the mechanism underlying wave propagation in the context of a bistable system [Bernitt et al., 2017]. They are also connected with the formation of actin waves in *Dictyostelium*, neutrophiles and macrophages [Masters et al., 2016, Weiner et al., 2007, Bretschneider et al., 2004]. Small GTPases that link the upstreaming signals of growth factors to the actin cytoskeleton are explained in Section 2.3 and play a fundamental role in a model by Zeng et al., which proposed CDR propagation to be the result of an interplay between the two small GTPases Rac and Rho [Zeng et al., 2011]. Further, growth factor stimulation and the activation of RTKs are characterized (Section 2.5). Moreover, a significant contributor to CDR formationis presented by PI3K and phosphoinositides (Section 2.4). These are assumed to play a crucial role in CDR formation within the proposed mechanism by Bernitt et al. and in other kinds of actin waves, for example, in *Dictyostelium* and macrophages [Gerisch et al., 2009, Gerisch et al., 2011, Masters et al., 2016]. Finally, membrane deforming proteins participate in the formation of membrane protrusions and interact with actin assembly factors, as proposed in a model of CDR propagation by Peleg et al. [Peleg et al., 2011]. Hence they are also involved in CDR formation (Section 2.6). The above mentioned models of CDR formation will be

presented in detail in Chapter 3.

In addition to the key players listed above, there is a large number of signaling and adapter molecules that are also involved in the process of CDR formation but which will not be further explored here. This thesis does not investigate the detailed molecular pathway of CDR formation but instead focuses on the mechanism underlying CDR formation and dynamics. Therefore, this chapter summarizes the main components in this process that play a fundamental role in the present context, and are required to study the mechanism underlying CDR formation and propagation.

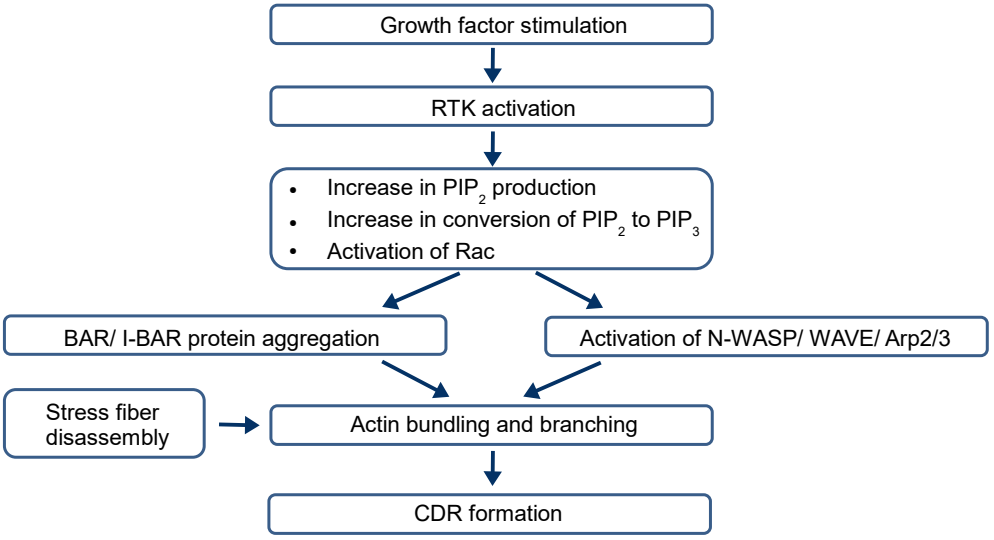

Figure 2.1: Schematic pathway of CDR formation after growth factor stimulation according to Hoon et al. [Hoon et al., 2012]. Growth factors lead to activation of RTKs and initiate a downstream signaling cascade. This includes an increased accumulation of PIP_2 at the cell membrane and a conversion of PIP_2 to PIP_3 via PI3K as well as activation of Rac by a signaling cascade downstream of PIP_3. Further, a remodeling of the actin cytoskeleton by curved membrane protein complexes with BAR and I-BAR domains, as well as recruitment of actin nucleators lead to CDR formation. Disassembly of stress fibers in the cell cortex provides the necessary amount of actin.

2.1 Actin

Actin is the most abundant protein in eukaryotic cells. One cell has been estimated to contain a concentration of around 150 µM of globular actin as well as around 500 µM of filamentous actin [Koestler et al., 2009]. The globular shaped monomers ("globular

actin“ or “g-actin“) consist of 375 amino acids and have the ability to form helical polymers (“filamentous actin“ or “f-actin“) [Sackmann and Merkel, 2010]. Filamentous actin assembles into branched or crosslinked networks, or into parallel or anti-parallel bundles to build various cellular structures in response to different stimuli. This enables, for example, lamellipodia and ruffles, which are sheet-like protrusions of the cell membrane, or finger-like membrane protrusions like filopodia [Chhabra and Higgs, 2007, Blanchoin et al., 2014].

To form actin filaments, g-actin assembly occurs head-to-tail. This leads to a molecular polarity of the filaments, and to structurally different filament ends: plus-ends (also called “barbed ends“) and minus-ends (also called “pointed ends“) [Pollard and Borisy, 2003, Alberts et al., 2015]. These single actin monomers bind one molecule of ATP, which is hydrolyzed to ADP during polymerization. Actin polymerization occurs with different rates at the barbed end and the pointed end. This leads to favorable filament elongation at the barbed end, whereas depolymerization occurs at the pointed end. At the steady state, barbed end polymerization of g-actin-ATP balances depolymerization of g-actin-ADP at the pointed end, leading to a “treadmilling“ process [Holmes et al., 1990, Clainche and Carlier, 2008].

2.2 Actin assembly factors

A large number of proteins participate in the regulation of actin filament assembly to form linear structures like filopodia or stress fibers, as well as branched actin structures like lamellipodia. These include, inter alia, actin nucleators, actin nucleation promoting factors, actin elongation factors and capping proteins. Spontaneous nucleation of actin filaments is prevented by profilin and β-thymosin, proteins that bind to actin monomers and sequester them, enabling only actin nucleators to initate *de novo* actin filament nucleation [Blanchoin et al., 2014, Chesarone and Goode, 2009]. Different kinds of nucleators have been identified, such as Arp2/3 complexes and formins [Rottner et al., 2017]. In contrast to formins, which lead to the formation of linear actin filaments, Arp2/3 complexes that consist of seven different proteins, play an important role in this work due to their ability to generate branched actin structures [Chesarone and Goode, 2009]. In this process, Arp2/3 complexes create new actin branches and link them to already existing filaments under an angle of 70° after activation by nucleation promoting factors from the Wiskott-Aldrich Syndrome protein (WASP)/WAVE family, such as WASp, N-WASP as well as WAVE1, WAVE2 and WAVE3 [Mullins et al., 1998, Higgs and Pollard, 1999]. These nucleation promoting factors link the upstreaming signals of proteins or molecules that regulate the activity or location of the nucleation promoting factors, such as small GTPases (see Section 2.3), WASp interactin protein, calmodulin, Grb2, Nck or PIP_2 (see Section 2.4) to the actin cytoskeleton [Higgs and Pollard, 1999, Takenawa and Miki, 2001].

After nucleation, filament elongation occurs in the presence of actin monomers un-

til capping proteins bind the barbed end of the filament, thus terminating its elongation. Capping proteins can be subdivided into two classes. The comprised proteins either sever and cap the filaments, such as Gelsolin and Severin, or only cap the filaments without severing them, like CapZ [Weeds and Maciver, 1993]. Elongating filaments may be protected from capping proteins by actin elongation factors, such as formins or Ena/VASP [Chesarone and Goode, 2009].

2.3 Rho GTPases

The signaling cascade of actin polymerization is governed by small Rho GTPases, GTP-binding proteins that constitute a subgroup of the Ras family [Takenawa and Miki, 2001, Ridley, 2006]. These are key regulatory molecules, which are involved in the signaling pathways of eukaryotic cells. Rho GTPases regulate many cellular processes, including membrane trafficking, cell division and cell growth, through a link of surface receptors to the organization of the actin cytoskeleton [van Aelst and D'Souza-Schorey, 1997, Hall, 1998]. In this regard, the best-studied members Rho, Rac and Cdc42 including their multiple isoforms affect actin polymerization and filament bundling in response to extracellular growth factors [Hall, 1998]. Rho activity induces the assembly of focal adhesions and actin stress fibers (actin-myosin filaments), Rac activity regulates the production of lamellipodia and membrane ruffles, and Cdc42 activity leads to filopodia formation [Ridley and Hall, 1992, Ridley et al., 1992, Hall, 1998]. Furthermore, Rho GTPases also can regulate each other, as Cdc42 can activate Rac and Rac can activate Rho [Hall, 1998]. On this basis, a model of CDR formation was proposed by Zeng et al. [Zeng et al., 2011], as introduced in Section 3.2. The model mainly focuses on a Rho-Rac antagonism due to an observed antagonistic relationship between stress fibers and CDRs.

The activity of GTPases depends on the binding of GDP and GTP, and can be switched between an inactive GDP-bound state and an active GTP-bound state. This conformation is controlled by three different categories of proteins: guanine nucleotide exchange factors (GEFs), GTPase-activating proteins (GAPs) and guanine nucleotide dissociation inhibitors (GDIs) [Boguski and McCormick, 1993, Jaffe and Hall, 2005]. GEFs activate GTPases by accelerating the exchange of bound GDP for GTP, whereas GAPs enhance the rate of hydrolysis of bound GTP to GDP to inactivate the molecular switch. GDIs act as an inhibitor of GAPs, thus inhibiting spontaneous activation [van Aelst and D'Souza-Schorey, 1997].

GTPases activate diverse effector proteins, which can interact selectively with the GTP-bound conformation of GTPases. These include, among others, a number of serine/threonine protein kinases, lipid kinases and scaffold proteins [Bishop and Hall, 2000]. The activation of two different kinds of target proteins induces actin polymerization: WASP/ WAVE proteins are target proteins of Rac and Cdc42, whereas

Diaphanous-related formins (DRFs) are activated by Rho [Jaffe and Hall, 2005, Ridley, 2006]. Furthermore, different activated kinases like Rho-associated protein kinase (ROCK) or p21-activated kinase (PAKs) also affect actin polymerization. These kinases regulate cofilin through activation and phosphorylation of LIM kinase [Jaffe and Hall, 2005, Ridley, 2006].

2.4 Phosphoinositides

Phoshoinositides are lipid molecules that are phosphorylated forms of phosphatidolinositol (PtdIns), playing an important role in transduction of extracellular signals from membrane receptors [Balla, 2013]. Seven different forms of these can be generated due to reversible phosphorylation and dephosphorylation of the inositol ring at position 3, 4 and 5, effected by various kinases and phosphatases. This interconversion schematic is summarized in Fig. 2.2 [Balla, 2013]. The phosphoinositides are accumulated at the intracellular membrane surface, where each of them has a particular distribution [DiPaolo and Camilli, 2006].

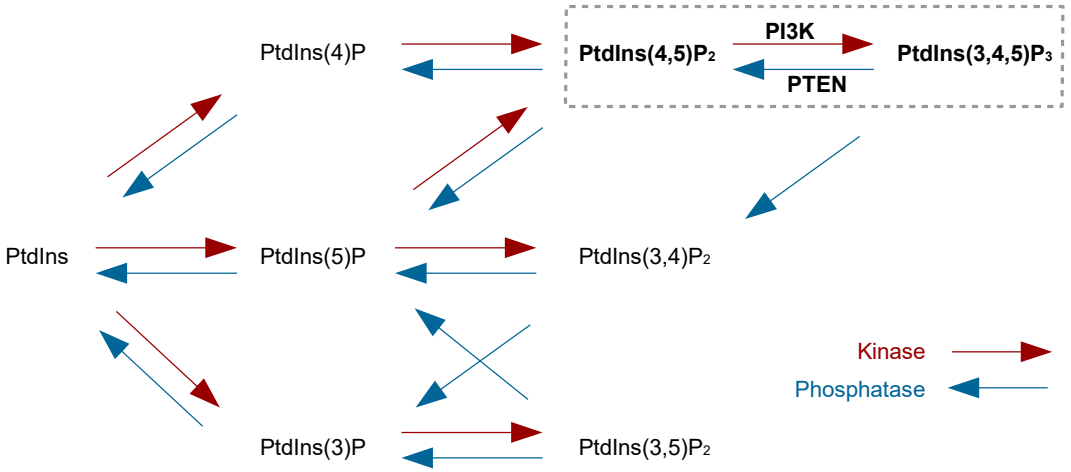

Figure 2.2: Interconversion between different Phosphoinositides. Graphical depiction of the interconversion between seven species of phophoinositides according to [Balla, 2013]. Phosphorylation of phosphoinositides mediated by different kinases is indicated by red arrows, whereas dephosphorylation mediated by various phosphatases is marked by blue arrows. Key players in CDR formation are PIP_2, PIP_3 and PI3K, highlighted by the grey box.

The greatest portion of phosphoinositides in cells is made up of PtdIns(4)P and PtdIns(4,5)P_2. PtdIns(4,5)P_2 is involved in many regulatory processes occuring at the plasma membrane, for example activation and recruitment of actin regulatory

proteins. In particular, PtdIns(4,5)P_2 in cooperation with the small GTPase Cdc42 participates in actin polymerization through direct binding of N-WASP, leading to Arp2/3-mediated nucleation of the actin network [DiPaolo and Camilli, 2006]. Moreover, PtdIns(4,5)P_2 also plays a critical role in dissociation of capping proteins, such as CapZ and gelsolin, as well as in the dissociation of actin-monomer-profilin complexes [Yin and Janmey, 2003].

PtdIns(3,4,5)P_3, the phosphorylated product of PtdIns(4,5)P_2, is negligible in resting cells, but upon stimulation with growth factors, its amount increases drastically. Therefore, phosphorylation of PtdIns(4,5)P_2 to PtdIns(3,4,5)P_3 is regulated by PI3K and, in reverse, the dephosphorylation of PtdIns(3,4,5)P_3 at the third position is mediated by PTEN [DiPaolo and Camilli, 2006]. PtdIns(3,4,5)P_3 is also involved in the recruitment of actin regulatory proteins, and its main target proteins are GEFs and GAPs for small GTPases.

Due to their important role in regulatory processes, for instance in regulation of actin polymerization, it seems obvious that PtdIns(4,5)P_2 (in the following referred to as PIP_2), PtdIns(3,4,5)P_3 (in the following named as PIP_3) as well as PI3K are also involved in CDR formation. This has been proven by studies in which Wortmannin, an inhibitor of PI3K, blocked the formation of CDRs [Buccione et al., 2004]. Furthermore, it is known that there is a PIP_2/PIP_3 asymmetry between the inside and the outside of CDRs. PIP_3 is localized in patches in the interior of CDRs, whereas PIP_2 is accumulated over the entire cell membrane [Bernitt et al., 2017]. On this basis, a bistable mechanism of CDR formation has been proposed (see Section 3.4).

2.5 Growth factors and receptor tyrosine kinases

Growth factors are signaling proteins promoting various cellular functions, such as proliferation, migration and wound healing [Tallquist and Kazlauskas, 2004,Deuel and Chang, 2014]. They have been shown to interact with extracellular binding sites of specific transmembrane proteins, namely receptor tyrosine kinases (RTKs). RTKs transmit extracellular signals into chemical signals by tyrosine phosphorylating itself or intracellular substrates to associate with corresponding signaling enzymes, such as Grb2, Nck, PI3K and Src family members via a Src homology 2 (SH2) domain binding site [Kazlauskas, 1994]. This leads to an activation of different signaling pathways including regulation of Ras activity and PI3K [Tallquist and Kazlauskas, 2004].

Growth factors, and thus, activated signaling pathways play a crucial role in CDR formation. CDRs form within minutes in response to stimulation with epidermal growth factors (EGF), hepatocyte growth factors (HGF) or platelet-derived growth factors (PDGF) [Mellström et al., 1983,Mellström et al., 1988,Dowrick et al., 1993,Chinkers et al., 1979]. The latter is regarded as one of the earliest and best characterized growth

factors for investigating CDR formation. Signaling pathways downstream of the PDGF receptor lead to CDR formation, including two main proteins, PI3K and Rac [Mellström et al., 1988, Hoon et al., 2012]. After activation of CDR formation signaling pathways, responsible RTKs are internalized, and either degraded or recycled [Hoon et al., 2012].

Furthermore, the interaction between growth factors and the extracellular matrix plays an important role for CDR formation, and is of special relevance to this work. They have been shown to bind to extracellular matrix molecules, in particular to fibronectin at its multiple binding sites [Sawicka et al., 2015]. Hence, fibronectin acts as a reservoir for growth factors, such that growth factors can be presented more effeciently to their receptors.

2.6 Membrane deforming proteins

Membranes can be deformed by three different interactions. First, the membrane can be shaped through interactions with the cytoskeleton from which actin filaments or microtubules can push, pull or stabilize the membrane. Second, the membrane can be curved by heterogeneous distributions of lipids with different sizes of head-groups or acyl chains. This is possible, for example by phosphoinositides, which induce a curvature by accumulation in the membrane due to their larger head-groups in contrast to phosphatidyl choline [Prinz and Hinshaw, 2009]. Third, membrane deformations can be obtained by directly binding to membrane deforming proteins that are connected to the membrane via electrostatical bindings between the protein's positively charged amino acids, and the negatively charged lipids of the membrane. They link the rearrangements of the membrane to actin dynamics by affecting actin polymerization due to activation of actin nucleation factors, such as WASP and WAVE, or interactions with Rho GTPAses [Stanishneva-Konovalova et al., 2016].

In this context, important membrane deforming proteins are so-called BAR-domain proteins. These are banana-shaped proteins, which are divided into three classes according to their curvature shaping the membrane either concave or convex: BAR-, F-BAR- (both concave) and inverse BAR (I-BAR)-domain proteins (convex) [Mim and Unger, 2012]. Prominent examples of membrane deforming proteins are Tuba, which contains a BAR-domain, as well as IRSp53 and MIM with an I-BAR-domain. IRSp53 and MIM also participate in the formation of membrane protrusions and regulate the cytoskeleton by involving in the Arp2/3-mediated actin polymerization. Therefore, IRSp53 interacts with the small GTPases Cdc42 and Rac, as well as with WAVE2, whereas MIM interacts with cortactin [Mattila et al., 2007]. The BAR-domain protein Tuba is also involved in the formation of membrane protrusions due to its ability of binding directly to N-WASP and interacting with the Rho GTPase Cdc42. Moreover, it has been shown that an overexpression of Tuba leads to the formation of dorsal ruffles in the absence of growth factors [Kovacs et al., 2006]. This leads to the inference that membrane deforming

proteins play an important role in CDR formation, thus having a key part in different models of CDR formation [Gov and Gopinathan, 2006, Shlomovitz and Gov, 2007, Peleg et al., 2011] (introduced in Section 3.5).

3 The Mechanism Underlying CDR Formation

The molecular signaling pathway and underlying mechanism of wave phanomena in *Dictyostelium*, neutrophiles, macrophages and fibroblasts were investigated in various studies [Vicker, 2000, Weiner et al., 2007, Masters et al., 2016, Bernitt et al., 2015]. As described in Chapter 2, a large number of molecules has been identified to be localized to actin waves, in particular to CDRs, and is assumed to be involved in their formation. Nevertheless, the molecular main players and the underlying mechanisms are still debated.

Several studies on actin waves in *Dictyostelium* focused on a reaction-diffusion mechansim that lead to propagating self-organized f-actin waves [Vicker, 2000, Whitelam et al., 2009]. The interaction between activator and inhibitor, which gives rise to an excitable medium is speculated to be one of the possible reasons for emergent actin waves [Whitelam et al., 2009]. Such an activator-inhibitor mechanism was also proposed for Hem-1 waves in neutrophiles, and is based on an interaction between the Hem-1 component of the SCAR/WAVE complex and f-actin [Weiner et al., 2007].

However, the observation of a polarization between the interior and exterior of actin waves in *Dictyostelium* due to bistable kinetics of actin and different concentration of PIP_2 and PIP_3 have led to the suggestion of a possible underlying bistable mechanism [Gerisch et al., 2011]. The concept of bistability on the basis of two stable actin states and distinct distributions of two kinds of phosphoinositides has been proposed for actin waves in macrophages as well [Masters et al., 2016].

Furthermore, the concept of excitability and bistability was also used to investigate CDR dynamics [Zeng et al., 2011, Bernitt and Döbereiner, 2017, Bernitt et al., 2017]. This has led to the proposal of alternative mechanisms for CDR propagation, featuring different molecular main players. The aim of this study is to identify the mechanisms underlying CDR formation. Therefore, this chapter summarizes the diversity of mechanisms underlying actin waves, focusing on the concepts of excitability and bistability, the triggering of actin waves and the spatial coupling of neighbouring regions for wave propagation (Section 3.1). Furthermore, it summarizes the various approaches of modeling CDR dynamics (Section 3.2 - 3.5).

3.1 Models of actin waves

To date, it is still unclear whether the different kinds of actin waves in various cell types underly the same mechanisms. At first glance, the differences in their appearence and the involvement of various molecules in different cell types led to the conclusion that there are diverse underlying mechanisms. However, the main characteristic feature of actin waves is the fact that they typically annihilate upon collision. This signature was the reason why the concept of excitability, which is based on interactions between activators and inhibitors, has been applied to the study on actin waves [Allard and Mogilner, 2013].

An excitable system is characterized by one steady state. Small perturbations decay, whereas larger perturbations induce a large excursion before returning to the steady state, and may lead to a traveling wave pulse [Allard and Mogilner, 2013]. In contrast, bistable systems are characterized by two stable states with, for example, low and high activity levels. Triggering the system locally from the lower to the higher activity level causes a propagating wavefront, which shifts the system in the neighbouring region to a higher level as well [Deneke and Di Talia, 2018].

In both cases, to initiate wave propagation, the system has to be stimulated by perturbations greater than a threshold. This can be achieved either due to random fluctuations in concentrations of filamentous actin or other molecules, as well as due to a perturbation in form of a global negative feedback effected by membrane tension or a fast-diffusing inhibitor [Allard and Mogilner, 2013].

Furthermore, the coupling of neighbouring cellular regions, which is a prerequisite for progagation of wave pulses and wavefronts, plays a critical role. Summarized by Allard and Mogilner, there are three possibilities underlying the spatial coupling: diffusion, f-actin polymerization or mechanical stress [Allard and Mogilner, 2013]. The most common assumption is spatial coupling by diffusion of regulatory molecules of polymerization or branching of f-actin. Consequently, these actin waves are classified as reaction-diffusion systems in which the propagation velocity is proportional to the square root of a diffusion coefficient of regulatory molecules. Moreover, alternative possibilities are spatial coupling by polymerization of f-actin itself, or mechanical spatial coupling, for example based on the interplay of the curved membrane and membrane proteins [Peleg et al., 2011]. For these two cases, the wave velocitiy is either proportional to the protrusion velocity of the cell, or proportional to the cytoskeletal mechanical moduli.

In the context of CDRs, the concept of excitability was taken into account by Zeng et. al [Zeng et al., 2011], who proposed an antagonistic model including the small GTPases Rac and Rho, that based on observations of an antagonistic relationship between stress fibers and CDRs (Section 3.2). Moreover, Bernitt and Döbereiner [Bernitt and

Döbereiner, 2017 employed the FitzHugh-Nagumo model as a prototype model for an excitable system with noisy initial conditions to study confined CDRs in fibroblasts on fibronectin substrates (Section 3.3). Furthermore, a bistability based mechanism was proposed by Bernitt et. al [Bernitt et al., 2017], based on the observations of distinct actin densities in the interior and exterior of CDRs (Section 3.4). In contrast, other studies mainly focus on the interplay of the membrane and their deforming proteins [Peleg et al., 2011] (Section 3.5).

3.2 Modeling CDRs with a Rac-Rho antagonism

Previous studies have shown that there is a depletion of stress fibers in the CDR interior [Buccione et al., 2004]. This finding inspired Zeng et al. to study the relationship between stress fibers and CDR formation by investigating the dependence of CDR formation on varied substrate stiffness, which is suspected to modulate stress fiber formation [Zeng et al., 2011]. Based on their experimental findings, they proposed an antagonistic reaction scheme between the signaling proteins Rac and Rho, of which stress fibers and CDRs are proposed to be markers. In detail, Zeng et al. explained that CDR formation results from a downstream signaling pathway after PDGF stimulation. In this process, the small GTPase Rac is assumed to be activated by PIP_3, and leads to an activation of WAVE1, which further causes an Arp2/3 mediated nucleation of actin filaments. In turn, WAVE1 also inactivates Rac by activating a RacGAP named WGAP, to prevent an overactivation of Rac. Furthermore, activated Rac binds to a RhoGAP and thus inhibits the formation of stress fibers by inactivating Rho. Activated Rho, which is proposed to be regulated by focal adhesion kinases (FAK), whose amount is increased on stiff substrates, induces mDia1-nucleated actin and thus causes the formation of stress fibers. The suggested pathway by Zeng et al. is shown in Fig. 3.1 and has been comprised in a coupled partial differential equation model. Numerical analysis of the model provided similar results compared to their experimental findings. For instance, they found longer CDR lifetimes as a result of stiffer substrates and higher amounts of FAK. Based on these results, Zeng et al. for further studies proposed investigations of CDR formation after inhibiting Arp2/3. In accordance with their model, they propose that a reduction of Arp2/3 leads to a decrease in the amount of CDRs.

In addition, Zeng et al. reduced the ful signaling pathway to a feedback scheme between Rac and WGAP. Rac is activated by PDGF, thus leading to an activation of WAVE1, which further activates WGAP. In turn, activated WGAP inactivates Rac (see grey dashed box in Fig. 3.1). This leads to a simplified model with Michalis-Menten kinetics and a Hill equation, which can create an excitable system. The model, which

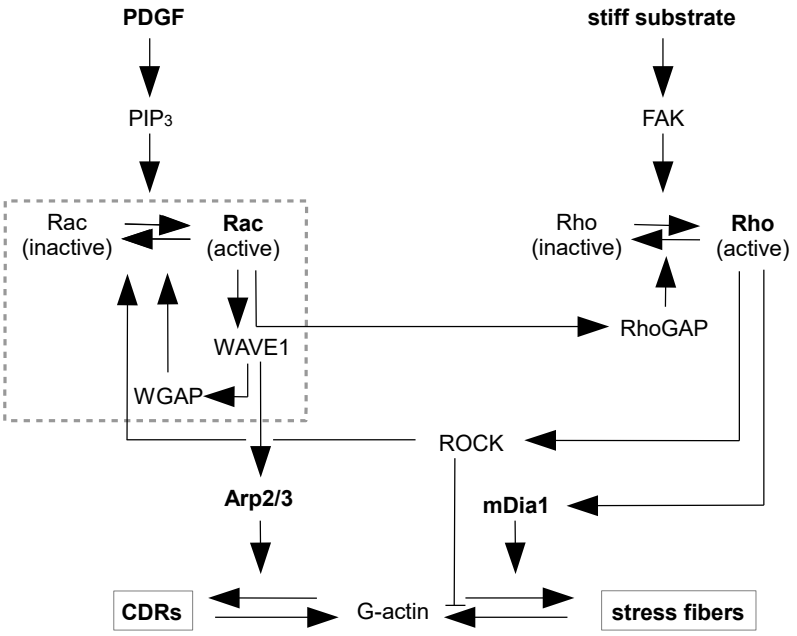

Figure 3.1: Signal pathway of CDR formation after PDGF stimulation and formation of stress fibers in response to stiff substrates incorporated in the complete model of Zeng et al. The dashed box contains the interactions of the key players in the reduced model: Rac, WAVE1 and WGAP [Zeng et al., 2011].

includes active Rac X, active WGAP Y, total Rac X_t and total WGAP Y_t reads:

$$\frac{\partial X}{\partial T} = D\frac{1}{R}\frac{\partial}{\partial R}\left(R\frac{\partial X}{\partial R}\right) + \frac{V_1(X_\mathrm{t} - X)}{K_\mathrm{m1} + X_\mathrm{t} - X} - \frac{V_2 X^2 Y}{K_\mathrm{m2}^2 + X^2}, \tag{3.1}$$

$$\frac{\partial Y}{\partial T} = D\frac{1}{R}\frac{\partial}{\partial R}\left(R\frac{\partial Y}{\partial R}\right) + \frac{V_3 X(Y_\mathrm{t} - Y)}{K_\mathrm{m3} + Y_\mathrm{t} - Y}. \tag{3.2}$$

The parameters of the enzymatic activation of Rac after PDGF stimulation are given by V_1 and K_{m1}, the parameters of the deactivation of Rac by WGAP are given by V_2 and K_{m2} and the activation of WGAP after Rac activation are given by V_3 and K_{m3}. T and R describe the temporal and spatial dimensions, and D is the diffusion constant. Numerical analysis of this reduced model demonstrated, that characteristic dynamics of CDRs, in particular ring growth and decay, can be explained as a wave propagation in an excitable medium.

3.3 Modeling CDR dynamics with a noise-driven excitable system

To identify the mechanism underlying CDRs, experimental studies quantitatively analyze the dynamics of CDRs in random shaped fibroblasts and fibroblasts of controlled morphology [Bernitt et al., 2015, Bernitt and Döbereiner, 2017]. CDRs in random shaped fibroblasts exhibit phaenomena like annihilation of wavefronts upon collision, spiral waves or stalled wavefronts close to the cell edge [Bernitt et al., 2015]. Moreover, in disk-shaped fibroblasts with a centered nuceleus, CDRs are confined between nucleus and cell edge leading to a wave propagation on a one dimensional trajectory. Kymographs resemble spatiotemporal patterns of coherence resonance [Bernitt and Döbereiner, 2017]. These characteristics can be compared to waves in an active medium and therefore it appears appropriate to study CDR dynamics via reaction-diffusion systems.

One of the most prominent examples of an active medium is the FitzHugh-Nagumo model. It is a simplified version of the Hodgking-Huxley-model describing nerve impuls propagation in a single nerve fiber [FitzHugh, 1968]. It includes two variables of state: the membrane potential V and a recovery variable R. Hence, the model consists of a pair of equations with time t, propagation distance s, diffusion coefficient D and the constants Φ, a and b:

$$\frac{\partial V(s,t)}{\partial t} = D\nabla^2 V + V - V^3/3 - R + \eta(s,t), \tag{3.3}$$

$$\frac{\partial R(s,t)}{\partial t} = \Phi(V + a - bR). \tag{3.4}$$

The FitzHugh-Nagumo model is a prototype of an excitable system with key features that are important for actin waves, such as autocatalysis, inhibition and diffusivity [Bernitt and Döbereiner, 2017]. Hence, Bernitt and Döbereiner utilized this model consisting of an activation and an inhibiting field to study the role of noise in the actin wave machinery [Bernitt and Döbereiner, 2017]. To do so, they included a noise term $\eta(s,t)$ in the form of a Wiener process as a stimulus. Numerical solutions of this model reproduce experimental data of spatiotemporal patterns of confined waves, that have led to the conclusion that CDRs can be understood as waves in a noise-driven active medium.

3.4 Modeling CDRs with a bistability-based mechanism

In contrast to the concept of excitability, Bernitt et al. proposed a bistability-based mechanism of CDRs by a mass-conservative reaction-diffusion model [Bernitt et al., 2017]. This has been inspired by confocal fluorescence microscopy visualizing distinct actin densities between the interior and exterior of CDRs, manifesting in a depletion of stress fibers and cortical actin in the CDR interior. This gives rise to the conjecture that CDRs obey bistable kinetics of actin. The model contains three different states

of actin: branched actin incorporated in CDRs, indicated by B, immobile filamentous actin organized in stress fibers and in the cell cortex, indicated by F and globular actin monomers, denoted by G. Feedback loops between these organizational actin states are suggested, whereas the total amount of actin (A=B+F+G) is assumed to be constant. Inhibition of actin polymerization in the interior of CDRs is controlled by an inhibition control complex I, that includes the activity of Arap1 and PIP_3 [Hoeller et al., 2013, Hasegawa et al., 2012]. The dimensionless model equations read as follows:

CDR-incorporated actin

$$\frac{\partial B}{\partial t} = \overbrace{\frac{B^2 G}{1+I}}^{\text{autocat. recruitment and polym.}} - \overbrace{B}^{\text{degradation}} + \overbrace{D_\mathrm{b}\nabla^2 B}^{\text{diffusion}}, \tag{3.5}$$

Stress fibers and cell cortex

$$\frac{\partial F}{\partial t} = \overbrace{k_{\mathrm{f}1}\frac{G}{1+I}}^{\text{polymerization}} - \overbrace{k_{\mathrm{f}2}F}^{\text{degradation}}, \tag{3.6}$$

Actin monomers

$$\frac{\partial G}{\partial t} = \overbrace{-\frac{B^2 G}{1+I} + B - k_{\mathrm{f}1}\frac{G}{1+I} + k_{\mathrm{f}2}F}^{\text{conservation}} + \overbrace{\nabla^2 G}^{\text{diffusion}}, \tag{3.7}$$

Actin inhibitor

$$\frac{\partial I}{\partial t} = \overbrace{k_{\mathrm{i}1}B}^{\text{activation}} - \overbrace{k_{\mathrm{i}2}I}^{\text{degradation}} + \overbrace{D_\mathrm{i}\nabla^2 I}^{\text{diffusion}}. \tag{3.8}$$

The activation rate of the inhibitor I by the CDR-incorporated actin B is given by $k_{\mathrm{i}1}$, whereas $k_{\mathrm{i}2}$ is the associated degradation rate. The rate of actin polymerization into stress fibers and the cortical network as well as the degradation rate are $k_{\mathrm{f}1}$ and $k_{\mathrm{f}2}$, respectively. The conservation of total mass of actin is reflected by Eq. 3.7.

In accordance with its name, this reaction-diffusion model exhibits two main characteristics. Reaction implies a positive feedback due to polymerization of branched actin, which leads to an increasing number of filament ends (Eq. 3.5). On the one hand, it is induced by N-WASP, a member of the WASP/Scar family as a major nucleator in CDRs, and on the other hand, by curved nucleators accumulated at the undulated membrane of the CDR [Legg et al., 2007, Kovacs et al., 2006].

The second characteristic of the model is diffusion, that comprises distinct mobil-

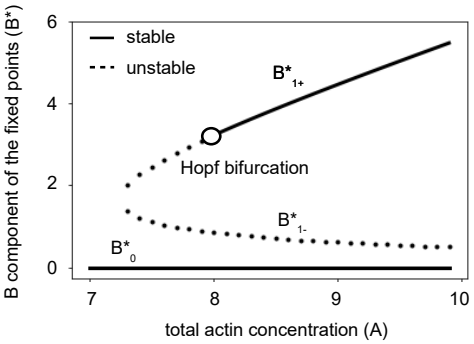

Figure 3.2: Bifurcation diagram of the bistable model (Eq. 3.5-3.8). The graph shows the B component of the fixed points P^*_0, P^*_{1+} and P^*_{1-} (B^*) dependant on the total actin concentration (A) according to Bernitt et al., 2017. The black unfilled circle marks the Hopf bifurcation.

ities of the actin components and the inhibitor of actin polymerization. Actin monomers G are free diffusive in three dimensions (Eq. 3.7), whereas branched actin B and the inhibitor of actin polymerization I are only diffusive at or in the two-dimensional dorsal cell membrane with small diffusion constants $D_\mathrm{b},\ D_\mathrm{i} < 1$ (Eq. 3.5 and 3.8). Filamentous actin in stress fibers and the cortical network F is immobile (Eq. 3.6).

Bistability

The system is characterized by the following two stables fixed points P^*_0=(B^*_0, F^*_0, G^*_0, I^*_0) and P^*_{1+}=(B^*_{1+}, F^*_{1+}, G^*_{1+}, I^*_{1+}) as well as one unstable fixed point P^*_{1-}=(B^*_{1-}, F^*_{1-}, G^*_{1-}, I^*_{1-}) as a function of the total amount of actin A:

$$B^*_0 = 0, \tag{3.9}$$

$$B^*_{1\pm} = \frac{A-a}{2} \pm \sqrt{\frac{(A-a)^2}{4} - (1-\alpha)}, \tag{3.10}$$

$$F^*_{0,1\pm} = \alpha \frac{A - B^*_{1\pm}}{\alpha + (1 + aB^*_{1\pm})}, \tag{3.11}$$

$$G^*_{0,1\pm} = A - B^*_{1\pm} - F^*_{1\pm}, \tag{3.12}$$

$$I^*_{0,1\pm} = aB^*_{1\pm}, \tag{3.13}$$

with $a = \frac{k_{\mathrm{i}1}}{k_{\mathrm{i}2}}$ and $\alpha = \frac{k_{\mathrm{f}1}}{k_{\mathrm{f}2}}$, the ratios of the kinetic constants of the inhibitor as well as filamentous actin and actin in stress fibers, respectively.

A saddle node bifurcation and a Hopf bifurcation are found for $P^*_{1\pm}$ dependent on the total actin concentration Bernitt et al., 2017. This leads to the existence of a bistable regime above a critical concentration of total actin A, in which P^*_0 corresponds to the CDR free state and P^*_{1+} to the state of the CDR interior (see Fig. 3.2).

Dynamics of wavefronts and wave instability

Numerical solutions of the model equations in the bistable regime reproduce oberserved CDR dynamics. It has been demonstrated that wavefronts can be formed from one point and grow radially after a local stimulation in the *B*-field (Fig. 3.3), followed by a second wave of a depletion of filamentous actin. The waves are reversed at the cell edge and collapsed in one point. Moreover, after a global noisy perturbation on the entire domain, a ring is formed near the domain edge, reverses at the boundary and collapses, again, in one point (Fig. 3.4). This is comparable to the CDR dynamics observed experimentally after growth factor stimulation.

Under certain biochemical conditions, CDRs show more complex dynamics, for example pinned wavefronts or chaotic dynamics of small actin clusters surrounded by a propagating front. These situations can also be found in numercial solutions of the bistable model of Bernitt et al. [Bernitt et al., 2017] (the latter is shown in Fig. 3.5).

To evaluate the hypothesis that CDRs are waves in a bistable system, in this study, a systematic analysis of biochemical condition in disk-shaped fibroblasts is performed (Chapter 6, 7 & 8) in comparison with simulations using the bistable model on an annulus domain under variation of the according parameters (Chapter 5 & 6).

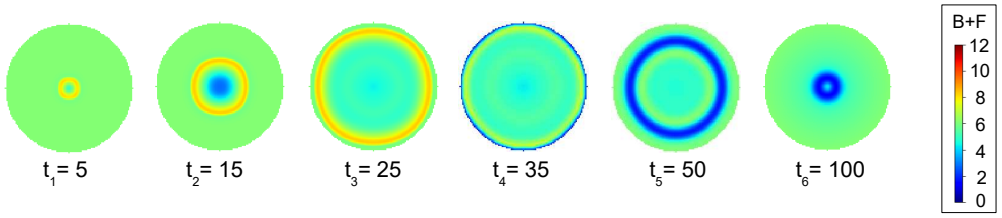

Figure 3.3: Propagating wavefront after local stimulation. Numerical solution of the bistable model with a spatially localized pertubation. Parameters are D=0.12, k_{i1}=2.09, k_{i2}=0.53, k_{f1}=2.05, k_{f2}=1.19 and A=10 according to [Bernitt et al., 2017].

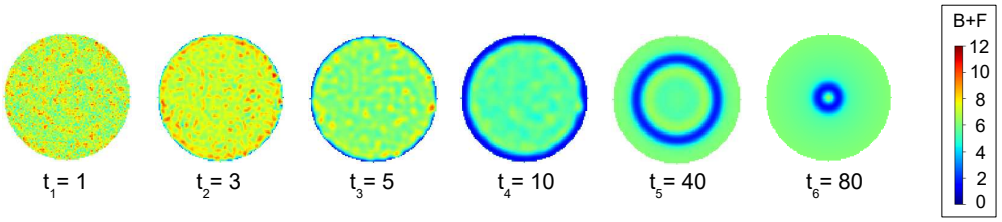

Figure 3.4: Propagating wavefront after a global stimulation. Numerical solution of the bistable model with a perturbation of the entire domain. Parameters are D=0.12, k_{i1}=2.09, k_{i2}=0.53, k_{f1}=2.05, k_{f2}=1.19 and A=9.67 according to [Bernitt et al., 2017].

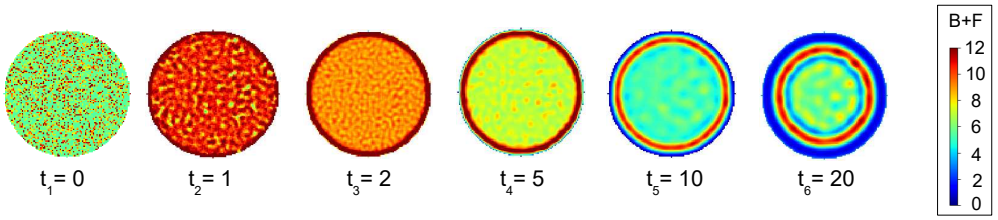

Figure 3.5: Unstable wavefront. Numerical solution of the bistable model with a perturbation of the entire domain. The parameters are D=0.12, k_{i1}=1.64, k_{i2}=0.30, k_{f1}=2.05, k_{f2}=2.05 and A=11.5 according to Bernitt et al., 2017.

3.5 Modeling CDRs with curved activators of actin polymerization

Several theoretical models describe the propagation of actin waves driven by potrusive forces of actin polymerization by the coupling of the elastic cell membrane and curved membrane proteins. Curved membrane proteins contain, for example, a BAR or a I-BAR domain, shaping the membrane either in a concave or in a convex form, respectively Peter et al., 2004, Mattila et al., 2007. Two prominent examples are Tuba (concave) or IRSp53 (convex), which are involved in the initiation of actin polymerization by recruiting actin activators like N-WASP or WAVE Kovacs et al., 2006. It was suggested that concave membrane proteins lead to damped actin waves Gov and Gopinathan, 2006. In contrast, addition of contractile forces mediated by myosin II motors and only convex membrane proteins are proposed to generate robust actin waves Shlomovitz and Gov, 2007. Controversely, experimental results have demonstrated that propagation of membrane ruffles like CDRs is unaffected by actomyosin contractility Peleg et al., 2011.

Based on these observations, Peleg et al. proposed a theoretical model explaining the interplay between both convex and concave membrane proteins Peleg et al., 2011. In the absence of curved membrane proteins, the elastic membrane is assumed to be flat. Proportional to their local concentrations, the membrane proteins induce a spontaneous membrane curvature (Fig. 3.6 A) and curve the membrane further by protrusive forces due to actin polymerization. In turn, the dynamics of these membrane proteins, which can either diffuse in the membrane or adsorb from the cytoplasm, are influenced by the membrane shape. This is because the membrane proteins accumulate locally, where the membrane shape fits to their curvature. According to Peleg et al., this leads to a feedback mechanism between the membrane curvature $h(\vec{r})$, and convex $\Phi_-(\vec{r})$ or concave membrane proteins $\Phi_+(\vec{r})$ (see Fig. 3.6 B). A positive feedback is caused by only convex membrane proteins with local membrane deformations leading to larger membrane protrusions, in which the concentration of convex membrane proteins rises. In contrast, only concave membrane proteins provoke a negative feedback with local

membrane deformations, but in combination with convex membrane proteins, they will produce unstable waves. In attempting to inhibit the protrusions, concave membrane proteins accumulate in this areas and thus shift local membrane protusions, induced by convex membrane proteins, laterally in space.

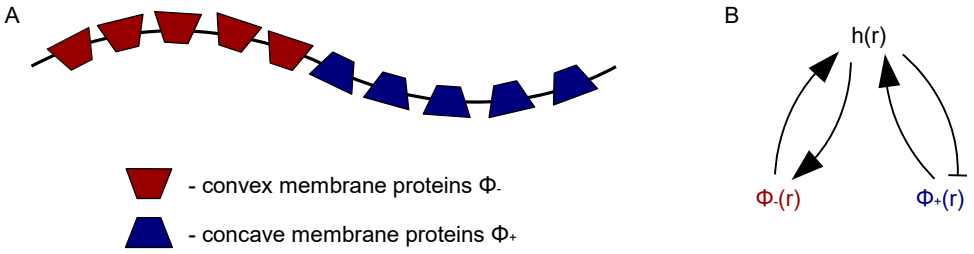

Figure 3.6: Interplay between concave and convex membrane proteins. A shows a sketch of accumulated concave and convex membrane proteins at the cell membrane according to their shapes. B visualizes the feedback loop between curved membrane proteins and the cell membrane. Convex membrane proteins provoke a positive feedback with the cell mebrane, in contrast concave membrane a negative. Figure was designed according to [Peleg et al., 2011].

This feedback mechanism (Fig. 3.6 B) is described by the following equation:

$$\frac{\partial h}{\partial t} = \frac{d}{4\eta}\left(-\frac{\delta \mathcal{F}}{\delta h} + f_{\text{actin}}\right). \tag{3.14}$$

It is composed of elastic forces on the membrane derived from the free energy $\mathcal{F}$, as well as potrusive forces from actin polymerization f_{actin} (Eq. 3.16). Additionally, local hydrodynamic interactions are included with fluid viscosity surrounding the membrane η and an effective distance d between cytoskeletal elements and the membrane.

The free energy $\mathcal{F}$ of the membrane is given by

$$\mathcal{F} = \int_S \frac{\kappa}{2}\left(\nabla^2 h - H_-\Phi_- - H_+\Phi_+\right)^2 + \frac{\sigma_{\text{eff}}}{2}(\nabla h)^2 + \left[T\sum_{i=\pm} n_i^s \Phi_i(\log\Phi_i - 1)\right] d^2r \tag{3.15}$$

in the limit of small undulations. The first term corresponds to the bending energy, which depends on the membrane curvature $(\nabla h)^2$ and the spontaneous curvature of the curved membrane proteins $H_- < 0$ and $H_+ < 0$, as well as the bending modulus of the membrane κ. Furthermore, the second term corresponds to the surface tension with the effective tension σ_{eff}, and the third term corresponds to the entropy of the membrane proteins with temperature T and saturation concentration n^s.

The pushing force f_{actin} generated by actin polymerization is characterized through

$$f_{\text{actin}}(\overrightarrow{r}) = A_+(\Phi_+(\overrightarrow{r}) - \overline{\Phi}_+) + A_-(\Phi_-(\overrightarrow{r}) - \overline{\Phi}_-) \tag{3.16}$$

with the activity of the actin polymerization $A_\pm$ induced by the curved membrane proteins $\Phi_\pm$ and their average concentration $\overline{\Phi_\pm}$.

Due to a comparison between experimental and theoretical results provided by linear stability analysis as a function of the membrane proteins activity A_- and A_+, Peleg et al. concluded that the interplay of both membrane proteins is the dominant mechanism in CDRs.

4 Materials and Methods

This chapter summarizes materials and methodes to investigate CDR dynamics in disk-shaped fibroblasts under constant physiological and varied biochemical conditions. Furthermore, the implementation of numerical solutions of the bistable model is detailed, which will be employed to theoretically investigate the mechanism underlying CDR formation.

4.1 Cell culture

Various cell types show different kinds of phenomena of actin waves. One of them are CDRs, that were discovered first and have been further examined in fibroblasts after growth factor stimulation [Mellström et al., 1988]. Hence, in this thesis all experiments to investigate CDR dynamics were performed with fibroblasts of type NIH WT 3T3 that in the following will be referred to as fibroblasts or cells. This standard cell line was cultured in Dulbecco's modified Eagle's medium (DMEM, Biochrom), containing $3.7\,\mathrm{g\,l^{-1}}$ $NaHCO_3$, $4.5\,\mathrm{g\,l^{-1}}$ D-Glucose and stable glutamine as well as 10 % Na-Pyruvate (100 mM, Biochrom), 10 % fetal bovine serum (FBS, Biochrom) and $100\,\mathrm{\mu g\,ml^{-1}}$ Penicillin/Streptomycin (Biochrom). Fibroblasts were grown at standard conditions of 37 °C and 5 % CO_2. They were split three times a week at 70 % confluence by using Trypsin/EDTA (Biochrom) and were tested as mycoplasma free.

4.2 Microcontact printing

Shaping highly dynamic fibroblasts into well-defined morphologies leads to comparable and reproducible experimental conditions. This is achieved by seeding fibroblasts on disk-like fibronectin patches of the same size that are stamped on glass coverslips according to a protocol of Théry and Piel with minor modifications [Théry and Piel, 2009]. Fibronectin was chosen as an adhesion protein for fibroblasts, that acts as a reservoir for growth factors and thus plays an important role in the formation of CDRs [Azimifar et al., 2012, Sawicka et al., 2015].

4.2.1 Fabrication of elastomeric stamps

For manufacture of the required stamps, a silicon wafer designed by Erik Bernitt was utilized as a negative [Bernitt et al., 2015]. It was silanized through vaporization of trimethylchlorosilane (Carl Roth GmbH) in a desiccator for several hours to ensure a

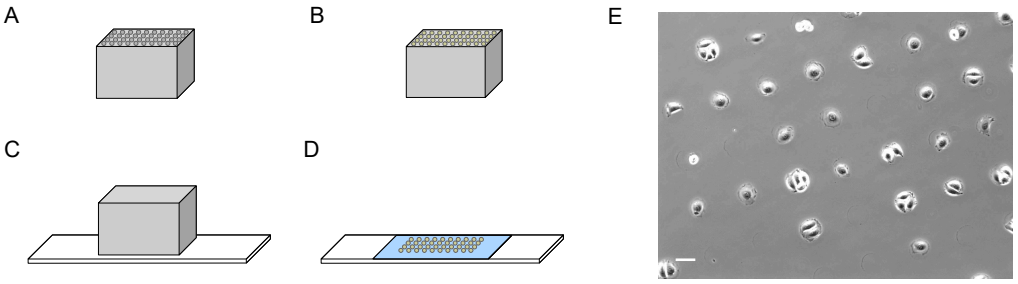

Figure 4.1: Microcontact Printing. A stamp with cylindric protrusions is coated with a drop of fibronectin (A). After removal of excess fibronectin, the stamp with wetted disk-like surface areas of cylindric protrusions (B) is pressed onto a glass coverslip (C) for printing fibronectin patches. After removal of the stamp, the areas in between are coated with PEG (D). Fibroblasts adhere on these disk-like fibronectin patches and adapt their morphology (E, scale bar: $50\,\mu m$).

residue-free detaching of the fabricated stamps. Then, a few millimeter elastomeric layer out of a polydimethylsiloxane(PDMS) mixture was casted onto the silicon wafer. It was prepared by mixing PDMS and the curing agent (both Sylgard 184) according to the manufacturer's instructions and centrifuged for five minutes to eliminate air bubbles. After hardening in an oven for two hours at 60 °C, the PDMS layer could be gently removed from the silicon wafer and the individual stamps were cut to an appropriate size.

4.2.2 Preparation of adhesion patterns

To create microcontact printed disk-like adhesion patterns with radii of 31 µm (Fig. 4.1), PDMS stamps were coated with a 30 µl drop of fibronectin (50 µg ml^{-1} diluted in phosphate buffered saline (PBS), both Sigma-Aldrich). After 20 minutes incubation time, excess fibronectin was aspirated from the stamps so that only contact surfaces were wetted. Glass coverslips were pretreated and thus activated with an argon plasma pen (kinpen 11, Neoplas Control) before stamps were pressed gently with tweezers on glass coverslips to create adhesion patterns. After careful removal of the stamps, the grid-like printed area was completely covered for 20 minutes with Poly(L-lysine)-graft-poly(ethylene glycol) (PLL-g-PEG, SuSoS SurfaceSolutions, 100 µg ml^{-1} diluted in 10 mM HEPES buffer) to prevent the space between the fibronectin patches for cell adhesion. Afterwards, fibronectin patterns were washed and stored, covered with PBS.

4.3 Microfluidic perfusion system

To examine the influence of different proteins on the dynamics of CDRs and to gain a deeper understanding of their underlying molecular species by changing biochemical

conditions, a microfluidic perfusion system (see Fig. 4.2) established by Malte Ohmstede and Erik Bernitt, was used [Ohmstede, 2016, Bernitt, 2015]. Two 25 ml Duran glass bottles served as reservoirs for normal cell culture medium (DMEM) and cell culture medium with an added inhibitor, like Jasplakinolide, Wortmannin or Wiskostatin, respectively (see Section 4.5.2). Air-inpermeable Teflon tubes (Techlab GmbH) were used to connect the medium reservoirs to a microfluidic channel with bottom-adherent fibroblasts. The microfluidic channels consisted of two components: a bottomless six channel slide (sticky-Slide VI 0.4) and an affixed accompanied glass coverslip (both Ibidi), that allowed a prior preparation of the glass bottom before sticking both together. The microfluidic channel was further linked to a waste container via a silicone tube. Luer adapter (outer diameter of 2.4 mm) were used to couple the tubes to the reservoirs, the microfluidic channel or the waste container. Due to the small diameter of the Teflon tubes of 0.75 mm, they were overcoated with 1 cm long silicone tubes with similar diameters like the luer adapters to stabilize their connections and also to seal them airtight.

A three-way valve (Discofix C 3SC, B. Braun), driven by a small servo-motor RS-D10Y (Modelcraft), was interposed between the two medium reservoirs and the microfluidic channel. To generate a pressure driven flow, a p2cs pressure controller (Biophysical Tools) was connected to the medium reservoirs. The pressure control, as well as the controlling of the motorized three-way valve, was done by a custom written software by Malte Ohmstede [Ohmstede, 2016]. With the help of this setup, a complete exchange of the medium in the microfluidic channel was achieved within one minute by generating a flow of 6 mbar.

4.4 Imaging

A light microscope Axio Observer.Z1 (Zeiss microscopy) was used for live cell imaging. It was equipped with an incubation unit containing a Heating Unit XL S, a Temp Module S and a CO_2 Module S to ensure constant physiological conditions of 37 °C and 5 % CO_2. Connected with an AxioCam MRm digital camera, experimental data were recorded, and microscope as well as camera were controlled by the software AxioVision (also Zeiss microscopy).

Phase contrast microscopy, using a 10x objective with a numerical aperture of 0.25, enabled a stable focus for long term experiments. It was used for multidimensional image aquisition of several positions with multiple fibroblasts. A number of CDRs were recorded in one experiment, which allowed a quantitative analysis of CDR dynamics.

For a more detailed information of CDR structures, a 40x objective with numerical aperture of 0.95 was used. Additionally, visualization of actin distributions were investigated by using fluorescent microscopy. In these experiments, fibroblasts were

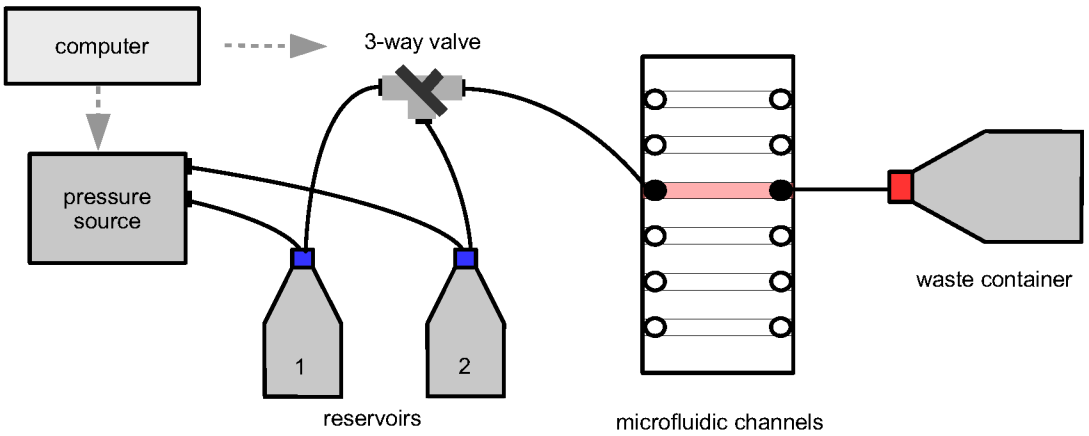

Figure 4.2: Setup of the microfluidic perfusion system. The system contains two reservoirs with DMEM and DMEM with an added inhibitor, a pressure source, a motorized three-way walve, a microfluidic channel and a waste container. A medium flow, and thus an exchange of medium in a microfluidic channel, can be generated and controlled using a computer.

illuminated with a mercury lamp HXP 120 (Zeiss microscopy), using a 488/10 Brightline filter (AHF Analysetechnik), as well as a 76 HE reflector filter set (Zeiss microscopy).

4.5 Experiments

Dynamics of spontaneously formed CDRs in disk-shaped fibroblasts under constant physiological conditions were investigated and compared to dynamics of stimulated and spontaneously formed CDRs in random shaped fibroblasts (Section 4.5.1). Moreover, to examine the influence of different proteins on the dynamics of CDRs, systematic experiments of controlled biochemical conditions were performed by using different chemical inhibitors (Section 4.5.2). Additionally, the detailed f-actin network was investigated by applying fluorescence microscopy (Section 4.5.3).

4.5.1 CDR dynamics in random shaped fibroblasts

Stimulated and spontaneously formed CDRs were observed in random shaped fibroblasts for a comparison with spontaneous CDR formation in disk-shaped cells. Therefore, in a first experiment, fibroblasts, that were seeded at low confluency one day prior to the experiment in plasma-treated glass bottom imaging dishes (WillCo Wells), were stimulated with 30 ng ml^{-1} PDGF-BB (Cell Signaling Technology). Furthermore, in a second experiment, spontaneously formed CDRs were observed in fibroblasts 20 minutes after spreading in plasma-treated glass bottom dishes, that had been coated with fibronectin (50 µg ml^{-1}, Sigma Aldrich) and incubated for 45 minutes with DMEM

plus FBS.

4.5.2 CDR dynamics in disk-shaped fibroblasts under physiological and controlled biochemical conditions

CDR dynamics in disk-shaped fibroblasts under physiological and controlled biochemical conditions were observed on microcontact printed substrates (Section 4.2) in microfluidic channels. To perform experiments with the microfluidic perfusion system (Section 4.3) in order to change protein densities in fibroblasts, it was important to avoid air bubble formation, as these would interfere with the pressure generated flow and destroy fibroblasts on fibronectin patches. Therefore, the perfusion system was prepared and filled with DMEM one day prior to the experiment, and all tubes were flushed with DMEM by using a 10 mL syringe [Bernitt, 2015]. Additionally, 50 mL DMEM for the reservoirs had to be degased one day prior to the experiment as well.

45 minutes before seeding fibroblasts into the microfluidic channel, PBS in the channels was replaced by DMEM with FBS and Penicillin/Streptomycin covering the fibronectin substrates (Section 4.2). Then, fibroblasts were allowed to spread for 20 minutes, and non-adhering cells were flushed out. CDR dynamics in spread fibroblasts were recorded with the imaging system (Section 4.4) under variation of the biochemical environment. The runtime of the experiments is described below and dependent on the biochemical compound and its produced effect.

Jasplakinolide

Jasplakinolide (Sigma Aldrich) is a membrane-permeable cyclodepsipeptide isolated from the marine sponge, *Jaspis johnstoni*. It binds to f-actin [Bubb et al., 1994, Lee et al., 1998] and has been used to investigate the influence of total actin. Jasplakinolide induces actin polymerization into amorphous strucures, and stabilizes the actin cytoskeleton [Bubb et al., 2000]. Two types of experiments were performed: short experiments taking 90 min and long experiments taking 180 min. In the 90 minutes experiments, fibroblasts spent 45 minutes during a DMEM environment and afterward 45 minutes in a DMEM environment with 15 nM, 20 nM or 25 nM Jasplakinolide. Each of the long-time experiments took three hours; the fibroblasts spent half of this time in a DMEM environment, afterwards DMEM was replaced by DMEM with 20 nM Jasplakinolide.

Wortmannin

To investigate the influence of the phospholipid PIP_3, Wortmannin (Sigma Aldrich), a known cell permeable inhibitor of the enzym PI3K, isolated from *Penicillium funiculosum*, was used to suppress the phosphorilation from PIP_2 to PIP_3 (see manufacturer's product information). A series of experiments was performed for two hours: 60 minutes with a

DMEM environment before replacing DMEM by DMEM with 0.5 µM, 1.0 µM or 1.5 µM Wortmannin, respectively.

Wiskostatin

Wiskostatin (Sigma Aldrich), a chemical inhibitor of N-WASP was deployed to examine the influence of Arp2/3-mediated actin nucleation on CDR formation and propagation. It binds to the GTPase-binding-domain of N-WASP keeping it in its autoinhibited conformation, and thus it suppresses the activation of Arp2/3 [Peterson et al., 2004]. A series of experiments was carried out by using Wiskostatin concentrations of 1 µM, 1.5 µM and 2 µM. Due to its reversibility, experiments were performed over two hours changing between DMEM and DMEM with the added inhibitor every 30 minutes.

4.5.3 Visualizing filamentous actin

To get detailed information about the distribution of actin filaments, fibroblasts were transfected with p^{CMV}-LifeAct®-TagGFP2 (Ibidi). The marker TagGFP2, bound to the actin binding domain LifeAct and the CMV promoter, allows a fluorescent labelling of actin filaments in various living eukaryotic cells. Its excitation and emission wave length maxima are 483 nm and 506 nm, respectively. Moreover, p^{CMV}-LifeAct®-TagGFP2 does not interfere with cellular processes, so that it is well suited for visualization of filamentous actin in living fibroblasts (see manufacturer's instructions).

To transfect fibroblasts with p^{CMV}-LifeAct®-TagGFP2 plasmid, Lipofectamine 2000 (Invitrogen) was utilized as a transfection reagent. These are cationic liposomes, building complexes with negatively charged nucleic acid molecules. This facilitates the overcoming of the electrostatic repulsion between the negatively charged LifeAct®plasmids and the also negatively charged cell membrane, ensuring an uptake of the LifeAct®plasmid by the cell [Dalby et al., 2004]. Following the manufacturer's protocol of Lipofectamine 2000, 8 µg of the plasmid p^{CMV}-LifeAct®-TagGFP2 and 18 µL of Lipofectamine 2000 were respectively diluted in 500 µL antibiotic- and serum-free DMEM. After five minutes of incubation, both mixtures were combined to allow complex formation for 20 minutes at room temperature. Subsequently, the LifeAct-Lipofectamine 2000 complexes were added to cells, plated one day prior to transfection at 90 % confluence in antibiotic-free DMEM.

4.6 Data analysis

For a detailed analysis of CDR dynamics in fibroblasts, time-lapse sequences of phase contrast micrographs with a time interval of 15 s or 20 s were recorded using the imaging set-up (described in Section 4.4). The experimental system of disk-shaped fibroblasts, in which propagating CDRs were limited to travel on a one-dimensional trajectory between cell boundary and nucleus, enabled a systematic analysis of the recorded data by means

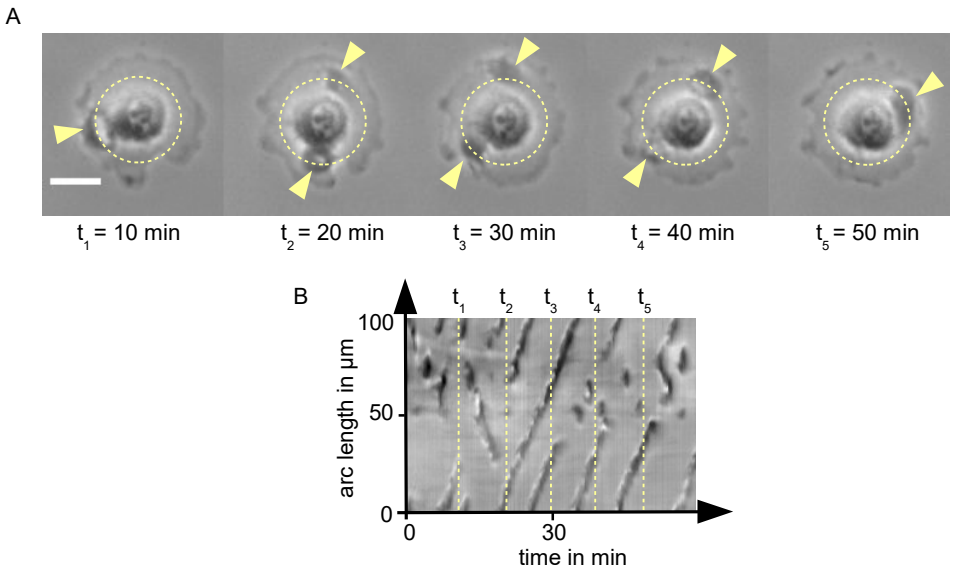

Figure 4.3: Creating a kymograph from time-lapse sequences of micrographs. A shows a time-lapse sequence of micrographs (scale bar: 20 µm) of a fibroblast with CDRs (indicated by yellow arrowheads) travelling along a circle around the nucleus. Image intensities along the circle around the nucleus are plotted as a function of space and time in B.

of circular kymographs (Section 4.6.1). These allowed a visualization and comparison of CDR dynamics and interactions as well as measurements of parameters like CDR velocities, periodicities, lifetimes and travelling distances (Section 4.6.2 & 4.6.3).

4.6.1 Visualization of CDR dynamics and interactions via circular kymographs

One-dimensional circular kymographs were created from time-lapse sequences of micrographs with FIJI (FIJI is just ImageJ), using a custom-written routine of Erik Bernitt [Schindelin et al., 2012; Bernitt et al., 2015]. These graphs are space-time-plots of image intensities along a circle around the nucleus as a function of space and time (Fig. 4.3). The kymograph patterns created in this manner uncovered a lot of important characteristics of CDR dynamics and their interactions, as well as the number of concurrently occurent CDRs. Moreover, it enabled to measure systematically CDR velocities and periodicities [Bernitt et al., 2015], as well as their lifetimes and travelling distances for a detailed study of CDR dynamics under physiological and controlled biochemical conditions.

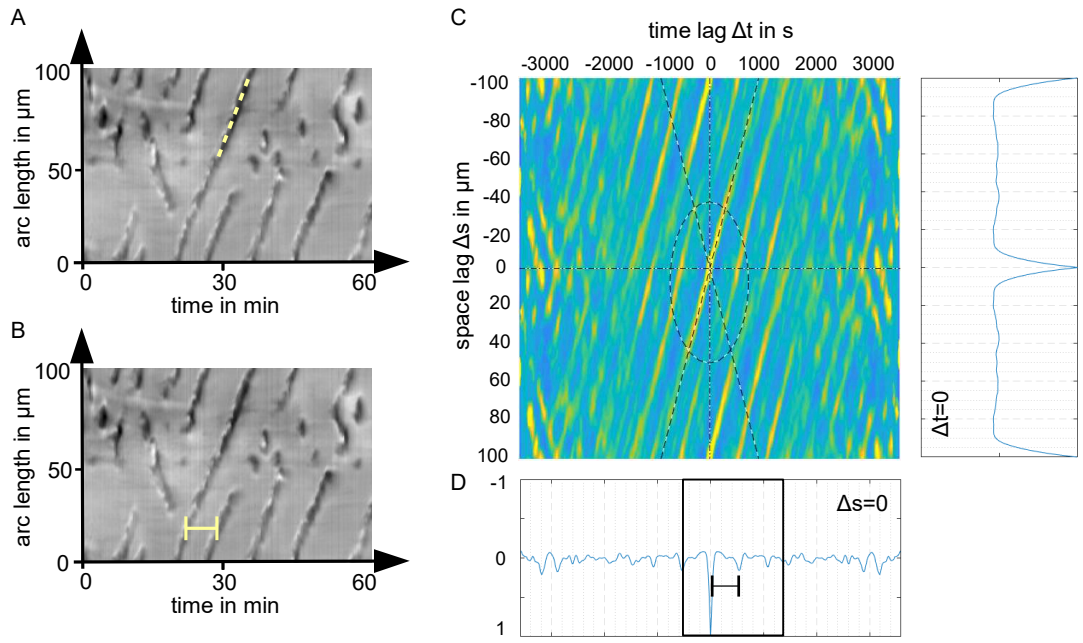

Figure 4.4: Measuring CDR velocities and periodicities via autocorrelation functions. A selected part of a CDR trajectory is highlighted by a yellow dashed line in an example of kymograph in A. The slope of the dashed line corresponds to CDR velocity. The time interval between two successive CDRs at the same position is referred to as the periodicity and highlighted by a yellow line in B. C displays the autocorrelation function in time and space of the kymograph example from A and B. CDR periodicites were measured from the intensity profile at zero space lag presented in D.

4.6.2 Measuring CDR velocities and periodicities

Constant velocities of CDRs correspond to the slope of line patterns in kymographs, which can be calculated by the difference quotient $v = \frac{\Delta s}{\Delta t}$ with arc length s and time t (Fig. 4.4 A). Moreover, CDR periodicities are time intervalls of two successive CDRs at the same position (Fig. 4.4 B). Both, CDR velocities and periodicities were measured using a custom-written routine by Erik Bernitt [Bernitt et al., 2015], that calculated autocorrelation functions in space and time of binarized kymographs. The routine has been implemented in Matlab R2017b (The Mathworks). The averaged CDR velocity over a selected time intervall was calculated by the routine via a Radon transform. Moreover, averaged CDR periodicities were read out from cuts in autocorrelation functions through $\Delta s = 0$ (Fig. 4.4 D).

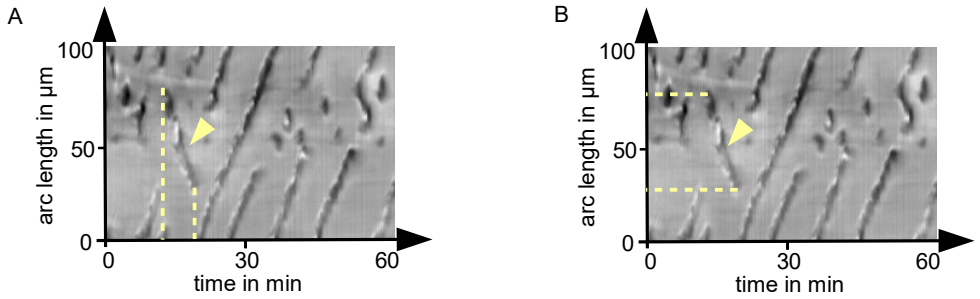

Figure 4.5: Measuring CDR lifetimes and traveling distances. In A yellow dashed lines visualize the lifetime of the CDR that is marked with a yellow arrowhead. In B yellow dashed lines highlight the travelling distance of the marked CDR.

4.6.3 Measuring CDR lifetimes and traveling distances

In this thesis, CDR lifetimes are defined as the time intervalls between emergence and disappearence of the same CDRs. This measurement value was directly read out from kymographs for individual CDRs (Fig. 4.5 A). Average CDR lifetimes in the same fibroblast over a certain time period were calculated manually as the mean of a series of lifetimes of individual CDRs. Moreover, CDR traveling distances are referred to as the spatial distances individual CDRs traveled on its one-dimensional trajectory around the nucleus during its lifetime (Fig. 4.5 B). Average traveling distances were also calculated manually as the mean of a series of traveling distances of individual CDRs in the same fibroblast over a certain time period.

4.7 Numerical simulations

Numerical solutions of the following coupled partial differential equations of the bistable model system proposed by Bernitt et al. [Bernitt et al., 2017] (Eq. 4.1-4.4, description of the model in Section 3.4) were calculated by using forward Euler method with Python 3.7 after initiating the system at its CDR free fixed point P_0^* (B_0^*=0, F_0^*, G_0^*, I_0^*=0):

$$\frac{\partial B}{\partial t} = \frac{B^2 G}{1+I} - B + D_\mathrm{b}\nabla^2 B, \tag{4.1}$$

$$\frac{\partial F}{\partial t} = k_{\mathrm{f}1}\frac{G}{1+I} - k_{\mathrm{f}2}F, \tag{4.2}$$

$$\frac{\partial G}{\partial t} = -\frac{B^2 G}{1+I} + B - k_{\mathrm{f}1}\frac{G}{1+I} + k_{\mathrm{f}2}F + \nabla^2 G, \tag{4.3}$$

$$\frac{\partial I}{\partial t} = k_{\mathrm{i}1}B - k_{\mathrm{i}2}I + D_\mathrm{i}\nabla^2 I. \tag{4.4}$$

Two-dimensional simulations were carried out on an annulus domain with Dirichlet boundary conditions at the inner and outer ring, which were set to constant values at the domain edges of the fixed point P_0^*. The ratio between inner and outer diameter was chosen as one half, similar to spatial extensions in experimental data. A time increment of about 10^{-4} was chosen as a step width in integration.

The dynamics of wavefronts (in the $B+F$-field) within the bistable regime are investigated on an annulus domain and compared with experimental data of CDRs to examine, if coherently propagating wavefronts on an annulus domain also occur after perturbations in a bistable regime of a system, similar to waves in an excitable regime (see Chapter 5). Furthermore, the role of the total amount of actin is investigated through performing simulations under variation of the the total amount of actin A (see Chapter 6).

The dynamics of these wavefronts are also visualized by circular kymographs for a systematic comparison of signatures in kymographs between experiments and simulations and they also allow a velocity measurement to identify the mechanism underlying CDRs and its molecular nature. The other model parameters (see Eq. 4.1 - 4.4) are given at the relevant text passages in the following chapters.

5 CDR Dynamics in Disk-Shaped Fibroblasts

CDRs were first observed and characterized by Mellström et al. after stimulation with the growth factor PDGF [Mellström et al., 1988]. Subsequently, they have been typically investigated in randomly shaped cells after an extensive stimulation with growth factors. After Bernitt et al. noted the impact of cellular boundaries on CDR formation and propagation, they investigated CDR dynamics in disk-shaped fibroblasts attached to microcontact printed substrates of fibronectin so that no further addition of growth factors like PDGF was necessary [Bernitt et al., 2015]. This system enables comparable cell morphologies and reproducible conditions, and furthermore allows a systematic analysis of CDRs that propagate around a centred nucleus on a one dimensional trajectoy confined between nucleus and cell boundary. For that reason, it provides an appropriate standard system for a detailed interesting study of CDR formation and propagation under physiological (Chapter 5) and changed biochemical conditions (Chapter 6, 7 and 8) to examine the mechanism underlying CDR dynamics.

This chapter focuses on the fascinating dynamics of CDRs in disk-shaped fibroblasts of the cell line NIH 3T3 WT (referred to as fibroblasts or cells) attached on fibronectin patches under physiological conditions. There are questions to answer concerning what factors may influence CDR velocities or CDR lifetimes, and how interactions between concurrently occuring CDRs influence each other and their velocities and lifetimes. In this regard, the role of actin itself or mechanical factors which may regulate CDR dynamics are discussed. Therefore, at the beginning the system of disk-shaped fibroblasts is introduced and the influence of boundary conditions and growth factors on the formation and propagation of CDRs is depicted (see Section 5.1). It is followed by a quantitative analysis of characteristic parameters like CDR velocities, periodicities as well as lifetimes and traveling distances in different fibroblasts in a comparable and reproducible manner (see Section 5.2, 5.3 & 5.4).

Furthermore, the overall objective of this study is to understand the wave machinery underlying CDR formation. Earlier studies of actin waves in fibroblasts, neutrophiles or *Dictyostelium* mainly focused on the concept of excitability [Vicker, 2000, Weiner et al., 2007, Whitelam et al., 2009, Gerhardt et al., 2014, Bernitt et al., 2015, Bernitt and Döbereiner, 2017] leading to propagating waves with similar features like actin waves in experimental systems. However, Beta as well as Bernitt et al. proposed models of bistable systems for propagating actin waves in *Dictyostelium* or fibroblasts [Beta,

2010, Bernitt et al., 2017.

In order to understand the wave machinery underlying CDR formation, the question arises whether CDRs can be understood as fronts in a system within a bistable regime. For that reason, numerical simulations of a theoretical system within a bistable regime are run on an annulus domain to investigate whether this system can generate coherent propagating wavefronts. So far, these coherent propagating pulses, similar to CDRs in the experimental system (see Section 5.5), are only known from excitable regimes.

5.1 Influences of boundary conditions and growth factors on CDR formation and propagation

In this study, CDR formation and propagation are investigated in disk-shaped fibroblasts. Therefore, fibronectin patches with radii of 31 µm were stamped on glass coverslips, on which fibroblasts were attached and adapted to this geometry very well. This led to comparable morphologies and boundary conditions in different fibroblasts. CDRs were formed in fibroblasts on fibronectin patches spontaneously without further addition of growth factors, for example PDGF. It is possible that they were stimulated by a small amount of growth factors contained in FBS, a common supplement in cell cultivation Bernitt et al., 2015.

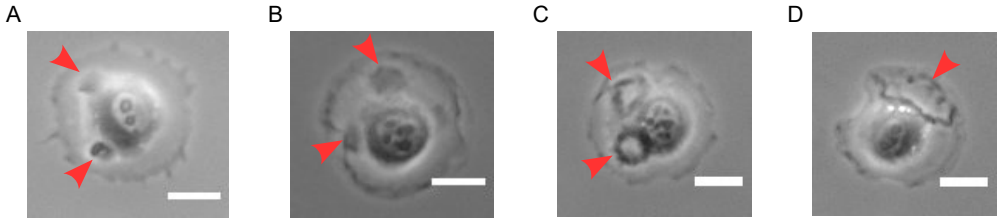

Figure 5.1: Different forms and sizes of CDRs in disk-shaped fibroblasts. CDR were formed under the same conditions either as small dots (A), wave pulses (B) or rings of different sizes (C & D). Scale bars: 20 µm.

Comparing CDRs formed in different disk-shaped fibroblasts under physiological conditions, differences in CDR sizes and shapes were observed (Fig. 5.1), but so far it is not clear why such a wide variability exists and what factors may influence the formation of CDRs. CDRs appeared, for example, as small dots or smaller wave pulses with no apparent ring-structures (Fig. 5.1 A & B) as usually observed, but this is also due to a small resolution of the 10x objective (numerical aperture of 0.25) that was deliberately chosen to observe dynamics of a number of simultaneous CDRs in fibroblasts and for long term experiments due to avoid focus drift. Moreover, also ring-shaped CDRs

in different sizes were observed (Fig. 5.1 C & D). The different CDRs were either formed from local points (Fig. 5.2 a1) or appeared already as an initial faint larger ring (Fig. 5.2 a2). This is similar to different kinds of CDR formation in randomly spread fibroblasts. In fibroblasts of random shapes attached on glass coverslips covered with fibronectin without further addition of growth factors, CDRs emerged usually from local points (Fig. 5.2 b1). In contrast, in fibroblasts that directly spread on glass coverslips and were stimulated with PDGF ($30\,\mathrm{ng\,ml^{-1}}$) causing the stimulation of a large area, a few minutes after PDGF stimulation an already very large but initially faint ring appeared (Fig. 5.2 b2) [Bernitt et al., 2015]. Due to this comparison of different kinds of stimulation underlying CDRs in random shaped fibroblasts, it is concluded that different forms and sizes of CDRs in disk-shaped fibroblasts, among other things, were also affected by different amounts and distributions of growth factors in FBS because fibronectin substrates are suspected to act as a reservoir for growth factors [Azimifar et al., 2012].

Moreover, comparing the dynamics of CDRs in random shaped fibroblasts without additional PDGF stimulation directly after their initial appearence they usually expanded, reversed at the cellular boundaries and collapsed at one point (Fig. 5.2 b1). Fibroblasts after PDGF stimulation directly exhibited CDRs as large rings that also shrunk after colliding at the cellular boundaries and collapsed in one point (Fig. 5.2 b2). This behavior was also found in disk-shaped fibroblasts (Fig. 5.2 A). However, it was more often observed that after CDRs were formed from a local point and expanded, they usually propagated on a circular trajectory between cell boundary and nucleus. These CDR dynamics can be visualized by using circular kymographs, space-time plots, in which image intensities along a circle around the nucleus are plotted as a function of space and time (Fig 5.3 A & B). This enables a good comparison between CDR dynamics in different disk-shaped fibroblasts. A propagation of the same CDR over minutes is shown by line signatures ("/" or "\"), whereas a stationary CDR, which appeared briefly and disappeared rapidly without propagating, is visualized by a dot-like signature. Due to these different kinds of dynamics, kymograph patterns can be subdivided into dotted (Fig. 5.3 C), fragmented (Fig. 5.3 D) and linear patterns (Fig. 5.3 B). The kind of pattern was hypothesized to be caused by an interplay between CDR collision events, stochastic CDR formation and recovery time of an excitable medium [Bernitt, 2015]. In contrast, the molecular nature underlying CDR dynamics resulting in different kymograph patterns was not investigated in detail. Therefore, this study focused on the role of three different macromolecules, actin, PIP_3 and N-WASP, in CDR dynamics (see Chapter 6, 7 & 8).

So far it is not clear why CDRs in disk-shaped fibroblasts often propagate over minutes in contrast to CDRs in random shaped cells. In random shaped fibroblasts, CDRs have the space for their formation and radial growth until they collide with cellular boundaries and collapse. In contrast, in disk-shaped fibroblasts, there is less space

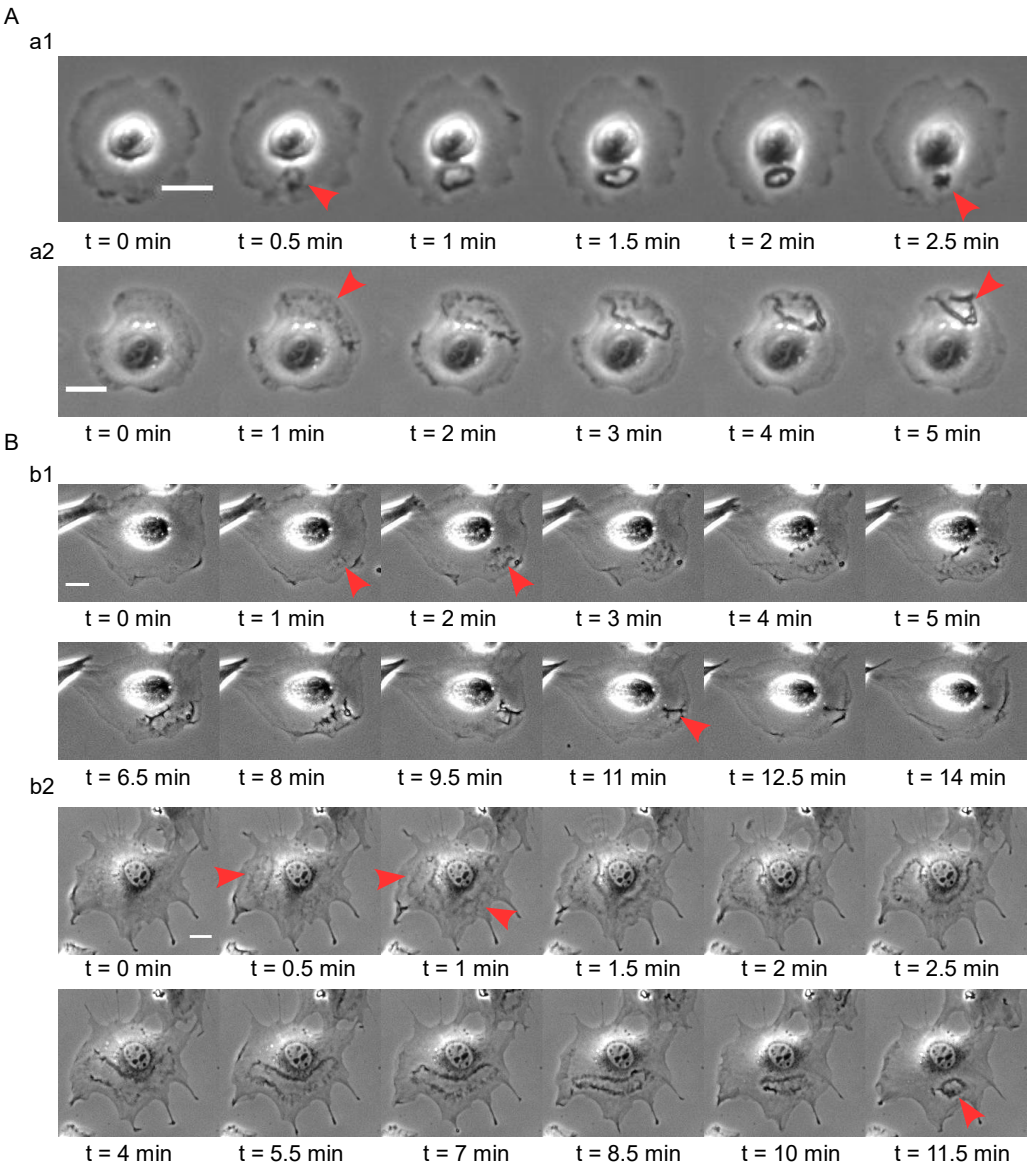

Figure 5.2: CDR formation in randomly spread and disk-shaped fibroblasts. A shows time-lapse sequences of micrographs of two different disk-shaped fibroblasts in which CDRs are formed either from one point (a1) or as a large faint ring (a2). B demonstrates time-lapse sequences of micrographs of CDR formation in a fibroblast on a fibronectin coated glass coverslip (b1) as well as in a fibroblasts attached on a glass coverslip stimulated with PDGF (b2). Red arrows highlight CDR formation and closure. Scale bars are $20\,\mu\mathrm{m}$.

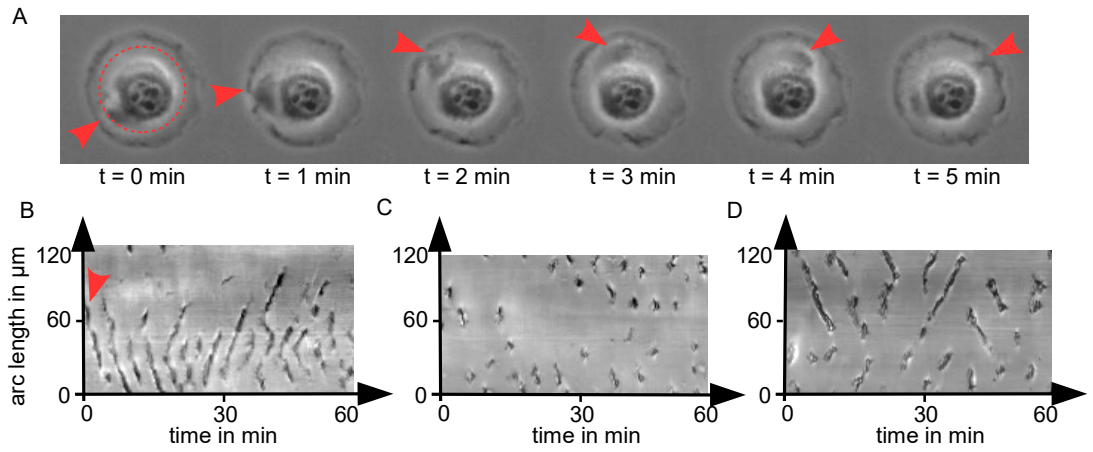

Figure 5.3: CDR propagation in disk-shaped fibroblasts. Time-lapse sequence of micrographs visualizes CDR propagation along a circle around a centred nucleus (A). Kymograph with specific patterns (B, C & D) visualize CDR dynamics along a circle around the nucleus. The red arrow in kymograph B indicates the first line that corresponds to the CDR propagation shown in A. Scale bars are 20 µm.

between cell boundary and nucleus, with which CDRs often collide shortly after their appearence. In many cases, this was followed by a splitting of CDRs into two twin-pulses through the round nucleus, see Fig. 5.4 A. After splitting, the twin pulses were only able to propagate in the opposite lateral direction that is visualized in kymograph patterns as a "<"-signature. However, the lifetimes and traveling distances of twin-pulses were usually not equal. In individual cases, both CDRs were able to travel undisturbed half around the nucleus, collided and annihilated each other (">"-signature in kymograph), but more often, CDRs did not collide but rather seemed to disappear, at first sight, spontaneously. This phenomenon is further analyzed in detail in Section 5.3. This leads to three different cases of propagating twin pulses after splitting. First, both twin pulses propagate around the nucleus nearly the same time (Fig. 5.4 b1), second, one of the two twin pulses travels much shorter than the other (Fig. 5.4 b2), or, third, the second twin pulse disappears directly after splitting and is nearly invisible (Fig. 5.4 b3), whereas the other twin pulse propagates further.

The splitting into two coherently propagating twin-pulses due to these boundary conditions is an interesting signature of this system. To uncover the mechanisms underlying the CDR machinery, it raises the question, if a bistable regime of a system can constitute such propagating ring-like wavefronts. That is, to date, only known from excitable regimes, like in an excitable regime within the FitzHugh-Nagumo system [Bernitt and Döbereiner, 2017]. This is investigated in detail in Section 5.5.

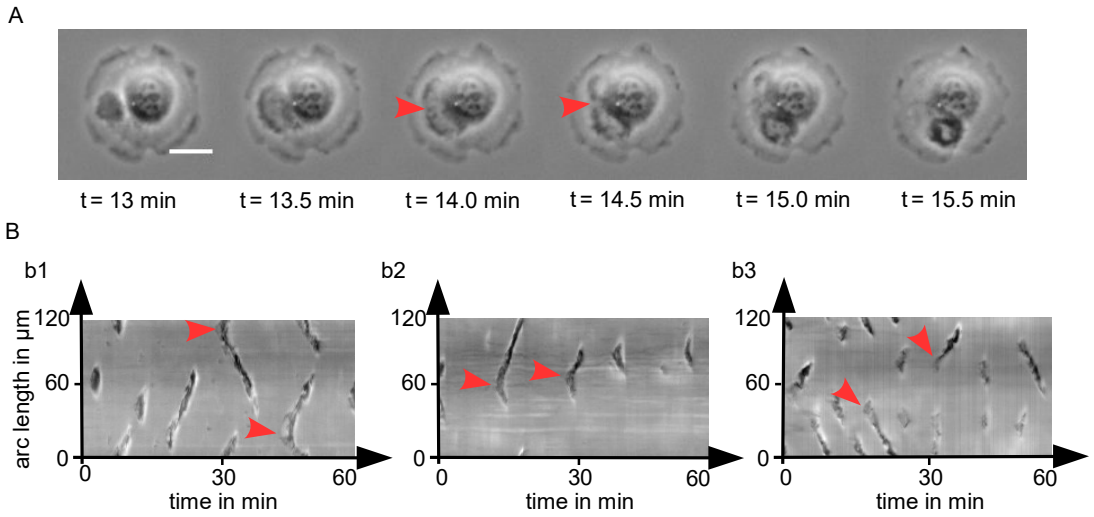

Figure 5.4: Splitting of CDRs. Example of a CDR that is split upon collision with the nucleus (A). Kymographs of B visualize CDR splitting with a "<"-signature. In b1 both twin pulses propagate around the nucleus after splitting in opposite directions. In b2 and b3 only one of two twin pulses travel, whereas the other twin pulse either disappeared a little later or directly after splitting. The splittings are indicated by red arrowheads. The scale bar is 20 µm.

5.2 Capturing CDR dynamics in disk-shaped fibroblasts

Kymograph patterns demonstrate the diversity of CDR formation and propagation and provide characteristic parameters to capture CDR dynamics, like CDR velocities and periodicites [Bernitt et al., 2015] as well as lifetimes and traveling distances. They play a fundamental role in this work not merely to characterize CDR dynamics but also to investigate CDR dynamics and their interactions in single cells (see Section 5.3 & 5.4). Additionally they aide in identifying the underlying wave machinery as well as examining the influence of actin, PIP3 or N-WASP on CDR formation and dynamics (see Chapter 6, 7 & 8).

In this section, CDR dynamics in disk-shaped fibroblasts observed over 60 minutes under physiological conditons are analyzed. Lines in kymograph patterns visualize CDR propagation with constant velocities, which can be measured from the slope of the line (see Fig. 5.5 a1), whereas CDR periodicities are time periodes between two successive CDRs occuring at the same position (see Fig. 5.5 a2). Averaged CDR velocties and periodicities in single fibroblasts were calculated via autocorrelation functions and Radon transforms of binarized kymographs. Averaged CDR velocities of 53 different fibroblasts are distributed between $0.10\,\mu m\,s^{-1}$ and $0.22\,\mu m\,s^{-1}$ with a mean CDR velocity ($\pm$ SE) of $0.14 \pm 0.01\,\mu m\,s^{-1}$ (see Fig. 5.5 b1). This is in line with observations by Bernitt,

who measured a mean CDR velocity of $0.14\,\mu m\,s^{-1}$ in disk-shaped fibroblasts, that was also similar to observations in random shaped fibroblasts [Bernitt, 2015]. Moreover, he found a correlation between CDR velocities and the kind of kymograph patterns. The reasons for this observation as well as the factors influencing CDR velocities are still under debate. This is investigated in detail in this study in the following sections and chapters.

In the context of actin waves, the measured CDR velocities in disk-shaped fibroblasts are also in the range of propagation velocities of Hem-1 waves in neutrophiles and actin waves in *Dictyostelium* [Weiner et al., 2007, Bretschneider et al., 2009, Gerisch et al., 2012, Gerhardt et al., 2014]. This leads to the hypothesis that different kinds of actin waves in various cell types can be traced back to a similar underlying wave machinery even if their molecular nature differs.

Furthermore, the averaged CDR periodicites of 41 fibroblasts range from 3.3 min to 9.1 min and the mean value of averaged CDR periodicities (± SE) amounts 6.1 ± 0.2 min (see Fig. 5.5 b2). This is also similar to characteristic periodicites in the range of 5 min to 7 min measured by Bernitt et al. [Bernitt, 2015]. In this regard, the question arises what factors regulate or affect CDR periodicities and therefore the formation of these spatiotemporal patterns. In the context of an excitable system, Bernitt et al. assumed an interplay between stochastic excitations due to a noisy environment and the following refractory period of the excitable system [Bernitt and Döbereiner, 2017] similar to Gerhardt et al. [Gerhardt et al., 2014]. However, also a system in a bistable regime is expected to exhibit a refractory period directly after transition from one to another fixed point. In combination with a reappering stimulation it may also cause a periodic reappearence of wavefronts similar to a system in an excitable regime.

Moreover, there are other parameters to capture CDR dynamics, which do not seem to be of particular interest at first sight, but but are indeed important to complete the whole picture of CDR dynamics and play an important role in this work. These characteristic parameters are lifetimes and traveling distances of CDRs, ,which have never been previously investigated in detail. In this study, the period of time between the emergence and disappearence of the same CDR is referred to as CDR lifetime (see Fig. 5.6 a1), whereas the spatial distance a CDR propagates around the nucleus during its lifetime is named CDR traveling distance s (see Fig. 5.6 a2), a composite measured quantity of CDR velocity v and lifetime λ calculated by

$$s = \lambda \cdot v. \tag{5.1}$$

Comparing averaged CDR lifetimes between 47 different fibroblasts ranging from 1.6 min to 6.5 min, a mean CDR lifetime (± SE) of 3.4 ± 0.2 min was found (see Fig. 5.6 b1). The averaged traveling distance in 43 different fibroblasts range from 13 µm to 58 µm with a mean traveling length of 28 ± 1 µm (see Fig. 5.6 b2). The factors leading to the

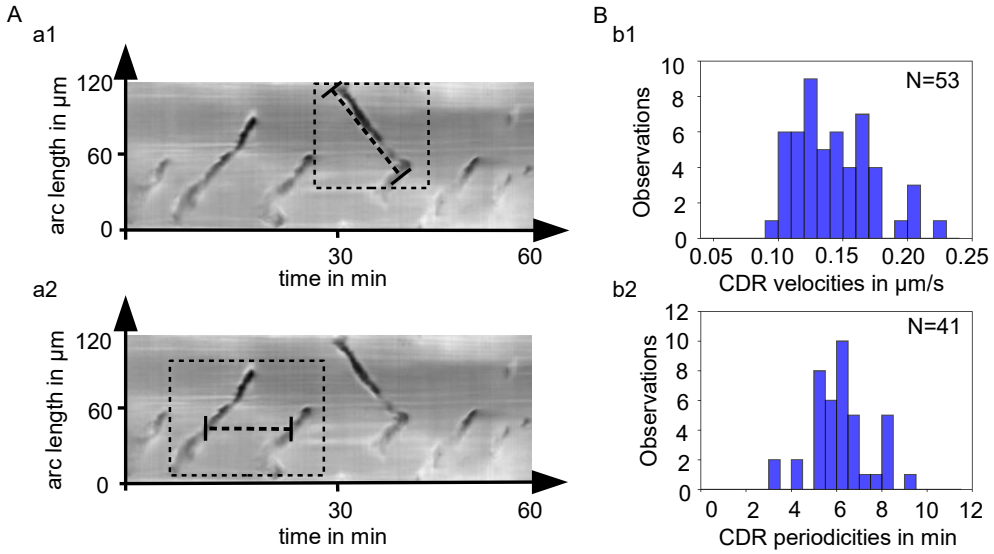

Figure 5.5: Mean CDR velocities and periodicities. In A are examples of kymographs visualizing propagating CDRs from which CDR velocities (a1) and periodicies (a2) were calculated. B show distributions of averaged CDR velocities (b1) from 53 fibroblasts and periodicities from 41 fibroblasts (b2).

differences in CDR lifetimes and traveling distances between different fibroblasts may be interactions between several CDRs within one fibroblast (see Section 5.3) as well as different molecular compositions in different fibroblasts. In this context, Zeng et al. discovered that an increase in substrate stiffness led to an increase in CDR lifetimes. This was ascribed to the antagonistic relationship between the small GTPases Rac and Rho regulating the formation of CDRs and stress fibers [Zeng et al., 2011].

5.3 Long-range interactions between CDRs restrict CDR lifetimes

In the previous section, CDR dynamics of different fibroblasts were analyzed quantitatively and distributions of characteristic parameters like averaged CDR lifetimes were presented. This distribution captures differences in CDR lifetimes between different fibroblasts but it does not provide informations about the distributions of single CDR lifetimes in individual fibroblasts. Hence, in the following, the lifetimes of single CDRs are investigated in more detail and the influence of CDR interactions on their lifetimes is examined.

Four selected examples of CDR dynamics within several fibroblasts are shown in form of kymographs in Fig. 5.7 A with corresponding distributions of CDR lifetimes in

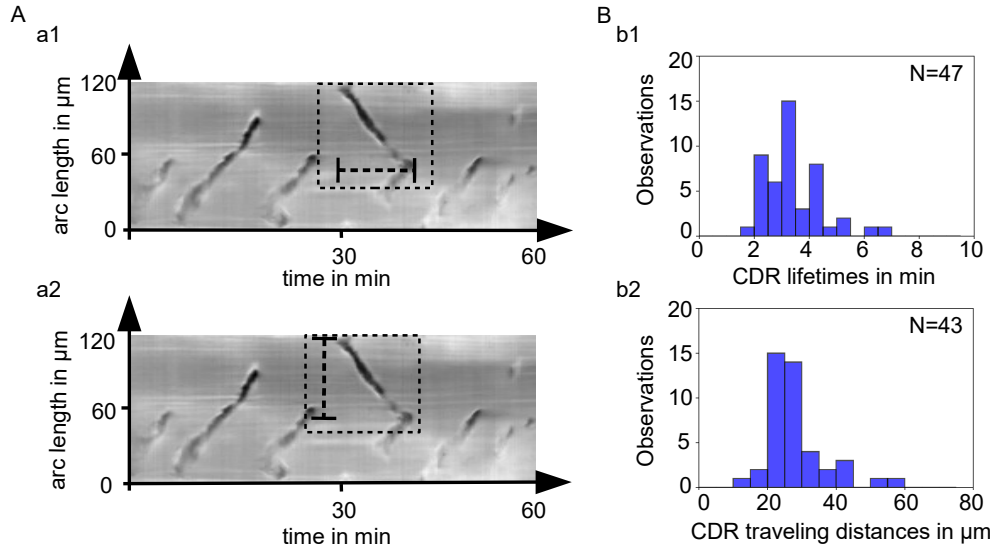

Figure 5.6: Mean CDR lifetimes and traveling lengths. In A are examples of kymographs from which CDR lifetimes (a1) and traveling lengths (a2) were calculated. B shows distributions of averaged CDR lifetimes (b1) from 47 fibroblasts and traveling lengths from 43 fibroblasts (b2).

Fig. 5.7 B. The different cells exhibit different distributions of CDR lifetimes resulting in distinct mean values (± SE) of 3.9 ± 0.3 min (b1), 3.1 ± 0.4 min (b2), 3.2 ± 0.4 min (b3) and 4.2 ± 0.5 min (b4). In most cases, lifetimes are limited between 2 min and 6 min, but there are also individual CDRs propagating over a longer time interval up to 12 min. Additionally, some CDRs only appear for up to one minute without propagating. This is also reflected by the distribution of single lifetimes of 132 CDRs within 20 fibroblasts (Fig. 5.8 A).

This raises the question of which factors restrict CDR lifetimes and thus cause their distributions within single cells. Bernitt and Döbereiner propose a model of the probability distribution of CDR occupational states within fibroblasts, which were suggested to be proportional to the distribution of CDR lifetimes [Bernitt and Döbereiner, 2017]. This model is mainly based on the assumption that the restriction of CDR lifetimes is due to annihilation of colliding CDRs. This leads to shorter CDR lifetimes when multiple CDRs propagate at the same time. Comparing the proposition of Bernitt and Döbereiner with experimental data of CDR lifetimes in this study subdivided into different occupational states, no correlation between CDR lifetimes and the number of concurrently occuring CDRs were found (demonstrated in Fig. 5.8 B). However, the model seems to predict an upper limit of CDR lifetimes but neglect other important factors influencing CDR lifetimes, which have yet to be uncovered.

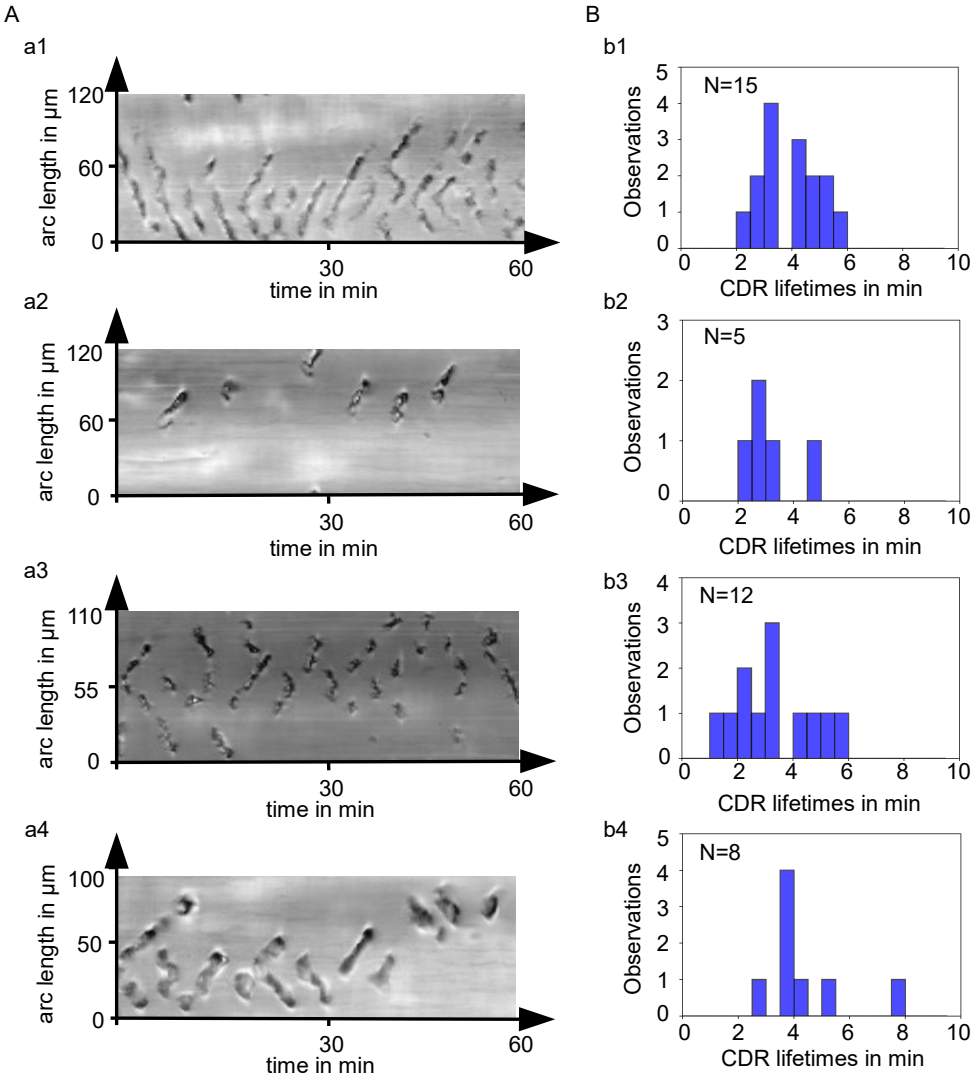

Figure 5.7: Distributions of CDR lifetimes in single fibroblasts. A presents examples of kymographs visualizing CDR dynamics in four different cells. B shows distributions of CDR lifetimes from the corresponding fibroblast out of A.

In many cases, there is a spontaneous disappearence of CDRs without direct interaction and annihilation of CDRs. However, there are CDR interactions which are not obvious at first sight. It was observed that often emerging CDRs have an influence on already existing and propagating CDRs causing a stop of their propagation and leading to a disappearence from the moment in which the other CDR appears (see Fig. 5.9 A). This leads to the conclusion, that CDR lifetimes may be restricted by a limiting species, for example the total actin concentration or mechanical factors like the membrane tension.

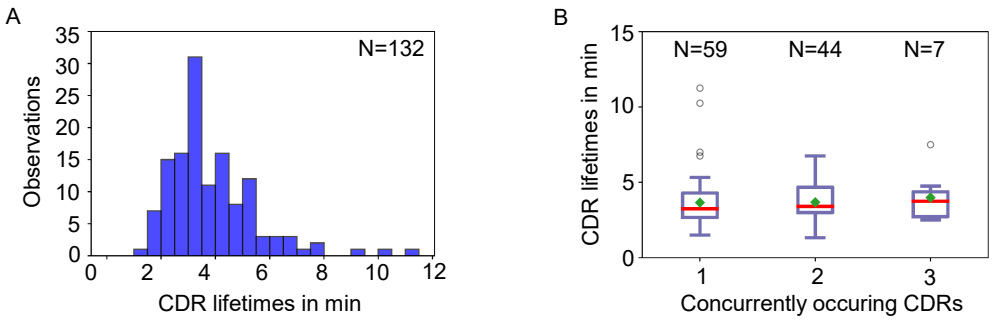

Figure 5.8: Dependence of CDR lifetime on concurrent occuring CDRs. A shows distribution of lifetimes of 132 single CDRs. The boxplot in B presents the dependence of CDR lifetimes on the number of concurrent occuring CDRs.

Considering the actin monomer diffusion within two dimensions due to the small height of the lamellipodium in the range of 200 nm, with a diffusion constant of 3 µm^2 s^{-1} - 30 µm^2 s^{-1} [Kiuchi et al., 2011] actin monomers are able to diffuse within a radius of 13 µm-42 µm in a time interval of 15 s complying with the temporal resolution of the image data. This means, that on the time scale of actin monomer diffusion, a reduction of available actin in a radius of 42 µm around the newly initiated CDR is possible. This may lead to a disappearence of the second CDR. However, the volume of one CDR with an assumed cylindric form with a diameter of 6 µm and a ring width of 2 µm in disk shaped fibroblasts, as well as an estimated height of 1 µm (1 µm-3 µm in random shaped cells [Bernitt, 2015]) is calculated to be 25 µm^3. This is very small compared to the cell size of estimated 3000 µm^3, in which various other actin-dependent processes still take place. In this regard, it seems to be more likely that the observed long-ranged CDR interactions are governed by the membrane tension instead of the actin concentration.

Furthermore, a potential influence of the membrane tension or the total amount of actin on CDR lifetimes is also enhanced by observations from examples of kymographs, in which two or more simultaneously propagating CDRs have a brighter signature when appearing at the same time as CDRs which travel alone around the cell nucleus (see Fig. 5.9 B). The brighter signature in phase contrast images might be related to a reduced height of CDRs, which is believed to be governed by the membrane tension.

Moreover, alongside molecular or mechanical restrictions of CDR lifetimes due to their long-range interactions, there are more factors regulating CDR lifetimes which must be taken into account. They include stochastic processes of CDR stimulation constituting a CDR periodicity [Bernitt, 2015]. The periodicity seems to generate an upper limit of CDR lifetimes due to the restriction of a distinct number of concurrently occuring CDRs. Furthermore, another important factor seems to be spatial inhomogenities, for example in protein densitites or stress fiber formation [Zeng et al., 2011]. This

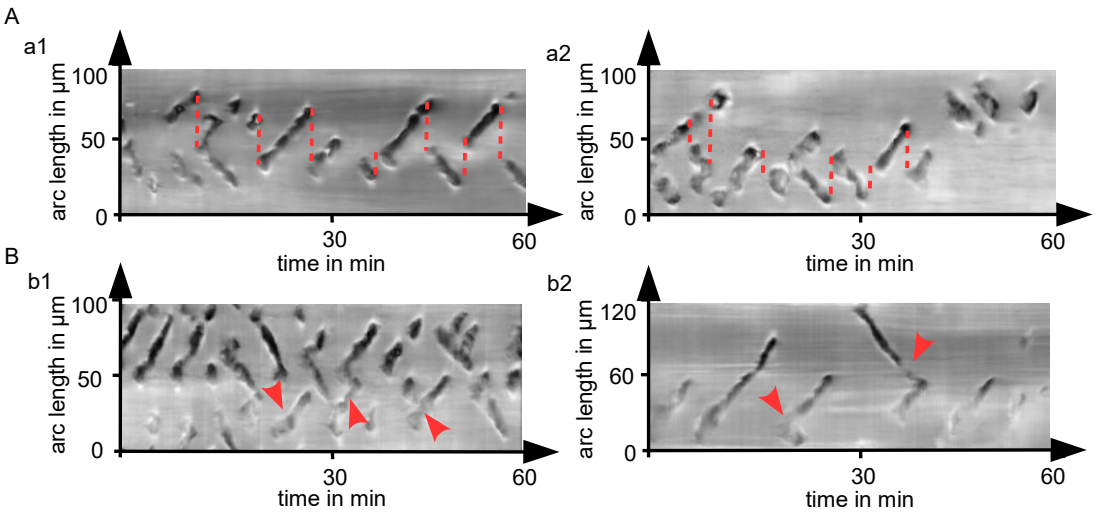

Figure 5.9: Interactions between single CDRs. Four examples of kymographs visualize the possible interactions of concurrent occuring CDRs. The dashed lines in A highlight disappearence of CDRs at the same time points at which other CDRs emerge at different places. Arrowheads in B indicate a brighter signature of propagating CDRs.

was derived from observations from kymograph patterns exhibiting formation of CDRs frequently in the same areas and, vice versa, rarely in other distinct regions (see Fig. 5.7 A).

5.4 CDR velocities and traveling distances are functions of the number of concurrently occuring CDRs

Following an analysis of characteristic distributions of averaged CDR velocities and periodicities (Section 5.2) and an investigation of CDR interactions and their lifetimes (Section 5.3), in this section CDR velocities of individual CDRs are analyzed to go into more detail and examine which factors may influence these velocities and thus the dynamics of CDRs. First, it is interesting to analyze individual CDRs within single fibroblasts to test whether the averaged velocities (Section 5.2) originated from constant velocities or from a velocity distribution within one cell, which may vary from cell to cell. Velocities of single CDRs were calculated for the appropriate time interval using the same routines as described above via autocorrelation functions to get comparable measurement values. Fig. 5.10 presents characteristic examples of CDR dynamics within four different fibroblasts in form of kymograph patterns (a1-a4) and their corresponding velocity distributions (b1-b4). This figure very nicely demonstrates that every fibroblast has its own characteristic CDR velocity distribution varying from cell to cell like its

corresponding kymograph pattern. It leads to different mean values (± SE) of CDR velocities of $0.15 \pm 0.01\,\mu m\,s^{-1}$ (b1), $0.19 \pm 0.01\,\mu m\,s^{-1}$ (b2), $0.14 \pm 0.01\,\mu m\,s^{-1}$ (b3) and $0.10 \pm 0.01\,\mu m\,s^{-1}$ (b4). Interestingly, one can identify two parts of the velocity distributions in which they are split up and seperated by a gap in between which no measured velocities exist. (see Fig. 5.10 b1-b4).

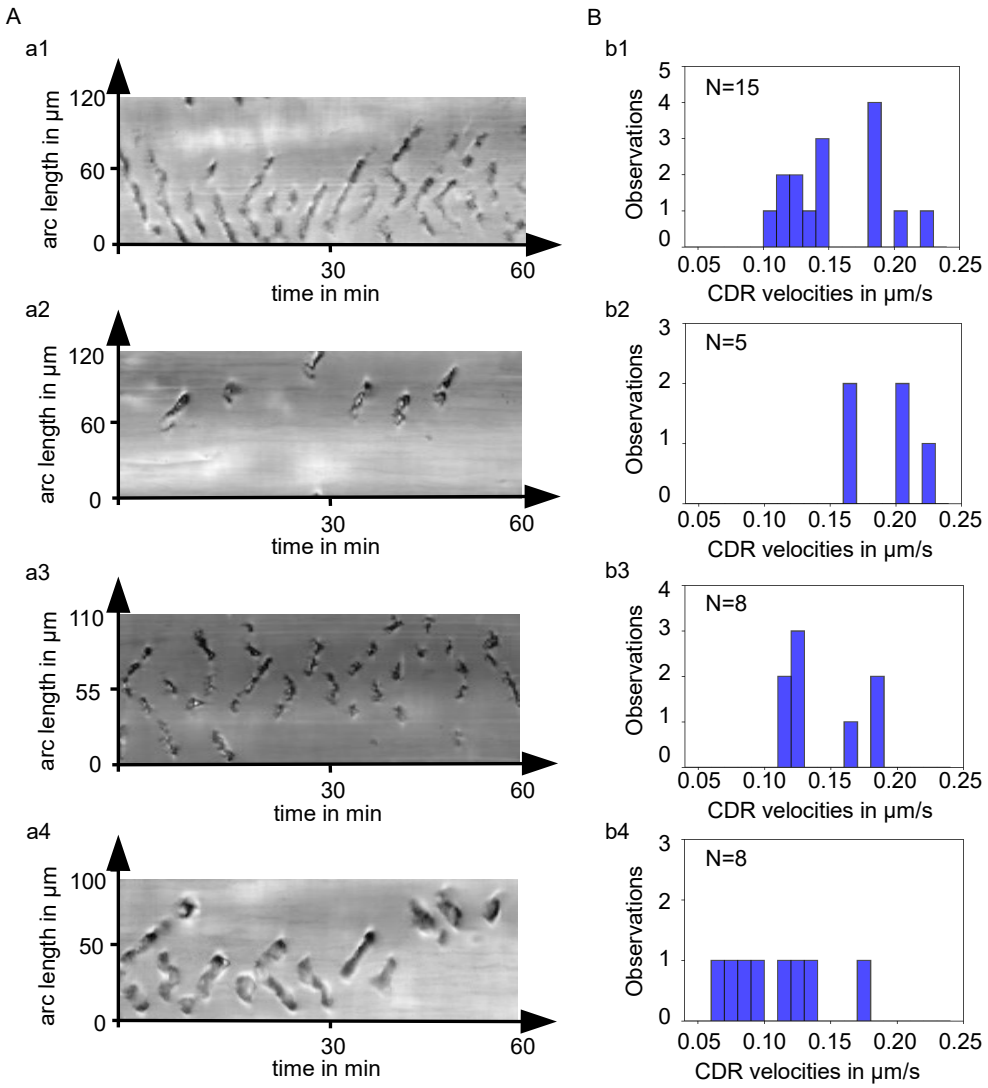

Figure 5.10: Velocity distribution of CDRs in single fibroblasts. A presents examples of kymographs visualizing CDR dynamics in four different cells. B shows velocity distributions of CDRs from the corresponding fibroblast out of A.

In order to gain a better understanding of factors influencing CDR velocities and

provoking the characteristic distributions (Fig. 5.10 b1-b4), the dependence of the number of simultaneously occuring CDRs on their velocities was analyzed. This was inspired by changes observed in CDR velocities from the moment at which a second CDR appears or disappears (see Fig. 5.11 A). In the case of a second emerging CDR (green unfilled arrowheads), the velocity of the other CDR decreased from that moment (green filled arrowheads). In the opposite case of a disappearing second CDR (yellow unfilled arrowheads), the velocity of the still existing CDR increased (yellow filled arrowheads). In regard to these interactions CDR velocities of 125 CDRs from 20 fibroblasts were calculated (see 5.11 B). The dependence of the CDR velocity on the number of simultaneously occuring CDRs is shown in Fig. 5.11 C. It demonstrates a clear correlation between CDR velocities and the number of CDRs propagating at the same time. The mean values differ between $0.17 \pm 0.01\,\mu m\,s^{-1}$ (for one CDR), $0.12 \pm 0.01\,\mu m\,s^{-1}$ (for two CDRs) and $0.09 \pm 0.01\,\mu m\,s^{-1}$ (for three CDRs). This explains in most cases the splitting of the characteristic distributions of CDR velocities into two parts (Fig. 5.10 B, with the exception of b2), because most of the time, one or two CDRs propagate at the same time having different velocities dependent on the number of concurrently propagating CDRs. Three simultaneously occuring CDRs constitute a minority in fibroblasts on fibronectin patches with radii of 31 µm (observed in Fig. 5.10 a4).

Furthermore, the traveling distance s around the nucleus of each single CDR was calculated with measured lifetimes λ and velocities v (see Eq. 5.1). Comparable to characteristic parameters of CDRs like lifetimes and velocities, each fibroblast has a characteristic distribution of CDR traveling distances with mean values (± SE), for example, of $36 \pm 4\,\mu m$ (b1), $34 \pm 3\,\mu m$ (b2), $30 \pm 4\,\mu m$ (b3) and $25 \pm 3\,\mu m$ (b4) (see Fig. 5.12). Calculating the traveling distances of 125 CDRs within 20 fibroblasts, they are distributed around a mean value (± SE) of $32 \pm 1\,\mu m$ and range from 8 µm up to 81 µm, where its upper limit nearly corresponds to one full rotation of the traveling CDR around the nucleus (see Fig. 5.13 A). Moreover, there is a clear correlation between the CDR traveling distance and the number of concurrently occuring CDRs (see Fig. 5.13 B). The more CDRs appear at the same time, the shorter they travel while exhibiting the same lifetimes. The mean values differ between $37 \pm 2\,\mu m$ (for one CDR), $25 \pm 1\,\mu m$ (for two CDRs) and $21 \pm 3\,\mu m$ (for three CDRs), that results from different upper limits of CDR traveling lengths ranges from 81 µm (for one CDR) to 32 µm (for three CDRs) while the lower limit is nearly identical in all three cases.

This leads to the conclusion, that CDR velocities and traveling distances around the nucleus are functions of the number of concurrently occuring CDRs. The more CDRs appear at the same time, the slower and shorter they propagate. This supports the hypothesis of a governing factor like membrane tension or a limiting factor like the total amount of actin as already discussed in the context of CDR interactions in Section 5.3. Moreover, in this regard, in the following chapters the influence of the different macromolecules actin (Chapter 6), PIP_3 (Chapter 7) and N-WASP (Chapter 8) on CDR

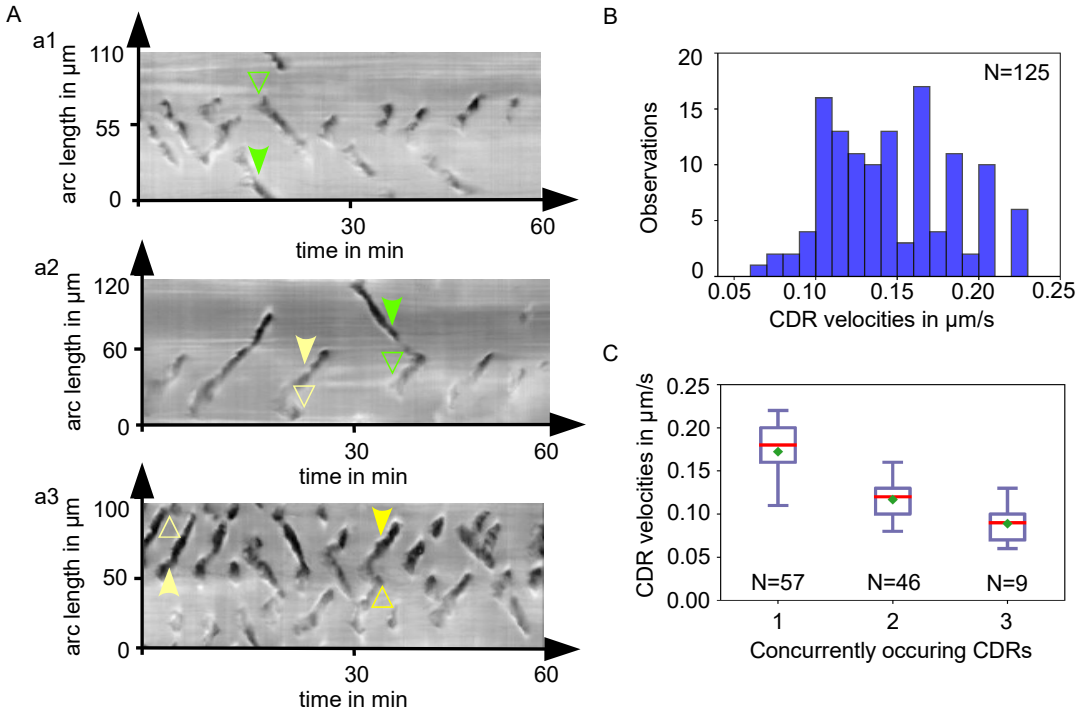

Figure 5.11: Velocities of CDRs. A presents three different kymographs visualizing the influence of emerging (unfilled green arrowheads) or disappearing (unfilled yellow arrowheads) CDRs on the velocities of previously or still existing CDRs (green and yellow filled arrowheads). B shows velocity distribution of 125 CDRs of 20 different fibroblasts. The boxplot in C represents the dependence of CDR velocities on the number of concurrent occuring CDRs.

dynamics in disk-shaped fibroblasts are investigated to further examine the mechanism underlying CDR formation and propagation.

5.5 Propagating wavefronts on an annulus domain in a bistable system

An essential question to study the wave mechanism underlying CDRs is whether within a bistable regime of a system coherently propgating wave pulses, similar to CDRs on disk-like fibronectin patches (see Section 5.1), can be generated. To date, this is only known from an excitable system as described by Bernitt and Döbereiner [Bernitt and Döbereiner, 2017]. Therefore, the theoretical model of Bernitt et al. [Bernitt et al., 2017] was utilized and numerical solutions within the bistable regime on an annulus domain were run comparable to the experimental system of disk-shaped fibroblasts with a centred nucleus. The ratio between inner and outer diameter was chosen as

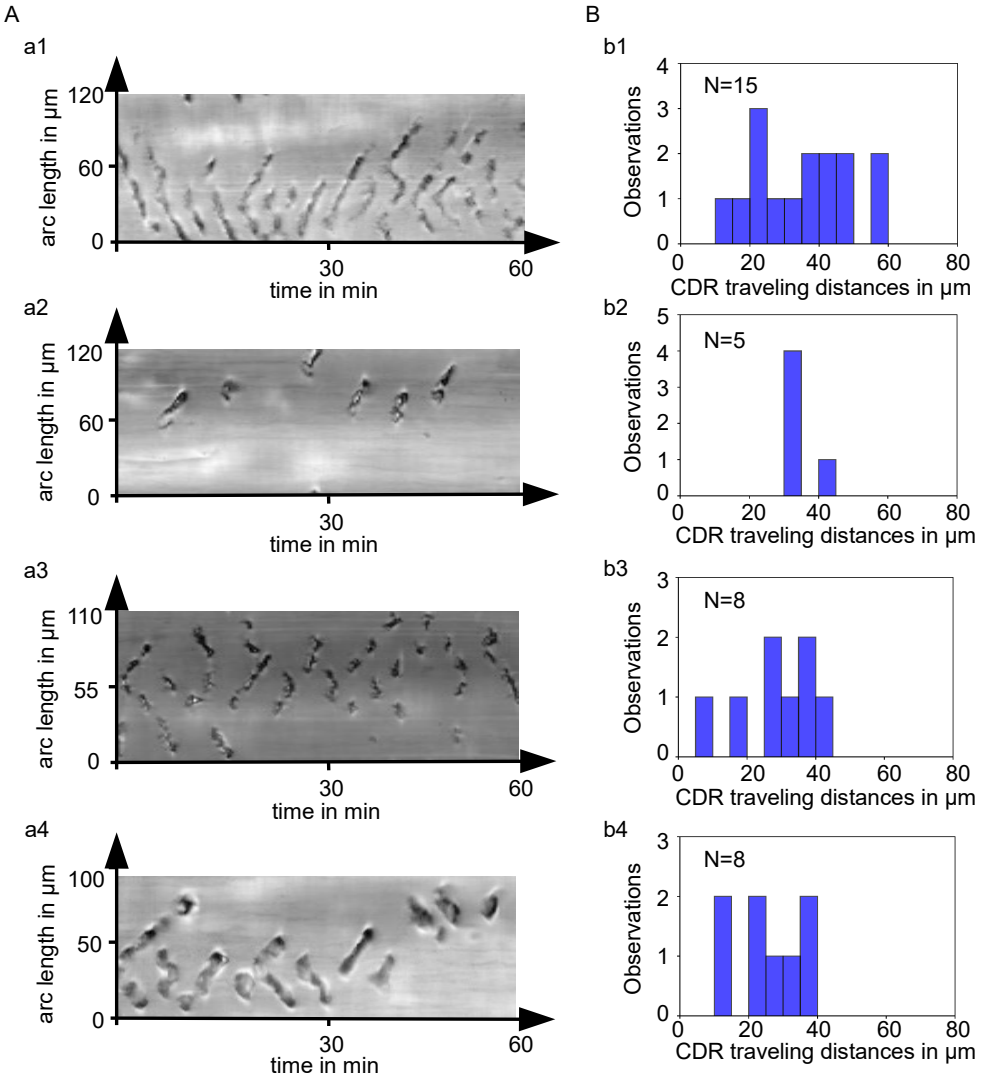

Figure 5.12: Distributions of CDR traveling distances in single fibroblasts. A presents examples of kymographs visualizing CDR dynamics in four different cells. Distributions of CDR traveling distances from the corresponding fibroblast out of A are presented in B.

one half corresponding to the experimental observations. After a local perturbation in the B-field, it was observed in the $B + F$-field, which corresponds to the experimental observable of filamenteous actin, a radially expanding ring from one local point with a depletion of filamenteous actin in the interior (see Fig. 5.14 a1 & a2). After interaction with the inner and outer boundary, the ring seemed to split into two twin-pulses with a half-moon shaped propagating front followed by a depletion zone of filamenteous actin

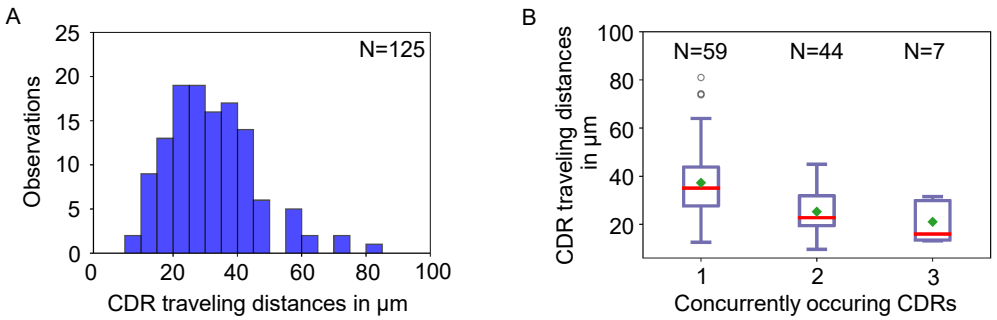

Figure 5.13: Dependence of CDR traveling distance on simultaneously occuring CDRs. A shows a distribution of traveling distances of 125 CDRs from 20 different fibroblasts. The boxplot in B represents the dependence of CDR traveling distance on the number of concurrent occuring CDRs.

and a second wavefront (see Fig. 5.14 a2-a4). After both twin-pulses traveled half around the nucleus, they collided and annihilated each other (see Fig. 5.14 a5). This behavior is comparable to experimental findings. In many cases a split of CDRs was observed, directly after their formation due to a collision with the cellular boundaries. This interaction with these certain boundary conditions seems to explain the traveling behavior of CDRs around the nucleus in contrast to their stationary open, reflection and closure behavior in randomly spread cells.

Moreover, the kymograph pattern (Fig. 5.14 B) also visualizes a lighter propagation front of high actin concentration followed by a darker depletion zone and a lighter second wavefront. This is in line with experimental observations by Bernitt, who recognized a depletion zone between two propagating fronts of CDRs in fibroblasts with visualized f-actin [Bernitt, 2015]. This signature strengthened the hypothesis that CDRs can be studied as wavefronts in a bistable regime of a system marked by different states of actin as proposed by Bernitt et al. [Bernitt et al., 2017]. Furthermore, it is also in line with Gerisch et al. inferring a bistable regime of two different actin states in *Dictyostelium* in which the transition from one to another is exhibited by a traveling wavefront [Gerisch et al., 2011].

Furthermore, the influence of multiple successive perturbations at the same location on an annulus domain was investigated. It was found, that a second perturbation after the disappearence of the first wavefront due to a collision of its two twin pulses, can stimulate a second wavefront (Fig. 5.15). This leads to the conclusion that this system is in the bistable regime which is also able to generate a periodic reappearence of wavefronts similar to excitable systems.

To examine the influence of higher numbers of concurrently occuring wavefronts, the

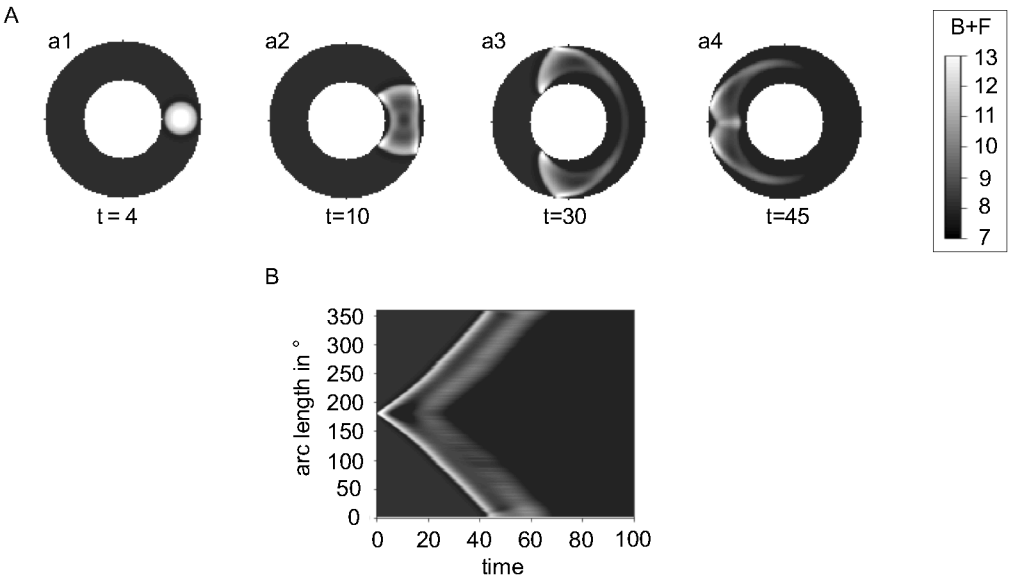

Figure 5.14: Propagating wavefronts on an annulus. Numerical solution of the bistable model on an annulus. The measured quantity is $B + F$, the CDR incorporated actin plus filamentous actin, comparable to observables in experimental data. A shows a time-lapse sequence of the propagating wavefront on an annulus domain, whereas B is kymograph, in which image intensities along a circle between inner and outer boundaries are plotted as a function of space and time. The parameters are D=0.12, k_{i1}=2.09, k_{i2}=0.53, k_{f1}=2.05, k_{f2}=1.19 and A=11.5.

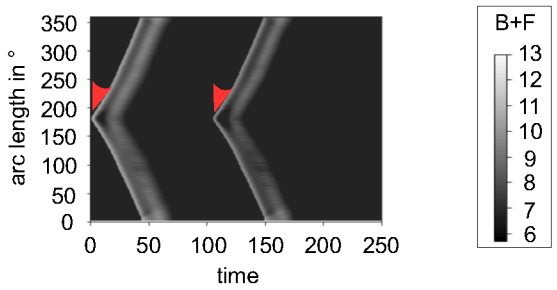

Figure 5.15: Successive wave stimulations on an annulus domain. The kymograph shows two successive perturbations in the B-field at the same location (red arrowheads), both lead to travelling wavefronts. Parameters are D=0.12, k_{f1}=2.05, k_{f2}=1.19, k_{i1}=2.09, k_{i2}=0.53 and A=11.5.

system was perturbated at two different positions in the B-field at the same time. Two ring-like wavefronts appeared at different positions and each split up into two twin pulses (see Fig. 5.16). Four twin pulses start traveling along a circular trajectory and annihilate after colliding with each other after a short time. The lifetimes of the

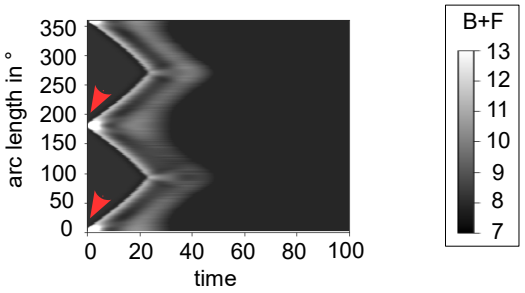

Figure 5.16: Simultanoeous stimulation on an annulus domain. Numerical solution of the bistable model on an annulus domain with two simultaneous stimulations (red arrowheads). The measured quantity is $B + F$, the CDR incorporated actin plus filamentous actin, comparable to observables in experimental data. The parameters are D=0.12, k_{i1}=2.09, k_{i2}=0.53, k_{f1}=2.05, k_{f2}=1.19 and A=11.5.

four twin pulses are shorter than in a case in which two pulses travel along a circular trajectory of the same length. These observations are in line with considerations by Bernitt et al., as described above, and lead to an upper limit of CDR lifetimes due to CDR collisions. Comparing the velocities of four concurrently occuring twin pulses (4.17° per unit time) with two simultaneously occuring twin pulses (3.83° per unit time), there are smaller propagation velocities the more wavefronts appear at the same time. This is in line with experimental observations, in which the propagation velocity depends on the number of concurrently occuring CDRs. In this regard, a limiting species, for example the total actin concentration, or a mechanical factor, like the membrane tension was taken into account to affect a decrease in CDR velocities with a rising number of CDRs that appear at the same time. However, the model does not provide information about mechanical factors, but the total amount of actin is incorporated as a main component. This leads to the conclusion, that similarities between the numerical and experimental results regarding the CDR velocities and their dependence on the number of concurrently occuring CDRs are provoked by the total amount of actin.

5.6 Summary

In this chapter, a detailed study of CDR formation and dynamics in disk-shaped fibroblasts under physiological conditions was presented in order to understand the mechanism underlying CDR propagation. In this regard, characteristic parameters like CDR velocities, periodicities, lifetimes and traveling distances were measured in various fibroblasts. Comparing the mean values of CDR velocities in different disk-shaped fibroblasts of $0.14\,\mu m\,s^{-1}$ with measured CDR velocities in disk-shaped fibroblasts and randomly shaped fibroblasts by Bernitt [Bernitt, 2015] as well as with other types of actin waves like Hem-1 waves in neutrophiles [Weiner et al., 2007] and actin waves in

Dictyostelium [Weiner et al., 2007, Gerisch et al., 2012, Gerhardt et al., 2014], propagation velocities in the same range were found. So far, it is not clear whether different types of actin waves in various cell types are constituted from a similar wave machinery but velocities in the same range could point to a similar wave machinery.

An important question for identfying the wave machinery underlying CDRs is which factors influence the characteristic parameters like velocities, lifetimes or traveling distances. Therefore, intracellular distributions of these parameters were analyzed and correlations between CDR velocities and the number of concurrently occuring CDRs were detected as well as between CDR traveling distances and the number of concurrently occuring CDRs. A decrease in CDR velocities and traveling distances with a rising number of concurrent occuring CDRs was exhibited. This leads to the conclusion that a governing factor such as the membrane tension or a limiting species like the total actin concentration has an important influence on the CDR velocities as well as the CDR traveling distances. To uncover the influencing factor, the role of the total amount of actin will be examined in detail in the next chapter (see Chapter 6).

Interestingly, in contrast to CDR velocities and traveling distances, it was demonstrated that CDR lifetimes do not correlate with the number of concurrently occuring CDRs, nevertheless, they seem to interact over long distances. For that reason, an upper limit of CDR lifetimes seems to be generated by an underlying stochastic process of CDR stimulation that leads to an apparent periodicity. Moreover, it is conjectured that CDR lifetimes are affected by spatial inhomogeneities for example in protein densities or stress fiber formation. This is in accordance with observations by Zeng et al. who demonstrated a correlation between increasing CDR lifetimes and increasing substrate stiffness [Zeng et al., 2011].

In contrast to studies by Zeng et al. proposing CDRs as waves in excitable media [Zeng et al., 2011], this study focuses on the examination of CDRs as wavefronts in a bistable regime of a system. It was investigated, whether a bistable regime of a system is also able to generate coherently propagating wave pulses. Therefore, numerical solutions of the bistable regime within the system of Bernitt et al. [Bernitt et al., 2017] on an annulus domain were run. It was found that after stimulation growing ring-like wavefronts arise with different actin concentrations between interior and exterior. After interactions at the domain boundaries, two twin pulses arise and propagate around the nucleus. This behavior is similar to experimental observations along with a periodic reapperence of wavefronts that are also known from excitable regimes. Furthermore, in contrast to excitable systems, a polarity between interior and exterior regarding different actin states was observed. This leads to the conclusion that CDRs behave as wavefronts in a bistable regime of a system.

In this regard, the next chapters focus on the molecular nature of the wave machinery.

First, the role of the total amount of actin will be investigated (see Chapter 6). In the subsequent chapters, the role of PIP_3 and N-WASP will be examined and discussed (Chapter 7 & 8).

6 Effect of Depletion of Total Available Actin on CDR Dynamics

Actin is the main component of CDRs and thus it is assumed to play a governing role in initiation and propagation of CDRs. Hence, various studies of actin waves focused on actin itself as a central component in wave formation, this includes, inter alia, a model by Weiner et al. for Hem-1 waves in neutrophiles as well as a reaction-diffusion model in an excitable regime for actin waves in *Dictyostelium* by Whitelam et al. [Weiner et al., 2007, Whitelam et al., 2009]. Furthermore, bistable kinetics of actin between the interior and exterior of actin waves led to the conclusion that actin waves can be percieved as propagating fronts between two stable actin states after observing in *Dictyostelium*, macrophages and fibroblasts [Gerisch et al., 2011, Masters et al., 2016, Bernitt et al., 2017]. In contrast, there are models of actin waves, which do not focus on actin itself, but are rather based on an interplay between regulatory molecules. In this regard, Zeng et al. proposed a model, which includes an antagonistic relationship bewteen the Rho GTPases Rho and Rac leading to propagating CDRs [Zeng et al., 2011].

Due to experimental observations of CDR dynamics in fibroblasts treated with latrunculin A, Bernitt assumed a direct regulation of CDR propagation by actin itself in contrast to an upstream regulation with Rho GTPases [Bernitt, 2015]. In the following, this speculation on the role of actin is proved in detail in a quantitative manner by depleting the total available actin using the biochemical compound Jasplakinolide. Moreover, the overall goal is to uncover the underlying mechanism. By assuming a system with a bistable regime as proposed in the model of Bernitt et al. [Bernitt et al., 2017], the bistable state of actin is suggested to be experimentally uncovered by identifying the proposed Hopf bifurcation due to a variation of the total amount of actin in fibroblasts.

In the following, the effect of Jasplakinolide on the cytoskeleton is studied. Afterwards, a low Jasplakinolide concentration was chosen to investigate the effect of Jasplakinolide on the initiation and propagation of CDR dynamics. In this regard, structural changes of CDRs are observed and portrayed to discuss a potential Hopf bifurcation in the context of a bistable regime of a system. Furthermore, parameters like CDR lifetimes, velocities and periodicities are measured and before/after comparisons of Jasplakinolide additions in the same cells are presented. This raises the question if CDR velocities and periodicities systematically change through a depletion of the total amount of actin. This should help to examine the suspected direct CDR regulation by actin itself. Furthermore, by assuming CDRs to be wavefronts in a system with a bistable

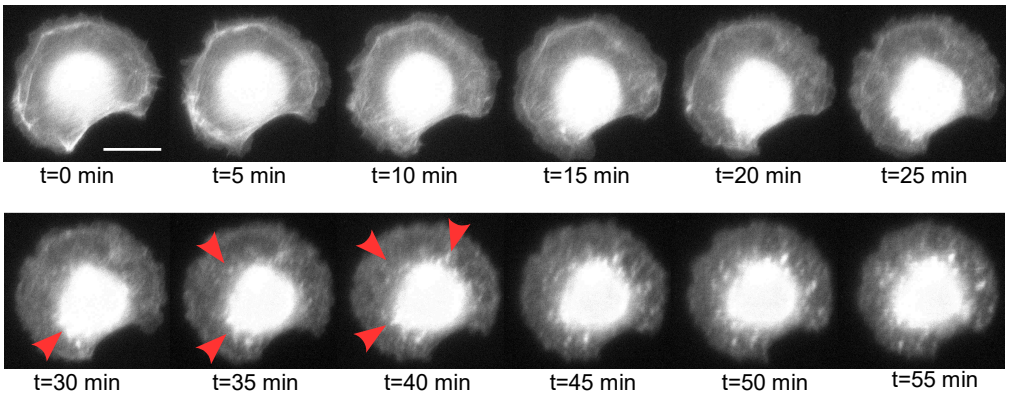

Figure 6.1: Effect of Jasplakinolide on actin cytoskeleton. A series of micrographs shows a fibroblast on a fibronectin patch, that was treated with 25 nM Jasplakinolide at time t=0 min. F-actin was labeled with p^{CMV}-LifeAct®-TagGFP2. Red arrowheads highlight actin clusters shown as white dots.

regime, numerical simulations of this model on an annulus domain are carried out. These simulations allow to determine how changes in the total amount of actin in the wavefront propagation differ in the theoretical system and the experimental one.

6.1 Degradation of actin leads to a structural loss and disappearance of CDRs

Jasplakinolide was used as a cell permeable biochemical compound, that binds to f-actin to induce actin polymerization and stabilize the actin cytoskeleton [Bubb et al., 1994, Bubb et al., 2000]. A series of micrographs shows an f-actin labeled disk-shaped fibroblast on a fibronectin patch, which was treated with 25 nM Jasplakinolide at time point t=0 min (Fig. 6.1) 30 minutes after it was completely spread. For the first 15 minutes after adding Jasplakinolide, the cytoskeleton shows no obvious change and consists of a network of actin filaments. 20 minutes after adding Jasplakinolide, the structure of the cytoskeleton begins to change, visualized by small dots indicating actin clusters. These actin clusters increase in size and number. In contrast, the number of visible actin filaments decreases and it seems there is a change from a filamenteous actin structure (at t=0 min) to an amorph clumpy structure of f-actin (at t=55 min). This change is not reversible, consequently, this implies that a Jasplakinolide treatment leads to a decrease of total available actin over time. Therefore, it seems to be an appropriate biochemical compound using for studying CDR dynamics.

To investigate the influence of Jasplakinolide and thus the resulting reduction in total actin on CDR dynamics, experiments had to be carried out with appropriate concentra-

tions of the biochemical compound. In this regard, a balance had to be found between influencing the CDR dynamics without completly destryoing the cytoskeleton. Therefore, experiments were performed with fibroblasts on disk-like fibronectin patches over 90 minutes, in which after 45 minutes under physiological conditions DMEM was replaced by DMEM with Jasplakinolide in concentrations of 15 nM, 20 nM or 25 nM by using a microfluidic perfusion system. Examples of kymographs are shown in Fig. 6.2 capturing CDR dynamics before and after adding Jasplakinolide subdivided in kymographs of experiments with Jasplakinolide concentrations of 15 nM (Fig. 6.2 A), 20 nM (Fig. 6.2 B) and 25 nM (Fig. 6.2 C). Direct before and after comparisons of fibroblasts treated with 25 nM Jasplakinolide show that CDR formation stopped almost immediately after adding 25 nM Jasplakinolide (see Fig 6.2 c1 and c2). Moreover, the rapid disruption of the cytoskeleton is visualized by horizontal lines in the kymograph (Fig. 6.2 c3). This effect occurs due to f-actin agglutination, as described above (see Fig. 6.1). Surprisingly, a few fibroblasts, which had shown no CDR formation at physiological conditions, began CDR formation after adding Jasplakinolide (see 6.2 c4). In contrast to experiments with 25 nM Jasplakinolide, before and after comparisons in fibroblasts treated with lower Jasplakinolide concentrations (15 nM and 20 nM) showed no termination of CDR formation after adding Jaslakinolide (see Fig. 6.2 A & B). Moreover, due to the diversity of CDR dynamic patterns in the kymographs, at first glance no systematic change in CDR dynamics in comparison between before and after adding Jasplakinolide can be identified. However, the kymographs in Fig. 6.2 a2, b2 and b3 give reason to the possibility of longer CDR lifetimes after adding Jasplakinolide. This is emphasized by the elongated lines or fragments in the kymograph patterns.

Due to these results, longer experiments over a runtime of 3 hours were performed, in which Jasplakinolide was added after 90 minutes. A concentration of 20 nM was chosen, so that the cytoskeleton was not as much disrupted and CDR formation could occur. Dynamics of CDRs are depicted in kymographs, which are depicted in Fig. 6.3 as a series of examples. As indicated above (Fig. 6.2), the data also show that kymograph patterns exhibited longer lines or fragments after adding Jasplakinolide (Fig. 6.3 B, C, D, E & F). In this regard, the data also function as a control experiment for the 90 minutes experiments to exclude that there was a time dependendent change in CDR dynamics instead that there was an effect due to the change of the biochemical environment.

Moreover, on occasion CDRs have appeared locally and not in all cases over the whole cell. After treatment with Jasplakinolide, these CDR behavior changes and CDRs appear all around the nucleus (see Fig. 6.3 C & D). When fibroblasts show CDR dynamics appearing as long line patterns in kymographs at physiological conditions, CDRs become unstructured after adding Jasplakinolide (Fig. 6.3 A-D & F) until they disappear. This means that the normally clearly defined propagating front and ring shape is less pronounced (Fig. 6.4). Moreover, in some cases CDRs appear as an unstructured accumulation of small actin cluster (Fig. 6.4 A). Nobody before has

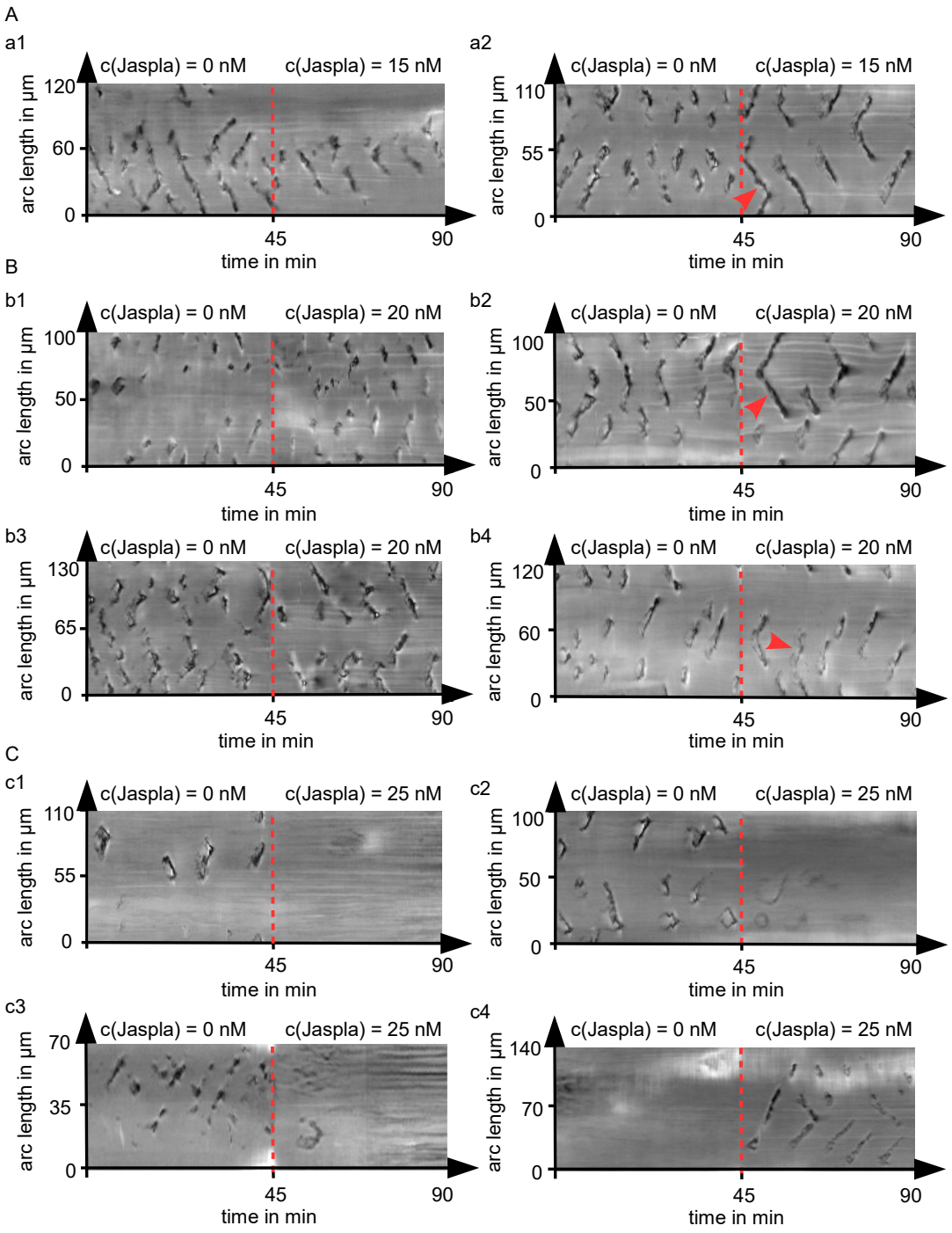

Figure 6.2: Examples of kymographs from fibroblasts treated with Jasplakinolide. Kymographs show CDR dynamics 45 minutes before and 45 minutes after adding Jasplakinolide. The medium exchange is visualized by red dashed lines. Panel A shows two examples of kymographs from fibroblasts treated with $15\,\mathrm{nM}$ Jasplakinolide, panel B with $20\,\mathrm{nM}$ Jasplakinolide and panel C with $25\,\mathrm{nM}$ Jasplakinolide, respectively. Red arrowheads highlight examples of longer lines or fragments after adding Jasplakinolide.

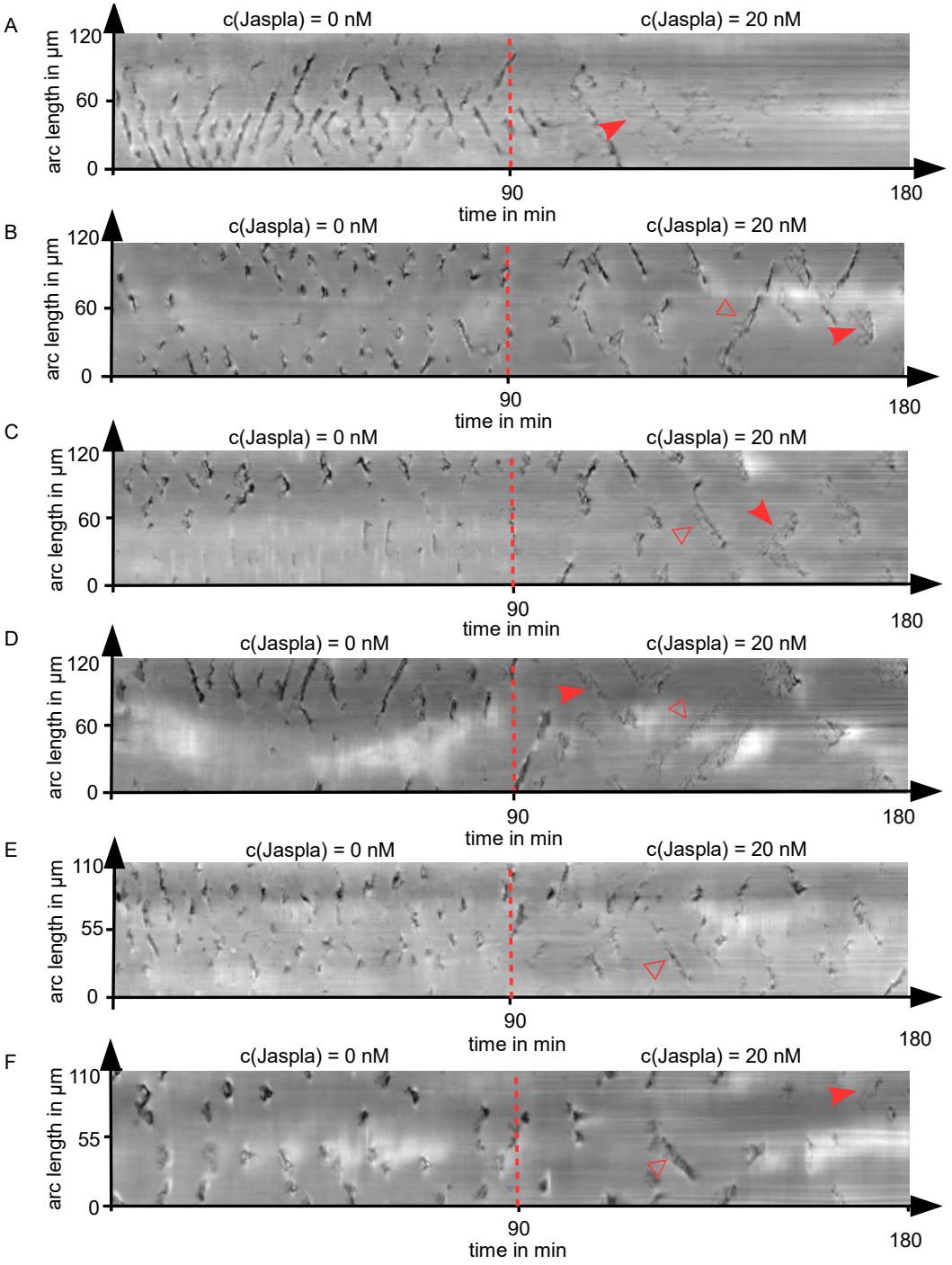

Figure 6.3: Examples of kymographs from fibroblasts treated with $20\,\mathrm{nM}$ Jasplakinolide over 90 minutes. A-F: Kymographs show CDR dynamics 90 minutes before and 90 minutes after fibroblasts were treated with Jasplakinolide. The medium exchange is visualized by red dashed lines. Red unfilled arrowheads highlight examples of elongated lines or fragments, whereas filled arrowheads indicate examples of unstructured lines or fragments.

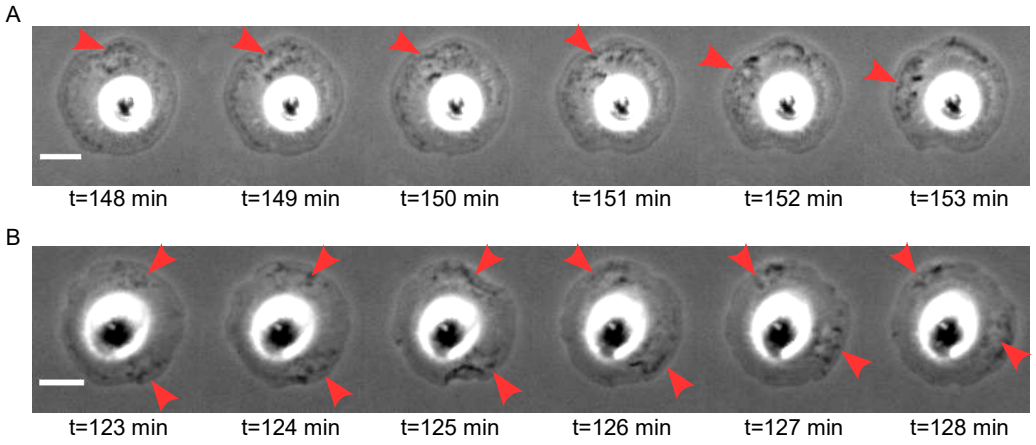

Figure 6.4: Unstructured CDRs in fibroblasts after adding Jasplakinolide. A and B are two examples of unstructured CDRs in fibroblasts. Their dynamics were presented in corresponding kymographs C (A) and D (B) in Fig. 6.3.

observed this interesting structural change when studying different wave dynamics in macrophages or neutrophiles with the biochemical compound Jasplakinolide [Weiner et al., 2007,Masters et al., 2016] but these experimental results are similar to a behavior of wavefronts in the model proposed by Bernitt et al. near the bistable regime [Bernitt et al., 2017]. They reproduced similar incidental findings in random shaped fibroblasts. Numerical results of their model also showed a chaotic behavior of small waves within a coherent wavefront under certain conditions and when the regime was unstable to waves (Section 3.4). Moreover, having taken a look at their bifurcation diagram of the model in dependence of the total amount of actin, Bernitt et al. proposed a Hopf bifurcation next to the bistable regime (see Fig. 6.5 A) [Bernitt et al., 2017]. This leads to the conclusion that the observed experimental results while decreasing the total amount of actin in this work are in line with an oscillatory behavior of a system at a Hopf bifurcation as proposed in the model. Furthermore, also transitions from dotted or fragmented to line patterns can be explained by a reduction of the total actin concentration in a bistable regime above the Hopf bifurcation (see Fig. 6.5 A & B).

6.2 Degradation of total available actin leads to longer CDR lifetimes

To quantify observations from kymographs (Section 6.1), CDR lifetimes were measured in 90 minutes experiments. In the same fibroblast, CDR lifetimes over the first 45 minutes before adding Jasplakinolide and the second 45 minutes after adding Jasplakinolide were calculated for concentrations of 15 nM and 20 nM (Fig. 6.6 a1 & a2) as well as for control experiments without adding Jasplakinolide (Fig. 6.6 a3). Comparing the

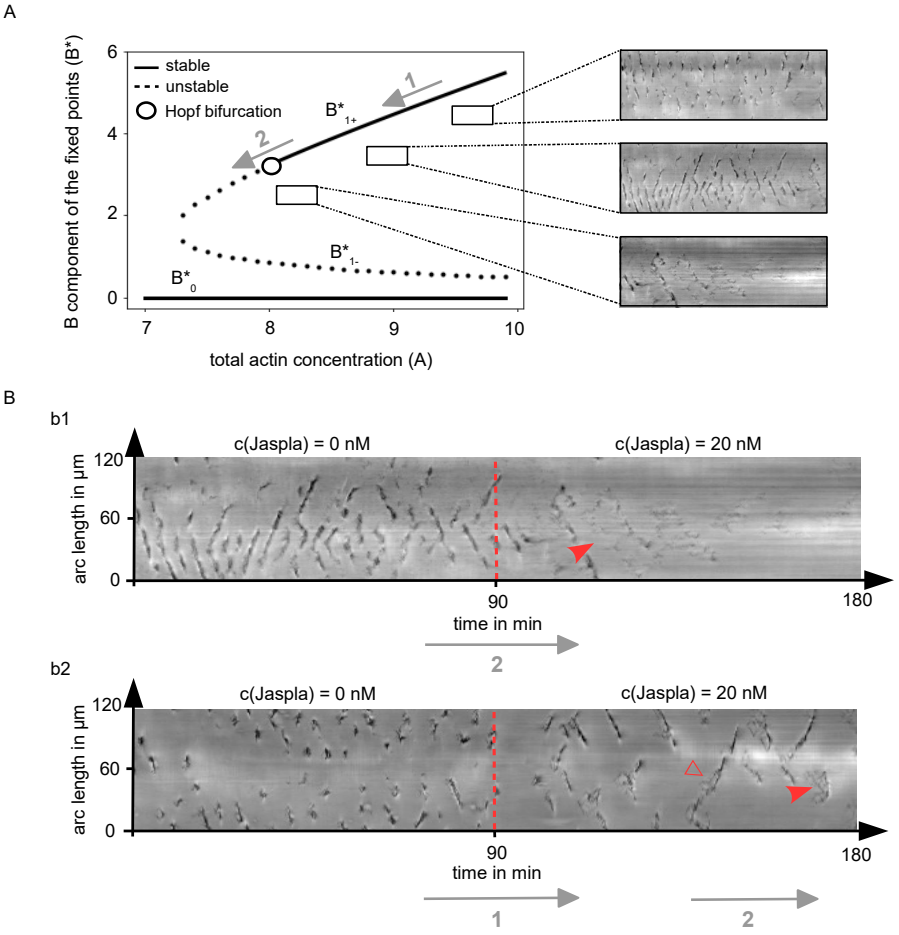

Figure 6.5: Visualizing the effect of Jasplakinolide within a bifurcation diagram. The bifurcation diagram in A shows the B components of the fixed points P_0^*, P_{1+}^* and P_{1-}^* (B^*) dependent on the total actin concentration (A) according to [Bernitt et al., 2017]. Three exemplary kymograph patterns (fragmented, line and unstructured) are inserted, that visualize the dependence of CDR dynamics on the total actin concentration. The grey arrow one highlights a degradation of total available actin in cells with a high total actin concentration within the bifurcation diagram, that is visible as a transition from a fragmented to a line pattern (unfilled red arrowhead) in a kymograph (b2). In contrast, the grey arrow two visualizes a decrease of the total available actin in cells with a lower actin concentration within the bifuraction diagram. In this case, at the Hopf bifurcation cells loose stability to waves, that is visible as unstructured patterns in kymographs (red filled arrowheads in b1 and b2).

average CDR lifetimes in 11 fibroblasts before and after adding 15 nM Jasplakinolide as well as in 7 fibroblasts exposed to 20 nM Jasplakinolide, longer CDR lifetimes in cells treated with Jasplakinolide were found. The mean values of CDR lifetimes amounted to 3.1 ± 0.3 min before and 3.7 ± 0.4 min after adding 15 nM, as well as in experiments with 20 nM Jasplakinolide 4.5 ± 0.9 min and 5.4 ± 0.6 min, respectively. In addition, histograms visualizing distributions of CDR lifetimes before and after adding 15 nM Jasplakinolide (see Fig. 6.6 a1) and 20 nM (see Fig. 6.6 a2) show a small shift of the distributions after adding Jasplakinolide to longer CDR lifetimes compared to the distributions before adding Jasplakinolide. In comparison, the mean values of CDR lifetimes in 14 fibroblasts in control experiments are similar in the first and second 45 minutes amounting to 2.9 ± 0.9 min in both cases. Additionally, these distributions show no differences between the first and second 45 minutes (see Fig. 6.6 a3).

Moreover, the data enables a calculation of the absolute differences in mean CDR lifetimes before and after adding Jasplakinolide in the same fibroblasts presented in Fig. 6.6 b1 & b2 as well as for control experiments without adding Jasplakinolide for the first and the second 45 minutes (see Fig. 6.6 b3). These histograms clarify the observations from Fig. 6.6 A. Fig. 6.6 b3 shows absolute differences in CDR lifetimes from control experiments, which are nearly normally distributed around a mean value of 0 min meaning that there is no systematic change between the data of the first and second 45 minutes. In contrast, the distribution of absolute differences in CDR lifetimes from experiments with 20 nM Jasplakinolide shows a shift to positive absolute differences which signifies longer CDR lifetimes after adding Jasplakinolide. The distribution of experiments with 15 nM Jasplakinolide also seems to be very slightly shifted to positive CDR lifetimes.

However, no statistical significance of the absolute differences in CDR lifetimes before and after adding Jasplakinolide for both concentrations, 15 nM and 20 nM, in 90 minutes experiments, as well as for the control experiments could be found. For all tests of statistical significance in this work, two-sided Wilcoxon signed-rank tests were performed to compare data of the same fibroblasts before and after treating with a biochemical compound. To clarify the indicated observations of longer CDR lifetimes after adding Jasplakinolide, CDR lifetimes of experiments with a longer runtime of 3 hours were calculated (as described in Section 6.1). From 14 fibroblasts the mean CDR lifetime calculated over 90 minutes before adding Jasplakinolide was 3.2 ± 0.2 min, whereas the mean CDR lifetime over 90 minutes after adding Jasplakinolide was increased to 6.9 ± 0.9 min. The distributions of the CDR lifetimes and their absolute differences are visualized in Fig. 6.7 A. It is shown that CDR lifetimes before and after adding Jasplakinolide are nearly similarly distributed, but the distribution of CDR lifetimes after adding Jasplakinolide is clearly shifted to longer lifetimes in comparison to the distribution of CDR lifetimes before adding Jasplakinolide (see Fig. 6.7 a1). The distribution of absolute difference between before and after adding Jasplakinolide shows only

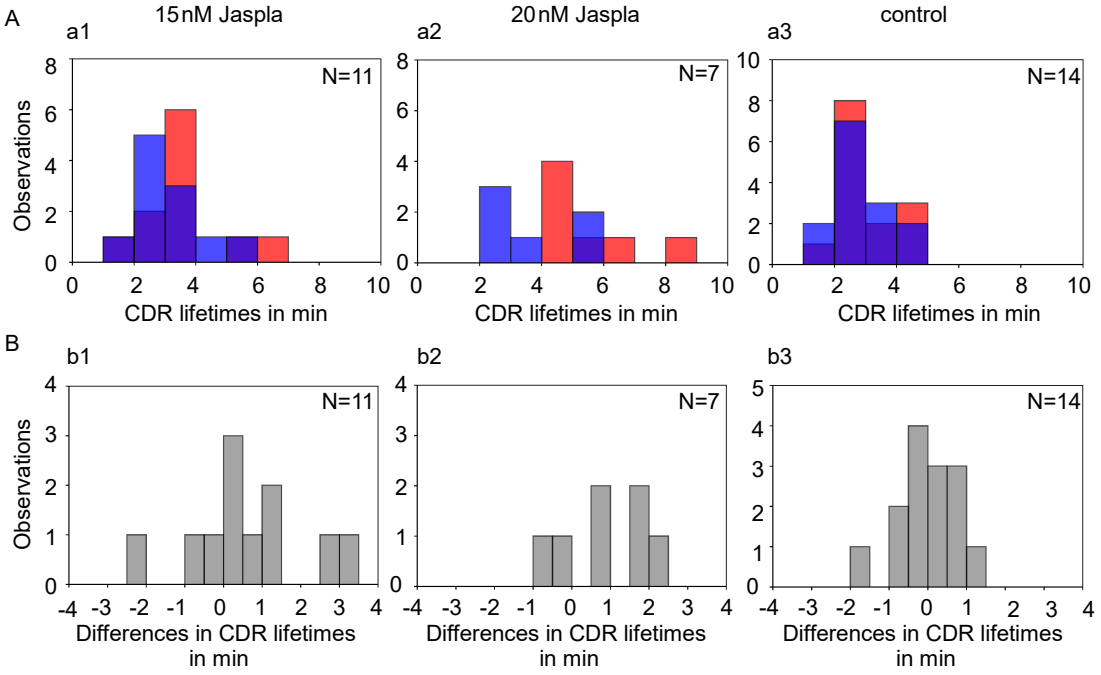

Figure 6.6: Histograms of CDR lifetimes in 90 minutes experiments. A: Average CDR lifetimes over time periods of 45 minutes before (blue bars) and 45 minutes after (red bars) adding Jasplakinolide with concentrations of $15\,\mathrm{nM}$ in a1 and $20\,\mathrm{nM}$ in a2. a3 shows mean CDR lifetimes in a control experiment subdivided into the first 45 minutes (blue bars) and the second 45 minutes (red bars). B: Absolute differences in mean CDR lifetimes before and after adding Jasplakinolide with concentrations of $15\,\mathrm{nM}$ in b1 and $20\,\mathrm{nM}$ in b2. b3 shows absolute differences in mean CDR lifetimes in single cells in a control experiment between the first and the second 45 minutes. N indicates the number of analyzed fibroblasts.

positive values implying a clear increase in CDR lifetimes after adding Jasplakinolide (see Fig. 6.7 a2). A statistical significance of the absolute differences in CDR lifetimes over 90 minutes before and 90 minutes after adding Jasplakinolide.

Comparing the results from the 3 hours experiments to those from the 90 minutes experiments regarding CDR lifetimes, the increase in CDR lifetimes after adding Jasplakinolide in experiments with longer runtimes seems to be larger than in experiments with shorter runtimes. This leads to the conclusion that time plays a fundamental role. This is speculated to be due to the time dependent actin agglutination induced by Jasplakinolide (see Fig. 6.1). The time dependence of CDR lifetimes in these experiments was investigated by calculating mean CDR lifetimes of three 30 minutes intervals of the 90 minutes section after adding Jasplakinolide in the 3 hours experiments (see Fig. 6.7 b1 & b2). Mean

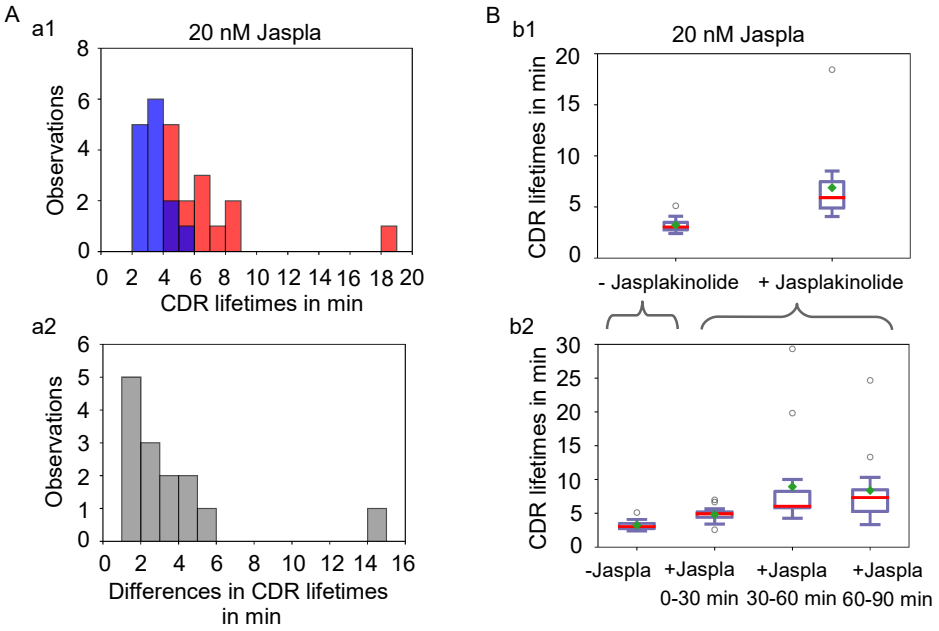

Figure 6.7: CDR lifetimes in 3 hours experiments. A: Histograms of CDR lifetimes in 3 hours experiments showing average CDR lifetimes before (blue bars) and after (red bars) adding Jasplakinolide. B: Boxplots of average CDR lifetimes before and after adding Jasplakinolide (b1) and average CDR lifetimes before adding Jasplakinolide as well as between 0 minutes and 30 minutes after adding Jasplakinolide, between 30 minutes and 60 minutes after adding Jasplakinolide as well as between 60 minutes and 90 minutes after adding Jasplakinolide (b2).

values were calculated to be 4.8 ± 0.3 min between zero and 30 minutes, 9.0 ± 1.9 min between 30 and 60 minutes and 8.4 ± 1.4 min between 60 and 90 minutes after adding 20 µM Jasplakinolide. This demonstrates an increase in CDR lifetimes after adding Jasplakinolide as a function of time (see Fig. 6.7 a2). It can therefore be concluded that the increase in CDR lifetimes is a function of total available actin depletion. It can be virtually excluded, that the increase in CDR lifetimes is an exclusive effect of time and it would not have been possible to cause this effect without adding Jasplakinolide. This was shown by the control experiment (see Fig. 6.6 a3), in which no difference in CDR lifetimes between the first and second 45 minutes was observed. In contrast, Jasplakinolide experiments over 90 minutes with concentrations of 15 nM and 20 nM exhibited a small increase in CDR lifetimes after adding Jasplakinolide (Fig. 6.6 a1 & a2).

The effect of an increase in CDR lifetimes and a weaker appearence of ring shapes of CDRs after adding Jasplakinolide, confirmed the important role of actin in CDR propagation. The influence of Jasplakinolide has also been tested in further studies, which investigated Hem-1 waves in neutrophiles [Weiner et al., 2007]. In contrast to

results in this study, Weiner et al. found decreased lifetimes and intensities after adding Jasplakinolide, and moreover, an increase in wave lifetimes after depolymerizing actin with Latrunculin A. This leads to the hypothesis of an opposite effect of actin in the wave machinery of Hem-1 waves, in which f-actin acts as an inhibitor of Hem-1, compared to the wave machinery of CDRs.

6.3 Degradation of total available actin leads to reduced CDR velocities

In addition to CDR lifetimes, CDR velocities and periodicities are important parameters to characterize CDR dynamics. Similar to the analysis of the dependence of CDR lifetimes on Jasplakinolide treatment (Section 6.2), in the following the influence of Jasplakinolide on CDR velocities and periodicities will be described. In experiments over 90 minutes, average CDR velocities were measured over 45 minutes before and 45 minutes after adding Jasplakinolide with concentrations of 15 nM and 20 nM (Fig. 6.8 a1 & a2) compared to CDR velocities calculated from control experiments of the first and the second 45 minutes without adding Jasplakinolide (Fig. 6.8 a3). Mean values of CDR velocities of 11 fibroblasts treated with 15 nM Jasplakinolide and 7 fibroblasts treated with 20 nM Jasplakinolide amounted to $0.14 \pm 0.01\,\mu m\,s^{-1}$ before adding Jasplakinolide and $0.11 \pm 0.01\,\mu m\,s^{-1}$ after adding Jasplakinolide for both Jasplakinolide concentrations. This demonstrates a decrease in CDR velocities after adding Jasplakinolide. Comparing the distributions of CDR velocities before and after adding Jasplakinolide, the CDR velocities are approximately equally distributed but a shift of the distributions after adding Jasplakinolide for both concentrations (15 nM and 20 nM) is also apparent. The average CDR velocities in 14 fibroblasts of control experiments over the first and second 45 minutes are nearly similarly distributed and show no systematic changes. They are also comparable in the first and second 45 min amounting to $0.16 \pm 0.01\,\mu m\,s^{-1}$ and $0.15 \pm 0.01\,\mu m\,s^{-1}$, respectively.

Furthermore, Fig. 6.8 b1 & b2 visualize the absolute differences in CDR velocities before and after adding Jasplakinolide (concentrations of 15 nM and 20 nM) in the same fibroblasts. Additionally, Fig. 6.8 b3 shows absolute differences in CDR velocities in the same fibroblasts of the control experiments between the first and second 45 minutes. CDR velocities in control experiments are distributed around a mean difference of 0 min, whereas the distributions of absolute differences in CDR velocities in Jasplakinolide treated fibroblasts appear shifted to negative values of absolute differences in CDR velocities. This is in line with results from Fig. 6.8 A leading to the conclusion that treating fibroblasts with Jasplakinolide results in decreased CDR velocities. It was found to be a statistical significance of the absolute differences in CDR velocities before and after adding Jasplakinolide for both concentrations, 15 nM and 20 nM, as well as no statistical significance of absolute differences in CDR velocities between the first and second 45 minutes in fibroblasts of control experiments.

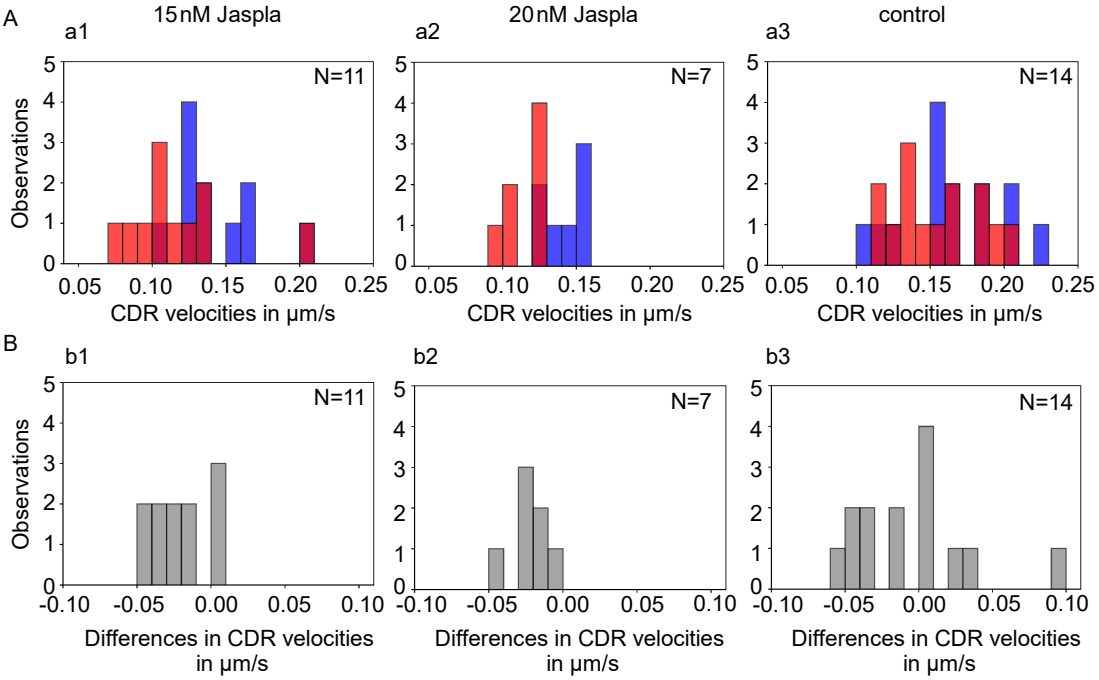

Figure 6.8: Histograms of CDR velocities in 90 minutes experiments. A: Mean CDR velocities over time periods of 45 minutes before (blue bars) and 45 minutes after (red bars) adding Jasplakinolide with concentrations of $15\,\mathrm{nM}$ in a1 and $20\,\mathrm{nM}$ in a2. a3 shows mean CDR velocities in a control experiment subdivided into the first $45\,\mathrm{min}$ (blue bars) and the second $45\,\mathrm{min}$ (red bars). B: Absolute differences in mean CDR velocities before and after adding Jasplakinolide with concentrations of $15\,\mathrm{nM}$ in b1 and $20\,\mathrm{nM}$ in b2. b3 shows absolute differences in mean CDR velocities in single cells in a control experiment between the first and the second 45 minutes. N indicates the number of analyzed fibroblasts.

Moreover, average velocities over 90 minutes before and 90 minutes after adding $20\,\mathrm{nM}$ Jasplakinolide in fibroblasts from 14 experiments with a 3 hours runtime (see Section 6.1 and Fig. 6.3) were calculated (see Fig. 6.9 a1). The distribution of CDR velocities after adding $20\,\mathrm{nM}$ Jasplakinolide is clearly shifted to lower CDR velocities compared to the distribution of CDR velocities before adding Jasplakinolide. In addition, the mean CDR velocity before adding Jasplakinolide was $0.16 \pm 0.01\,\mu\mathrm{m\,s^{-1}}$, whereas the mean CDR velocity after adding $20\,\mathrm{nM}$ Jasplakinolide amounted to $0.11 \pm 0.01\,\mu\mathrm{m\,s^{-1}}$. Fig. 6.9 a2 visualizes the absolute differences in CDR velocities between before and after adding $20\,\mathrm{nM}$ Jasplakinolide in the same fibroblasts. It shows only negative values. This demonstrates once more that the decrease in CDR velocities after adding Jasplakinolide and the absolute differences in CDR velocities before and after adding

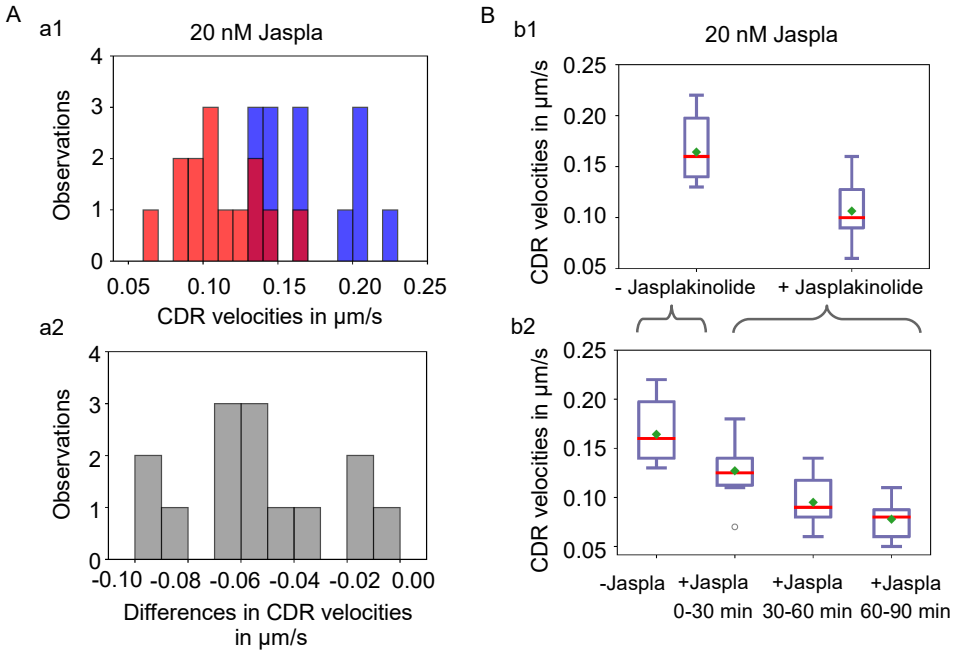

Figure 6.9: CDR velocities in 3 hours experiments. A: Histograms of CDR velocities in 3 hours experiments showing average CDR velocities before (blue bars) and after (red bars) adding Jasplakinolide (a1) as well as differences between before and after adding Jasplakinolide (grey bars) (a2). B: Boxplots of average CDR velocities before and after adding Jasplakinolide (b1) and average CDR velocities before adding Jasplakinolide as well as between 0 minutes and 30 minutes after adding Jasplakinolide, between 30 minutes and 60 minutes after adding Jasplakinolide as well as between 60 minutes and 90 minutes after adding Jasplakinolide (b2).

20 nM Jasplakinolide were verified to be statistically significant.

As described above, Jasplakinolide induces a time dependent actin agglutination which reduces the total available actin over time. To investigate the dependence of CDR velocities on time and thus a dependence on the total available actin, average CDR velocities of three 30 minutes time intervals from the 90 minutes section were calculated after adding 20 nM Jasplakinolide (see Fig. 6.9 b1 & b2). Comparing the average CDR velocity of $0.13 \pm 0.01\,\mu m\,s^{-1}$ from the intervall between zero and 30 minutes after adding 20 nM Jasplakinolide to the average CDR velocity of $0.09 \pm 0.01\,\mu m\,s^{-1}$ from the intervall between 30 and 60 minutes and to $0.08 \pm 0.01\,\mu m\,s^{-1}$ from the intervall between 60 and 90 minutes after adding Jasplakinolide, a stepwise decrease of CDR velocities was found. This leads to the conclusion that CDR velocities are a function of total available actin.

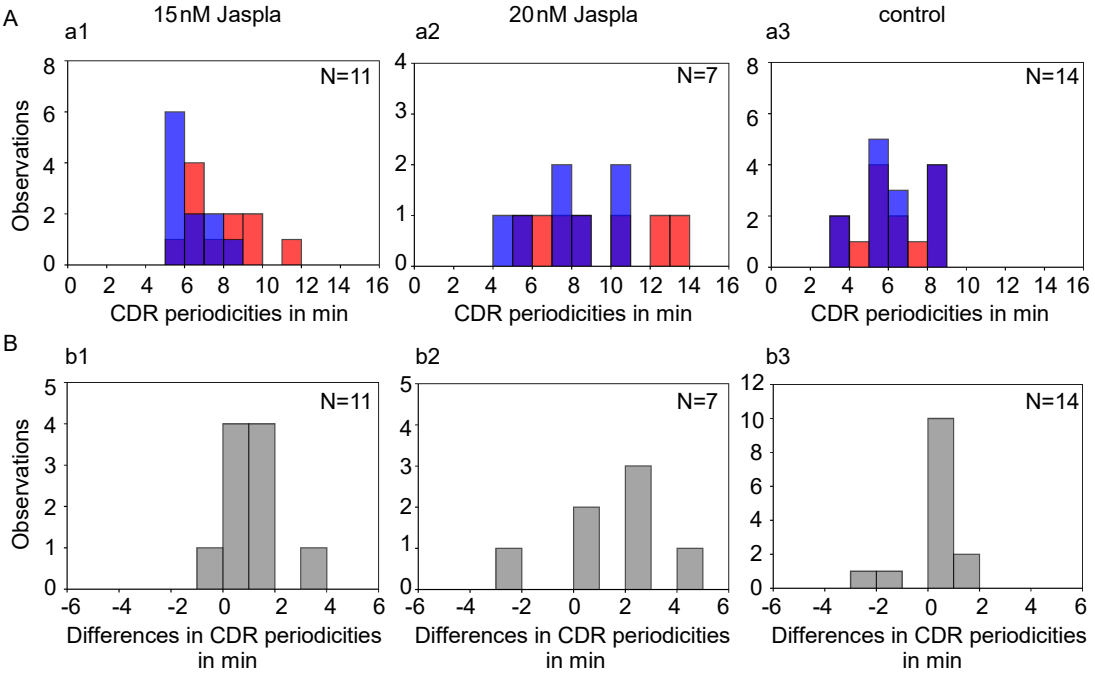

Figure 6.10: Histograms of CDR periodicities in 90 minutes experiments. A: Mean CDR periodicities over time periods of 45 minutes before (blue bars) and 45 minutes after (red bars) adding Jasplakinolide with concentrations of $15\,\mathrm{nM}$ in a1 and $20\,\mathrm{nM}$ in a2. a3 shows mean CDR periodicities in a control experiment subdivided into the first $45\,\mathrm{min}$ (blue bars) and the second $45\,\mathrm{min}$ (red bars). B: Absolute differences in mean CDR periodicities before and after adding Jasplakinolide with concentrations of $15\,\mathrm{nM}$ in b1 and $20\,\mathrm{nM}$ in b2. b3 shows absolute differences in mean CDR periodicities in single cells in a control experiment between the first and the second 45 minutes. N indicates the number of analyzed fibroblasts.

This is in line with the proposition of Chapter 6 that actin is a limiting species affecting a dependence of CDR velocities as a function of the number of the concurrently occuring CDRs. Moreover, it underlines the governing role of actin itself. It is in line with experimental observations of decreased Hem-1 wave velocities by affecting actin with Jasplakinolide in neutrophiles by Weiner et al. and also with decreased CDR velocities by affecting actin with latrunculin A by Bernitt [Bernitt, 2015]. However, it is contradictory to the assumption of Zeng et al. that CDRs are regulated upstream of actin by Rho GTPases Rac and Rho [Zeng et al., 2011].

6.4 Degradation of total available actin leads to larger CDR periodicities

The same 90 minutes experiments were analyzed regarding CDR periodicities (see Fig. 6.10). Comparing the mean values of CDR periodicities before and after adding Jasplakinolide, increased CDR periodicities of 7.9 ± 0.6 min were found after adding 15 nM Jasplakinolide compared to 6.4 ± 0.4 min before adding Jasplakinolide. Moreover, for a concentration of 20 nM Jasplakinolide mean values of 9.2 ± 1.1 min after adding Jasplakinolide and 7.7 ± 0.9 min before adding Jasplakinolide were measured. Fig. 6.10 a1 & a2 visualize the distributions of CDR periodicities before and after adding Jasplakinolide for concentrations of 15 nM and 20 nM. In both cases, CDR periodicities before and after adding Jasplakinolide are similarly distributed, whereas the distributions of CDR periodicities after adding Jasplakinolide appear shifted to larger CDR periodicities in contrast to the distributions of CDR periodicities before adding Jasplakinolide. Absolute differences in CDR periodicities before and after adding Jasplakinolide in the same fibroblasts exhibit, with the exception of one value in each case, only positive values, which also emphasizes an increase in CDR periodicities after adding Jasplakinolide (see Fig. 6.10 b1 & b2). The differences in CDR periodicites before and after Jasplakinolide were found to be of statistical significance, which is the case for the concentration of 15 nM, but not for 20 nM. This may, however, be inaccurate due to the small amount of 7 analyzed fibroblasts. The control experiments provided, as expected, no statistically significant differences in CDR periodicities between the first and the second 45 minutes. The data show nearly similar distributions and no shift between CDR periodicities of the first and second 45 minutes (see Fig. 6.10 a3). Absolute differences of CDR periodicities between the first and second 45 minutes are distributed around 0 min (see Fig. 6.10 b3).

In experiments with longer runtimes of 3 hours, the mean CDR periodicities differ between 6.3 ± 0.4 min over 90 minutes before and 11.7 ± 0.6 min over 90 minutes after adding 20 nM Jasplakinolide. The distribution of CDR periodicities after adding Jasplakinolide is distinguished from the distribution of CDR periodicities before adding Jasplakinolide due to a clear shift to larger values of CDR periodicities and a broader spread (see Fig. 6.11 a1). The values for the absolute differences of CDR periodicities between before and after adding Jasplakinolide are only positive and their difference is statistically significant. Splitting up the average values of CDR periodicities of the 90 minutes section after adding Jasplakinolide in three 30 minutes section, a stepwise increase in CDR periodicities with mean CDR periodicities of 8.7 ± 0.6 min between zero and 30 minutes, 10.9 ± 0.5 min between 30 and 60 minutes and 15.4 ± 1.6 min between 60 and 90 minutes was found (see Fig. 6.11 b1 & b2). This comparison demonstrates that CDR periodicities increased with the time after adding Jasplakinolide and are also a function of the total available actin concentration.

CDR periodicites were presumed to be a result of the interplay between stochastic

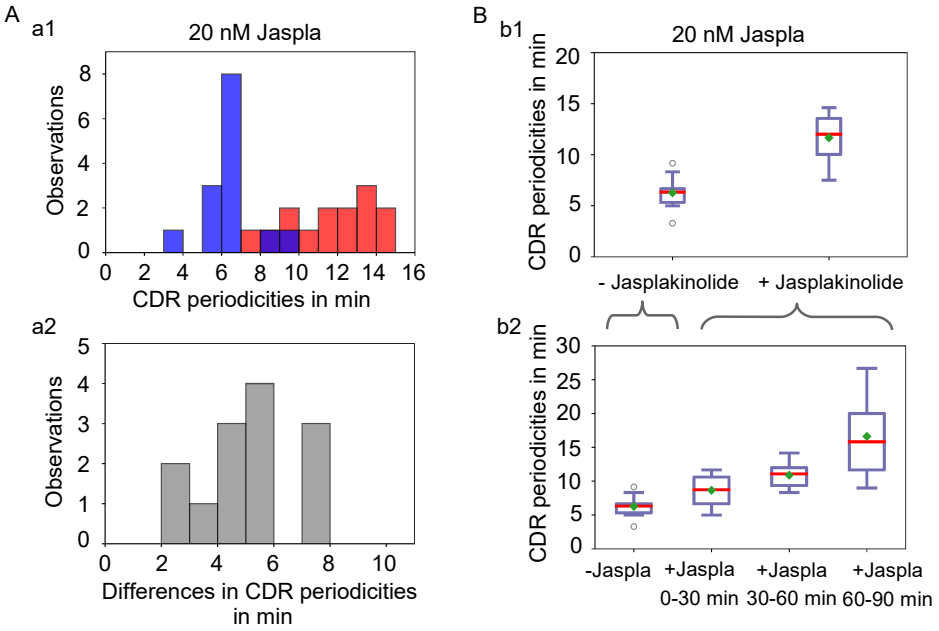

Figure 6.11: CDR Periodicities in 3 hours experiments. A: Histograms of CDR periodicities in 3 hours experiments showing average CDR periodicities before (blue bars) and after (red bars) adding Jasplakinolide (a1) and the differences between before and after adding Jasplakinolide (grey bars) (a2). B: Boxplots of average CDR periodicities before and after adding Jasplakinolide (b1) and average CDR periodicities before adding Jasplakinolide as well as between 0 minutes and 30 minutes after adding Jasplakinolide, between 30 minutes and 60 minutes after adding Jasplakinolide as well as between 60 minutes and 90 minutes after adding Jasplakinolide (b2).

perturbations and a recovery time of the system Bernitt et al., 2015. In this respect, a decrease of the total amount of actin may have two possible effects. On the one hand, it may lead to an increase in the recovery time of the system and therefore affect a larger periodicity. On the other hand, it is also possible that a decrease of the total available actin affects a higher threshold, which a perturbation has to overcome in oder to initiate CDRs. Furthermore, CDR periodicites are proposed to regulate CDR lifetimes (as described in Chapter 5), therefore, the observed longer CDR lifetimes after depleting the total available actin are also affected by larger CDR periodicities.

6.5 Propagating wavefronts on an annulus domain under variation of the total actin concentration

The main hypothesis in this work is that CDRs can be considered as wavefronts in a bistable regime of a system. An exemplary model of Bernitt et al. focused on the

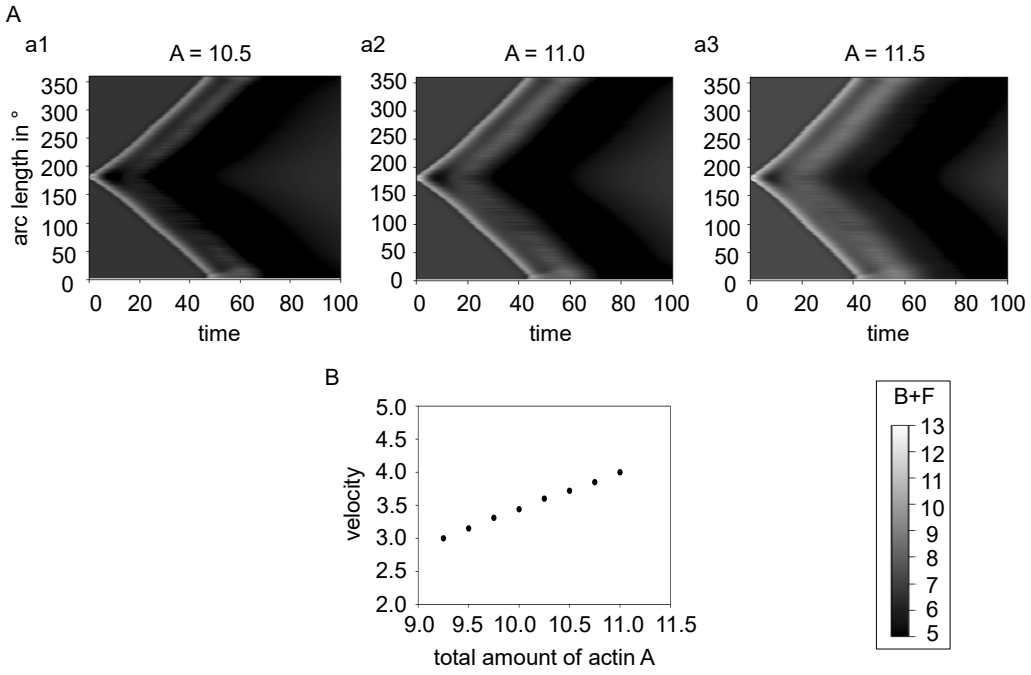

Figure 6.12: Dependence of propagating wavefronts on total actin concentration. A shows kymographs visualizing propagating wavefronts dependent on the total amount of actin A. The velocities of wavefronts as a function of the total amount of actin A are summarized in the plot B with arbitrary units. The parameters are D=0.12, k_{i1}=2.09, k_{i2}=0.53, k_{f1}=2.05, k_{f2}=1.19.

transition between two stable actin states, the basal CDR-free state (or CDR exterior) and the stress fiber depleted CDR interior [Bernitt et al., 2017]. The total amount of actin A is the main parameter in this model and it is assumed to be constant over the whole time. Within the model, it is split up in actin that occurs as globular monomers as well as in actin that is incorporated either in CDRs or in stress fibers and the cell cortex. The concentration of the latter changed over time. It raises the question how wavefronts in theoretical experiments, which are based on a model that uses actin as a main paramer, behave, when the total amount of actin is changed. Do wavefronts also propagate slower with a decreasing amount of actin?

Numerical solutions for the model on an annulus domain were calculated by varying the total amount of actin in the bistable regime, while keeping the other parameters constant. It seems to be evident that an increase in the total amount of actin leads to an increase in the actin concentration incorporated in the propagating front in the $B + F$ field (Fig. 6.12 A). Moreover, also the ring size increases with an increase in the total amount of actin. This effect is visualized in the kymograph by the larger distance between the beginning of the first propagating front and the back of the second

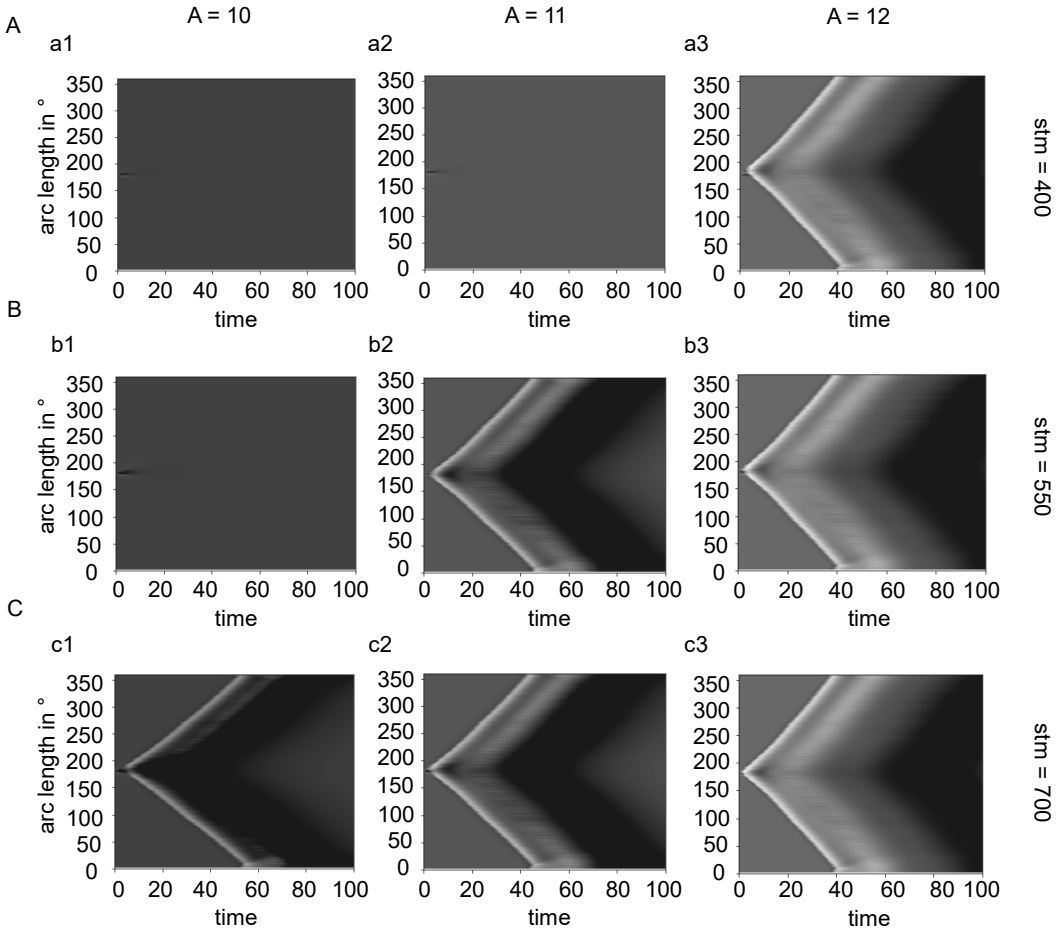

Figure 6.13: Dependence of the required stimulus for propagating wavefronts on the total amount of actin. Numerical solutions were calculated for three different parameters of the total amount of actin A (see different columns) and for three different values of the amplitude of the stimulus (see different rows, A-C). It is shown the $B + F$-field. The parameters are D=0.12, k_{i1}=2.09, k_{i2}=0.53, k_{f1}=2.05, k_{f2}=1.19.

propagating front.

Comparing velocities of the propagating fronts, an increase in wavefront velocities with a raised amount of the total actin concentration was found (Fig. 6.12 B). This is comparable to the main experimental findings presented in the previous section, in which a decrease of the total available actin also lead to a reduction in CDR velocities (Section 6.3). Both, experimental and theoretical experiments, lead to the conclusion that actin itself is the main parameter regulating CDR dynamics in contrast to, for

example, former studies by Zeng et al. which describe CDR dynamics as being mainly governed by the regulatory proteins Rho and Rac [Zeng et al., 2011].

Moreover, from experimental observations of longer CDR periodicities after degrading the total amount of actin (Section 6.3) a further question arises whether a reduction of the total actin concentration leads to an increase in the stimulation threshold for propagating CDRs. This was also tested with theoretical experiments within the bistable regime of the model by varying the amplitude of the stimulus for three different values of the parameter A (total amount of actin). In this regard, a correlation between the stimulation threshold for propagating wavefronts and the total amount of actin was found. Lower amplitudes of the stimulus were required to induce propagating wavefronts in theoretical experiments with higher actin concentrations (see Fig. 6.13). This leads to the conclusion, that longer CDR periodicities and longer CDR lifetimes result from an increase in the threshold for stimulation of propagating CDRs by decreasing the total amount of actin.

6.6 Summary

In this chapter, the influence of decreased total available actin on CDR initiation and propagation in disk-shaped fibroblasts was investigated. Therefore, the biochemical compound Jasplakinolide, that induces actin agglutination was used. This leads to a reduction of the total amount of available actin as a function of time. It was observed that a degradation of actin leads to a structural loss of the ring shapes of CDRs into an oscillatory behaviour of actin substructures before CDRs completely disappeared. This leads to the conclusion of a comparable behavior of wavefronts as proposed in the model of Bernitt et al. at a Hopf bifurcation next to the bistable regime [Bernitt et al., 2017].

Furthermore, decreased CDR velocities were found as a function of time and therefore as a function of the total available amount of actin. This seems to be in line with results from Chapter 5, in which a correlation between a decrease in CDR velocities with a rising number of concurrently occuring CDRs was demonstrated. This leads to the conclusion of a direct regulation of CDR dynamics by actin itself as also hypothesized in Chapter 5. It is also in line with experimental results of decreased velocities of actin waves after affecting actin in fibroblasts via latrunculin A and in neutrophiles with latrunculin A as well as with Jasplakinolide [Bernitt, 2015, Weiner et al., 2007]. However, it is contradictory to models focussing on CDR regulation upstream of actin via Rho GTPases as proposed by Zeng et al. [Zeng et al., 2011].

Moreover, a degradation of total available actin affects a larger periodicity and longer lifetimes of CDRs. It was concluded that longer CDR periodicities result from an increased recovery time or a heightened threshold for a stimulus to induce propagating CDRs for decreased concentrations of total amounts of actin. The longer CDR lifetimes

are believed to be affected by longer CDR periodicities generating an upper limit for CDR lifetimes (see Chapter 5).

To further examine the hypothesis that CDRs can be considered as wavefronts in a bistable regime, numerical simulations of the model by Bernitt et al. were run on an annulus domain under variation of the parameter A, the total amount of actin [Bernitt et al., 2017]. Decreased wave velocities as a function of the total amount of actin were also obtained from numerical solutions in the bistable regime. This emphasizes the hypothesis that CDRs can be considered as wavefronts between two stable states of actin as proposed by Bernitt et al. [Bernitt et al., 2017] and also confirms the assumption of actin itself as a main parameter regulating CDR dynamics. Moreover, the model also provides predictions concerning a correlation between the stimulus threshold for propagating wavefronts and the total amount of actin (A). This confirms the supposition that a heightened threshold for propagating wavefronts due to a degradation of the total amount of actin affects longer CDR periodicities and therefore also longer CDR lifetimes.

The following chapters focus in the same way on the influence of the macromolecules PIP_3 (Chapter 7) and N-WASP (Chapter 8) on CDR initiation and propagation. These two types of macromolecules are, apart of actin itself, of particular importance because they are also supposed to play a fundamental role in the underlying wave machinery by regulating actin organization [Bernitt et al., 2017].

7 Influence of PIP_3 on CDR Formation and Propagation

CDRs are ring-shaped protein density waves consisting of branched actin. A depletion of stress fibers in the CDR interior was observed by Bernitt [Bernitt, 2015]. In the previous chapter, the direct regulation of CDR formation and propagation by actin itself was demonstrated (see Chapter 6). Moreover, it is now necessary to examine the inhibition of actin polymerization in the CDR interior, that is supposed to be influenced by the phosphoinositide PIP_3 and the Arf GAP ARAP1 [Bernitt et al., 2017].

PIP_3 seems to play a key role in actin wave formation. It is known to localize to the CDR interior and disfavores the incorporation of actin into CDRs [Hoeller et al., 2013, DiPaolo and Camilli, 2006, Bernitt et al., 2017]. Moreover, it stimulates the Arf GAP ARAP1, which is assumed to regulate CDR ring sizes [Campa et al., 2009, Hasegawa et al., 2012]. In this context, a major player in phoyphorylation of PIP_2 ($PtdIns(4,5)P_2$) to PIP_3 at the third position of the phosphoinositol ring is PI3K. In contrast to PIP_3, PIP_2 is known to activate N-WASP, a major nucleator of actin filaments (see Chapter 8) and affect dissociation of the capping proteins capZ and gelsolin [DiPaolo and Camilli, 2006].

Moreover, phosphoinositides and their associated kinases and phosphatases are also localized to actin waves in *Dictyostelium* and macrophages [Gerisch et al., 2009, Gerisch et al., 2011, Masters et al., 2016]. Similar to CDRs in fibroblasts, PIP_3 patches surrounded by a propagating actin front occur in *Dictyostelium*. The interrelation between actin waves and PIP_3 patches also led to an interpretation of actin waves in the context of a bistable regime, whereas in former studies these actin waves were mainly interpreted as waves in an excitable system [Gerisch et al., 2011, Gerisch et al., 2009]. Furthermore, a bistable regime of a system was also suggested for actin waves in macrophages, in which a polarization was not induced by an association of actin waves with PIP_3 patches, but with $PI(3,4)P_2$ in their interior [Masters et al., 2016].

This chapter examines the influence of PIP_3 on the formation and propagation of CDRs. Therefore, Wortmannin is used as a biochemical compound to affect PIP_3 through inhibition of PI3K, an enzyme that catalyzes the phosphorylation of PIP_2 to PIP_3. Due to the localization of PIP_3 in the CDR interior and the association with ARAP1, there is the presumption that inhibition of PIP_3 could affect CDR ring sizes (see Section 7.1). Moreover, the dependence of CDR lifetimes, velocities and periodicities

(see Section 7.2, 7.3 & 7.4) are investigated in detail to uncover a direct influence of PIP_3 on CDR propagation as it is the case for actin itself.

7.1 Effects of inhibition of PIP_3

To identify the influence of PIP_3 on the formation and propagation of CDRs, experiments with Wortmannin of three different concentrations (0.5 µM, 1.0 µM and 1.5 µM) were performed. They were run over 2 hours, in which CDR dynamics were observed over 60 minutes under physiological conditions before adding Wortmannin and further 60 minutes after adding Wortmannin. In experiments with a lower concentration of 0.5 µM Wortmannin, the majority of fibroblasts did not display a change in CDR dynamics with added Wortmannin (Fig. 7.1 a1 & a2). In some cases, one might assume, that CDR lifetimes will be shorter after adding Wortmannin indicated by smaller fragments or more spotted kymograph patterns (Fig. 7.1 a3 & a4). In experiments with a higher Wortmannin concentration of 1.0 µM, the same results become apparent. There are examples of propagating CDRs showing no obvious change after adding 1.0 µM Wortmannin (Fig. 7.1 b1 & b2), but in contrast, other examples show an apparent effect of Wortmannin on CDR dynamics. In these cases, CDRs exhibited shorter lifetimes after adding Wortmannin and collapsed shortly after emerging without propagation (Fig. 7.1 b3 & b4). This change in CDR dynamics is visualized by a change in kymograph patterns from line patterns to more fragmented and spotted patterns. This effect seems amplified by a higher Wortmannin concentration of 1.5 µM Wortmannin. However, also in this case some fibroblasts show only shorter CDR lifetimes after adding 1.5 µM Wotmannin visualized by shorter fragments or lines in kymograph patterns (Fig. 7.1 c1 & c2). In contrast, other fibroblasts sparsely formed CDRs appearing for a very short time after adding Wortmannin visualized by small dots in kymograph patterns (Fig. 7.1 c3 & c4).

These observations are in line with results from experiments in the context of actin waves treating *Dictyostelium* and macrophages with the PI3K inhibitor LY-294002, that suppressed the phosphorylation of PIP_2 to PIP_3 [Gerisch et al., 2009, Masters et al., 2016]. In both studies, an inhibition of PI3K and thus a suppression of PIP_3 led to a rapid collapse of actin waves. This leads to the conclusion that PI3K affects actin wave formation in macrophages, in *Dictyostelium* and moreover, as shown in this study, also in fibroblasts. Despite these similar effects, the role of PI3K and its product PIP_3 in the underlying wave machinery of these different actin waves seems to be different. In *Dictyostelium*, a polarization between interior and exterior of actin waves due to different concentrations of PIP_3 was found, however, in macrophages different concentrations of $PI(3,4)P_2$ were observed. In this study, a similar role of PIP_3 in actin wave formation in fibroblasts and *Dictyostelium* is presumed, based on the proposed model of Bernitt et al [Bernitt et al., 2017].

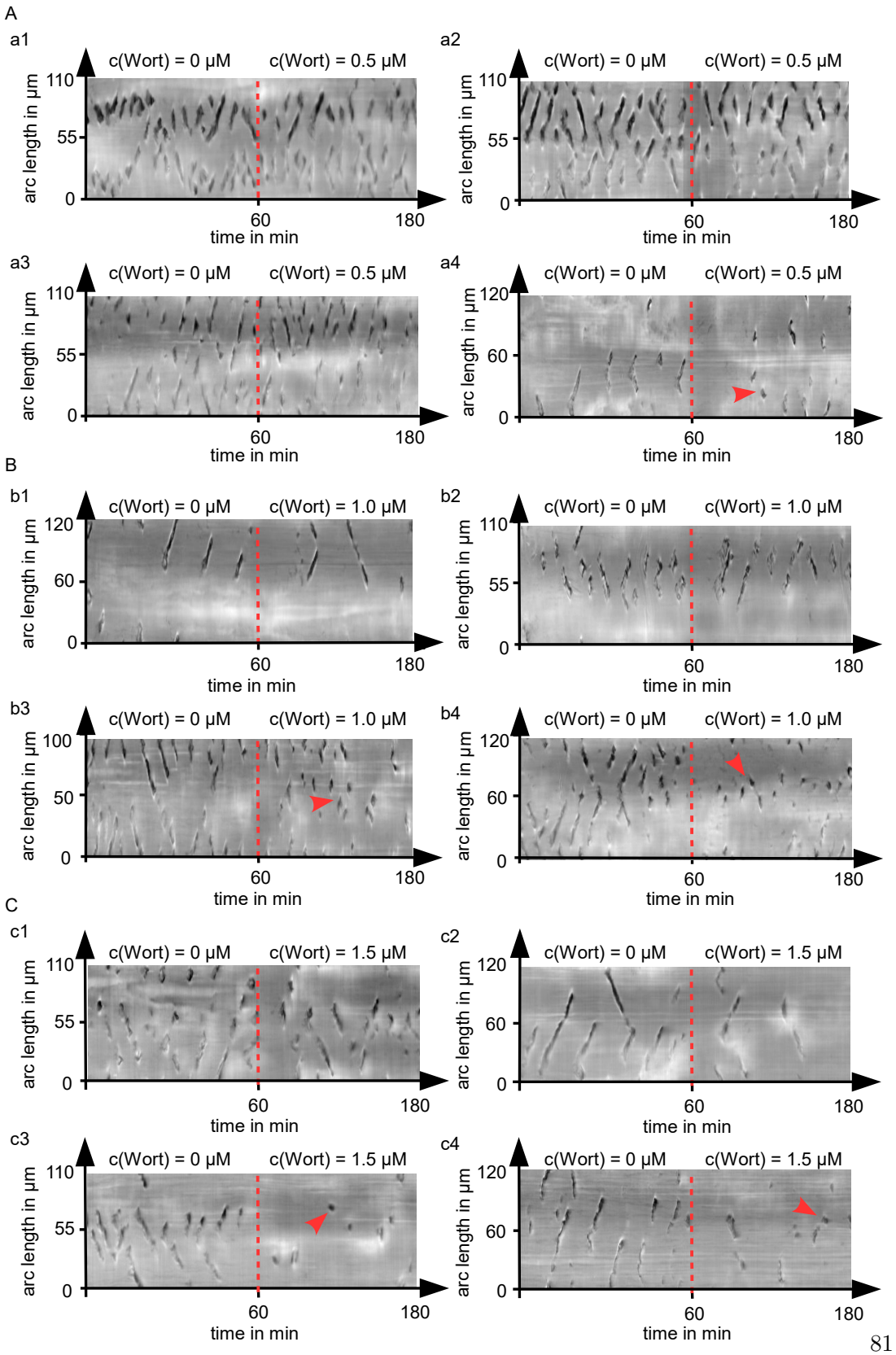

Figure 7.1: Examples of kymographs from fibroblasts treated with Wortmannin. Kymographs show CDR dynamics 60 minutes before and 60 minutes after adding Wortmannin. The medium exchange is visualized by red dashed lines. Panel A shows examples of kymographs from fibroblasts treated with $0.5\,\mu M$ Wortmannin, panel B with $1.0\,\mu M$ Wortmannin and panel C with $1.5\,\mu M$ Wortmannin, respectively. Red arrowheads highlight examples of shorter lines or dots after adding Wortmannin.

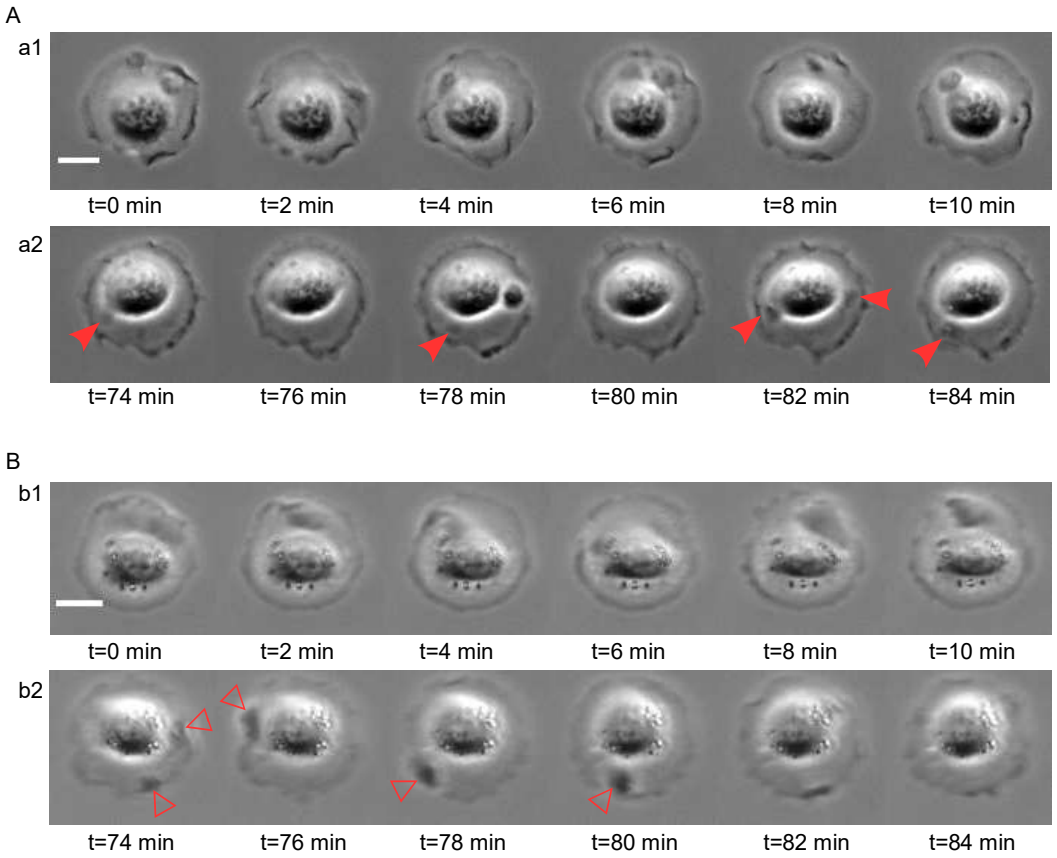

Figure 7.2: CDR formation in fibroblasts treated with Wortmannin. A shows a time series of micrographs of a fibroblasts forming CDRs before (a1) and after (a2) adding $1\,\mu M$ Wortmannin. Red filled arrowheads inidicate sparcely formed CDRs. B presents a time series of micrographs of a fibroblasts forming CDRs before (b1) and after (b2) adding $1.5\,\mu M$ Wortmannin. Red unfilled arrowheads inidicate smaller formed CDRs than before adding Wortmannin. The corresponding kymographs of CDR dynamics of A and B are shown in Fig. 7.1 b4 & c2, respectively. Scale bars are $20\,\mu m$.

Moreover, comparing the sizes of CDRs before and after adding Wortmannin, it was observed that CDR sizes decreased after adding Wortmannin (see Fig. 7.2), but different sizes of CDRs in different fibroblasts were observed. Sometimes CDRs were only sparsely formed and did not propagate (see Fig. 7.1 b4 and 7.2 A), in contrast, other CDRs with decreased sizes were still able to propagate over longer distances (see Fig. 7.1 c2 and 7.2 B). This leads to the suggestion, that lifetimes are coupled to CDR sizes, because the front propagates every time with nearly the same speed independent of the maximal ring size. This coupling seems to be evident for smaller CDRs, that expand slightly until they split up after collisions with the cellular boundaries and propagate along the

nucleus. For larger CDRs, it is assumed that there is no correlation between CDR ring sizes and their lifetimes.

Considering the similar localization of PIP_3 in the interior of actin waves in fibroblasts compared to *Dictyostelium* as described by Gerisch et al. [Gerisch et al., 2009], it seems to be evident that CDR sizes are determined by the amount of PIP_3. This leads to the hypothesis of similar interaction between PIP_3 and actin waves in *Dictyostelium* as presumed by Gerisch et al. [Gerisch et al., 2009]. They pointed out the coupling of actin wave formation to a steep PIP_3 gradient. This was considered in the context of an excitable system, whereas Bernitt et al. proposed similar interactions between actin waves and PIP_3 patches in fibroblasts in the context of a bistable regime [Bernitt et al., 2017]. In this regard, PIP_3 is known to disfavores the incorporation of actin in the interior of CDRs [Hoeller et al., 2013, DiPaolo and Camilli, 2006].

Moreover, the results from this study also seem to be consistent with results from Hasegawa et al. [Hasegawa et al., 2012]. They detected a dependence of the CDR ring shape in fibroblasts on the Arf GAP ARAP1 and its products Arf1 and Arf5. Due to a knockdown of ARAP1, decreased ring sizes were found. Moreover, it was detected that ARAP1 is stimulated by binding of phosphoinositides, particularly PIP_3 [Campa et al., 2009]. It seems to be evident that a decrease in the PIP_3 amount also leads to a decrease in the ARAP1 activity and therefore to decreased CDR ring sizes.

7.2 Suppression of PIP_3 leads to shorter lifetimes of CDRs

To quantify the observed effect of decreased lifetimes after adding Wortmannin, average lifetimes of CDRs in the same fibroblasts were measured before and after adding Wortmannin. Comparing the distributions of CDR lifetimes before and after adding Wortmannin, for all three inhibitor concentrations the peaks of the distributions after adding Wortmannin are shifted to lower lifetimes (Fig. 7.3 A). Consequently, decreased mean lifetimes after adding Wortmannin were found compared to the state before adding Wortmannin (see Table 7.1). Comparing the absolute differences in mean CDR lifetimes before and after adding Wortmannin in the same fibroblasts, nearly all fibroblasts exhibited decreased CDR lifetimes after adding Wortmannin for all three different Wortmannin concentrations (Fig. 7.3 B). The absolute differences in CDR lifetimes before and after adding Wortmnannin are statistically significant at a significance level of 10% for the data with 0.5 µM Wortmannin, 2% for the data with 1.0 µM Wortmannin and 5% for the data with 1.5 µM Wortmannin.

This leads to the conclusion that a reduction of PIP_3 results in a decrease in CDR lifetimes. It seems to be a reversed effect to the depletion of total available actin (see Chaper 6.2), where it has been shown that a decrease in total available actin leads to longer lifetimes of CDRs. This became apparent from kymograph patterns due to

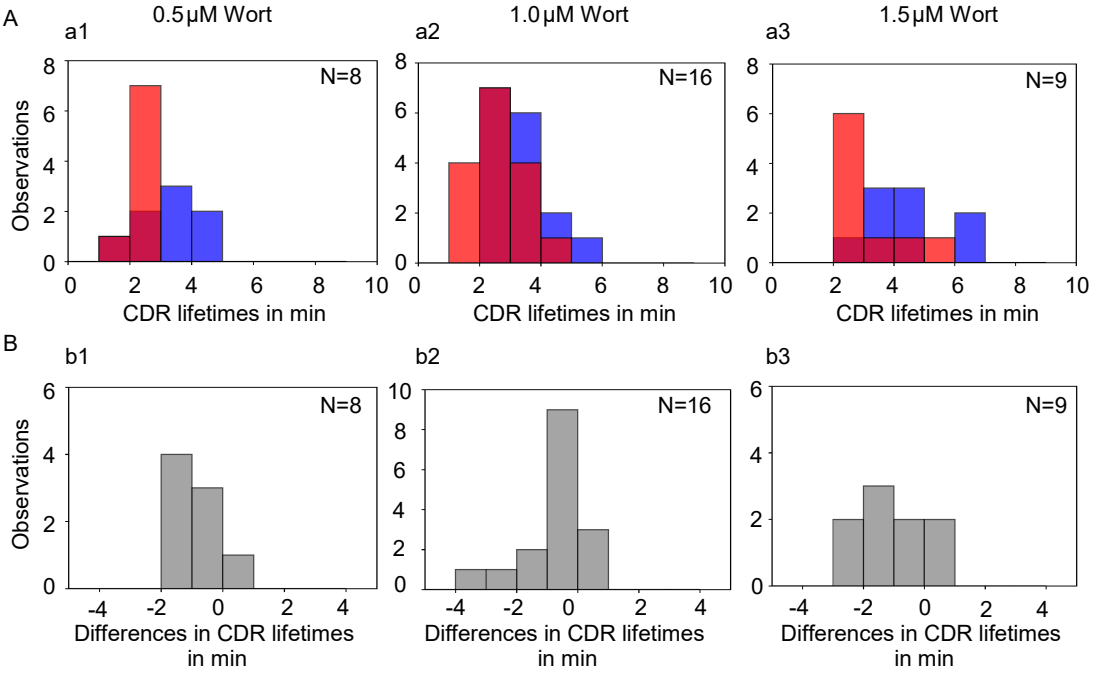

Figure 7.3: Histograms of CDR lifetimes before and after adding Wortmannin. A shows histograms of average CDR lifetimes before (blue) and after (red) adding Wortmannin in concentrations of 0.5 µM (a1), 1.0 µM (a2) and 1.5 µM (a3). B visualizes absolute differences in average lifetimes between before and after adding Wortmannin in the same fibroblast for Wortmannin concentrations of 0.5 µM (b1), 1.0 µM (b2) and 1.5 µM (b3). N indicates the number of analyzed fibroblasts.

a transition from dotted to line patterns (see Fig. 6.3). This effect increased with time and thus with a decrease in total available actin. However, in these experiments the effect of a decrease in CDR lifetimes seems to be independent of the Wortmannin concentration in the range between 0.5 µM and 1.5 µM, but it is believed that this is due to the relative small number of samples, especially for Wortmannin concentrations of 0.5 µM and 1.5 µM.

7.3 Velocities of CDRs are reduced after suppression of PIP_3

To characterize CDR dynamics after a suppression of PIP_3, similar to CDR lifetimes, average CDR velocities over 60 minutes before and over 60 minutes after adding Wortmannin with concentrations of 0.5 µM, 1.0 µM and 1.5 µM were measured. Analysing 8 fibroblasts treated with 0.5 µM Wortmannin, there is no change in average CDR velocities over 60 minutes after adding Wortmannin compared to over 60 minutes before

Table 7.1: Mean values of average CDR lifetimes (± SE) with different biochemical conditions due to the biochemical compound Wormannin, in 8 different fibroblasts with an inhibitor concentration of $0.5\,\mu M$, 16 different fibroblasts with $1.0\,\mu M$ and 9 different fibroblasts with $1.5\,\mu M$.

c(Wortmannin)	-Wortmannin	+Wortmannin
$0.5\,\mu M$	$3.6 \pm 0.3\,min$	$2.7 \pm 0.1\,min$
$1.0\,\mu M$	$3.2 \pm 0.2\,min$	$2.6 \pm 0.1\,min$
$1.5\,\mu M$	$4.1 \pm 0.5\,min$	$3.1 \pm 0.3\,min$

adding Wortmannin. The CDR velocities before and after adding $0.5\,\mu M$ Wortmannin are nearly similarly distributed (see Fig. 7.4 a1 and Table 7.2) as well as the absolute differences in CDR velocities between before and after adding $0.5\,\mu M$ Wortmannin in the same fibroblasts are distributed around a mean value of $0\,\mu m\,s^{-1}$ (see Fig. 7.4 b1).

Table 7.2: Mean values of average CDR velocities (± SE) with different biochemical conditions due to the biochemical compound Wormannin, in 8 different fibroblasts with an inhibitor concentration of $0.5\,\mu M$, 14 different fibroblasts with $1.0\,\mu M$ and 7 different fibroblasts with $1.5\,\mu M$.

c(Wortmannin)	-Wortmannin	+Wortmannin
$0.5\,\mu M$	$0.13 \pm 0.01\,\mu m\,s^{-1}$	$0.13 \pm 0.01\,\mu m\,s^{-1}$
$1.0\,\mu M$	$0.13 \pm 0.01\,\mu m\,s^{-1}$	$0.11 \pm 0.01\,\mu m\,s^{-1}$
$1.5\,\mu M$	$0.13 \pm 0.01\,\mu m\,s^{-1}$	$0.11 \pm 0.01\,\mu m\,s^{-1}$

In contrast, in fibroblasts treated with higher Wortmannin concentrations of $1.0\,\mu M$ and $1.5\,\mu M$ there is an apparent decrease in average CDR velocities after adding Wortmannin compared to the state before adding Wortmannin (see Table 7.2). The distributions of average CDR velocities after adding Wortmannin are shifted to slower CDR velocities compared to the corresponding distributions of CDR velocities before adding Wortmannin (Fig. 7.4 a2 & a3). In addition, the distributions of absolute differences in CDR velocities before and after adding Wortmannin demonstrate a decrease in CDR velocities after adding Wortmannin in most fibroblasts. The absolute differences in CDR velocities before and after adding Wortmannin with a concentration of $1.0\,\mu M$ are statistically significant at a significance level of 1% and with $1.5\,\mu M$ at a significance level of 5%.

This leads to the conclusion that the activity of PIP_3 affects CDR velocities but only in a weak manner unaffected by higher inhibitor concentrations of PI3K. However, the total amount of actin was found to influence CDR velocities massively and thus to regulate them directly (see Chapter 6). In conclusion it was found, that PIP_3 plays a

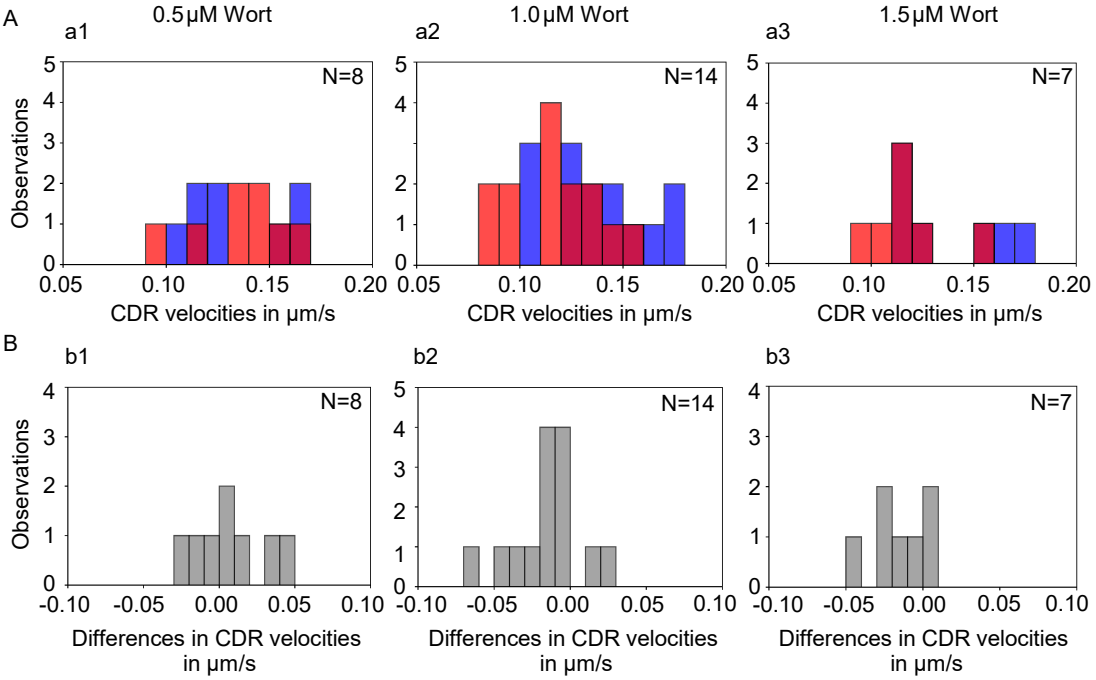

Figure 7.4: Histograms of CDR velicities before and after adding Wortmannin. A shows histograms of average CDR velocities before (blue) and after (red) adding Wortmannin in concentrations of $0.5\,\mu M$ (a1), $1.0\,\mu M$ (a2) and $1.5\,\mu M$ (a3). B visualizes absolute differences in average CDR velocities between before and after adding Wortmannin in the same fibroblast for Wortmannin concentrations of $0.5\,\mu M$ (b1), $1.0\,\mu M$ (b2) and $1.5\,\mu M$ (b3). N indicates the number of analyzed fibroblasts.

crucial role in regulating CDR formation and ring sizes, but it only weakly affects their propagation.

7.4 PIP_3 does not affect CDR periodicities

To complete the investigation of the influence of PIP_3 on CDR dynamics, CDR periodicities over 60 minutes before and over 60 minutes after adding Wortmannin for the same three concentrations as described above ($0.5\,\mu M$, $1.0\,\mu M$ and $1.5\,\mu M$) were analyzed. In contrast to CDR velocities and lifetimes, CDR periodicities seem to be unaffected by a suppression of PIP_3. No change in distributions of CDR periodicities after adding Wortmannin compared to before adding Wortmannin neither in 8 fibroblasts treated with a small concentration of $0.5\,\mu M$ Wortmannin, nor in 12 fibroblasts treated with a higher concentration of $1.0\,\mu M$ or 7 fibroblasts treated with $1.5\,\mu M$ were observed (see Fig. 7.5 A). Consequently, also the mean values of the distributions before and after adding

Wortmannin are nearly identical. They amount to 5.4 ± 0.5 min and 5.1 ± 0.4 min before and after adding 0.5 µM Wortmannin, 5.8 ± 0.2 min and 5.7 ± 0.4 min (1.0 µM Wortmannin) and 7.3 ± 0.4 min as well as 7.3 ± 0.6 min (1.5 µM Wortmannin), respectively. Furthermore, no statistical significance of the absolute differences before and after adding Wortmannin for all three concentrations were found (shown in Fig. 7.5 B).

Table 7.3: Mean values of average CDR periodicities (± SE) with different biochemical conditions due to the biochemical compound Wormannin, in 8 different fibroblasts with a concentration of 0.5 µM, 16 different fibroblasts with a concentration of 1.0 µM and 9 different fibroblasts with a concentration of 1.5 µM.

c(Wortmannin)	-Wortmannin	+Wortmannin
0.5 µM	5.4 ± 0.5 min	5.1 ± 0.4 min
1.0 µM	5.8 ± 0.2 min	5.7 ± 0.4 min
1.5 µM	7.3 ± 0.4 min	7.3 ± 0.6 min

This leads to the conclusion that PIP_3 does not influence CDR periodicities. Comparing these results to the results from experiments with Jasplakinolide, in which the total amount of actin was decreased, a strong dependence of CDR velocities and periodicities on the total amount of actin was found (Chapter 6). It confirms the hypothesis that actin directly affects CDR formation and propagation, whereas PIP_3 only weakly affects CDR propagation in contrast to CDR formation and their ring sizes.

7.5 Summary

To sum up, this chapter focused on the influence of PIP_3 in CDR formation and propagation. Therefore, the PI3K inhibitor Wortmannin was used to suppress the phosphorylation of PIP_2 to PIP_3. It was found, that CDRs emerged with shorter lifetimes and smaller ring sizes. This is in line with results by Hasegawa et al. that demonstrated a dependence of CDR ring sizes on the Arf GAP ARAP1, which is stimulated by PIP_3 [Hasegawa et al., 2012, Campa et al., 2009]. Furthermore, it leads to the proposition that PIP_3 affects actin wave formation in fibroblasts, which was also known for actin waves in *Dictyostelium* and macrophages [Gerisch et al., 2009, Masters et al., 2016]. However, the role of PIP_3 seems to be distinct in different kinds of actin waves in various cell types.

Due to these and previous results, it is assumed that PIP_3 is localized in the CDR interior in fibroblasts and the interior of actin waves in *Dictyostelium* [Gerisch et al., 2009]. It leads to the conclusion that actin waves can be seen as propagating wavefronts in a bistable regime of two stable actin states, that are interrelated with different phosphoinositide concentrations [Gerisch et al., 2011, Bernitt et al., 2017]. The assumption

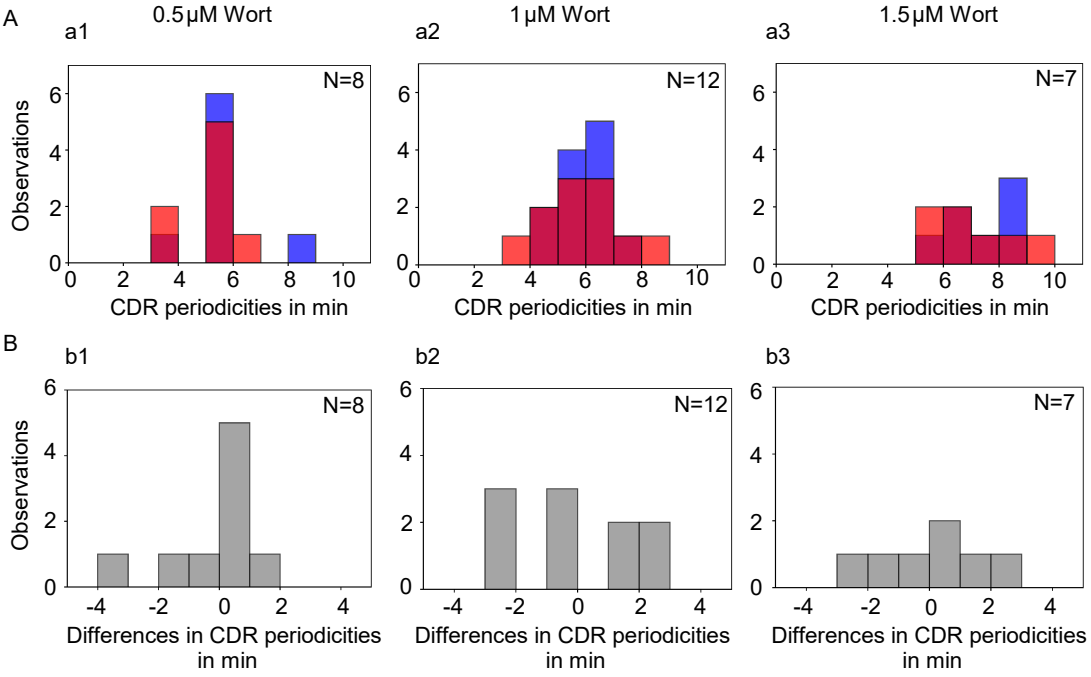

Figure 7.5: Histograms of CDR lifetimes before and after adding Wortmannin. A shows histograms of CDR periodicities before (blue) and after (red) adding Wortmannin in concentrations of $0.5\,\mu M$ (a1), $1.0\,\mu M$ (a2) and $1.5\,\mu M$ (a3). B visualizes absolute differences in CDR periodicities between before and after adding Wortmannin in the same fibroblast for Wortmannin concentrations of $0.5\,\mu M$ (b1), $1.0\,\mu M$ (b2) and $1.5\,\mu M$ (b3). N indicates the number of analyzed fibroblasts.

of wavefronts in a bistable regime is similar for actin waves in macrophages, but in contrast to fibroblasts or *Dictyostelium* a localization of $PI(3,4)P_2$ instead of PIP_3 in the interior of actin waves was observed.

Moreover, comparing the CDR velocities and periodicities before and after adding the PI3K inhibitor, only a slight dependence of CDR velcocities on the PIP_3 activity and no correlation between CDR periodicities and the PIP_3 activity was found. This leads to the conclusion, that in contrast to actin itself, there is no direct regulation of PIP_3 on CDR propagation.

8 Inhibition of Arp2/3-Mediated Actin Nucleation

Among actin itself, Arp2/3 and its mediated nucleation of actin filaments play a fundamental role in creating branched actin. Actin nucleation promoting factors, of which N-WASP is a prominent example, are required to link upstream signals to the cytoskeleton and activate the Arp2/3-complex [Takenawa and Miki, 2001]. In this context, it seems to be evident that Arp2/3 and N-WASP are crucial for CDR formation. Different studies demonstrated a localization of Arp2/3 and N-WASP in CDRs [Buccione et al., 2004, Hoon et al., 2012]. Futhermore, a direct involvement in CDR formation and also in other type of actin waves was proven by using an inhibitor of N-WASP or Arp2/3 or by knocking down these proteins [Legg et al., 2007, Masters et al., 2016].

This chapter focuses on the role of N-WASP in CDR propagation. Different studies proposed the influence of N-WASP and Arp2/3 on CDR propagation, for example, Zeng et al. postulated a reduction of the CDR amount due to an inhibition of Arp2/3. They modeled the interplay between Rac and Rho leading to traveling CDRs, where Rac could not effect Arp2/3 nucleation of actin if it was inhibited [Zeng et al., 2011]. A model by Peleg et al. proposed the Arp2/3-activator N-WASP within a protein complex together with a concave curved membrane protein, like Tuba, leading to traveling waves due to an interplay with convex membrane protein complexes [Peleg et al., 2011]. Moreover, also Bernitt et al. assumed an influence of N-WASP within their model of CDR propagation in a bistable regime. They presumed that N-WASP causes de novo formation of actin filaments and leads to positive feedback loops [Bernitt et al., 2017].

In this chapter, the influence of Arp2/3-mediated actin nucleation on the initiation and propagation of CDRs is examined. Therefore, N-WASP is affected by Wiskostatin, a biochemical compound binding directly to N-WASP in a reversible manner and stabilizing its native autoinhibited conformation [Peterson et al., 2004]. Wiskostatin concentrations are chosen low enough, so that CDRs reappear and CDR formation is not completely inhibited for the duration of the whole experiments. The effect of N-WASP inhibition on CDR dynamics is investigated in a quantitative manner, so that CDR lifetimes, velocities and periodicities are measured (see Section 8.2, & 8.3). The question, whether a decrease in N-WASP activity leads to a reduction in CDR velocity and therefore N-WASP directly regulates CDR propagation in a similar fashion as actin itself will be of particular focus. Furthermore, the effect of CDR reappearence without a Wiskostatin washout is examined by a quantitative investigation of CDR lifetimes

directly after CDR reformation and their recovery time dependent on the Wiskostatin concentration (see Section 8.1, 8.2 & 8.4).

8.1 Inhibition of N-WASP leads to a disappearance and reappearence of CDRs

To identify the role of N-WASP on CDR formation and propagation, experiments with Wiskostatin were carried out in a way that during a runtime of two hours every 30 minutes the cell culture medium was replaced by cell culture medium with added Wiskostatin, and vice versa. This led to four time intervals with different biochemical environments for fibroblasts in the same experiment, in which the fibroblasts were either observed under physiological conditions (from 0 to 30 minutes and 60 to 90 minutes after starting the experiment) or under changed biochemical conditions due to Wiskostatin (from 30 to 60 minutes and 90 to 120 minutes). Fibroblasts treated with 1 µM Wiskostatin (Fig. 8.1) showed no obvious systematic change in kymograph patterns, like elongated, shortened or unstructured lines, compared to changes in CDR dynamics after reducing the total amount of actin or inhibiting PIP_3 (see Chapter 6 & 7). In contrast, directly after adding 1 µM Wiskostatin, CDR formation seemed to be inhibited for a short time period until CDRs reappeared. This time period is referred to as "recovery time" and should not be confused with normal periodicity of CDRs. After the recovery time has elapsed, the first reappearing CDRs were mostly split into two twin pulses and showed longer lifetimes and traveling distances compared to the next emerging CDRs or CDRs that had emerged before adding Wiskostatin (see Fig. 8.1 B-G). This effect was particularly pronounced after adding Wiskostatin for the first time (after 30 minutes), but occured more rarely after adding Wiskostatin for the second time (after 90 minutes).

Fibroblasts treated with a higher concentration of 2 µM Wiskostatin showed the same effects as fibroblasts treated with 1 µM Wiskostatin (see Fig. 8.2). However, the recovery time after adding Wiskostatin until CDRs reappeared seemed to increase compared to the recovery time of CDRs after adding 1 µM Wiskostatin. In many cases, the recovery time after adding 2 µM Wiskostatin seemed to be larger than the observed time interval of 30 minutes, so a complete suppression of CDR formation was observed (see Fig. 8.2 G & H). In contrast, the effects of longer CDR lifetimes and the occurence of twin pulses seemed to be less frequent compared to fibroblasts treated with a lower Wiskostatin concentration.

These results are in line with experimental observations of Masters et al. investigating the behavior of actin waves in macrophages after treatment with 5 µM Wiskostatin [Masters et al., 2016]. They observed a collapse of actin waves rapidly after addition of Wiskostatin similar to observations in fibroblasts (see Fig. 8.1 and 8.2). In contrast, they did not find a spontaneous reapparence of actin wave formation in macrophages, but also observed a reformation of actin waves after a washout of Wiskostatin. This

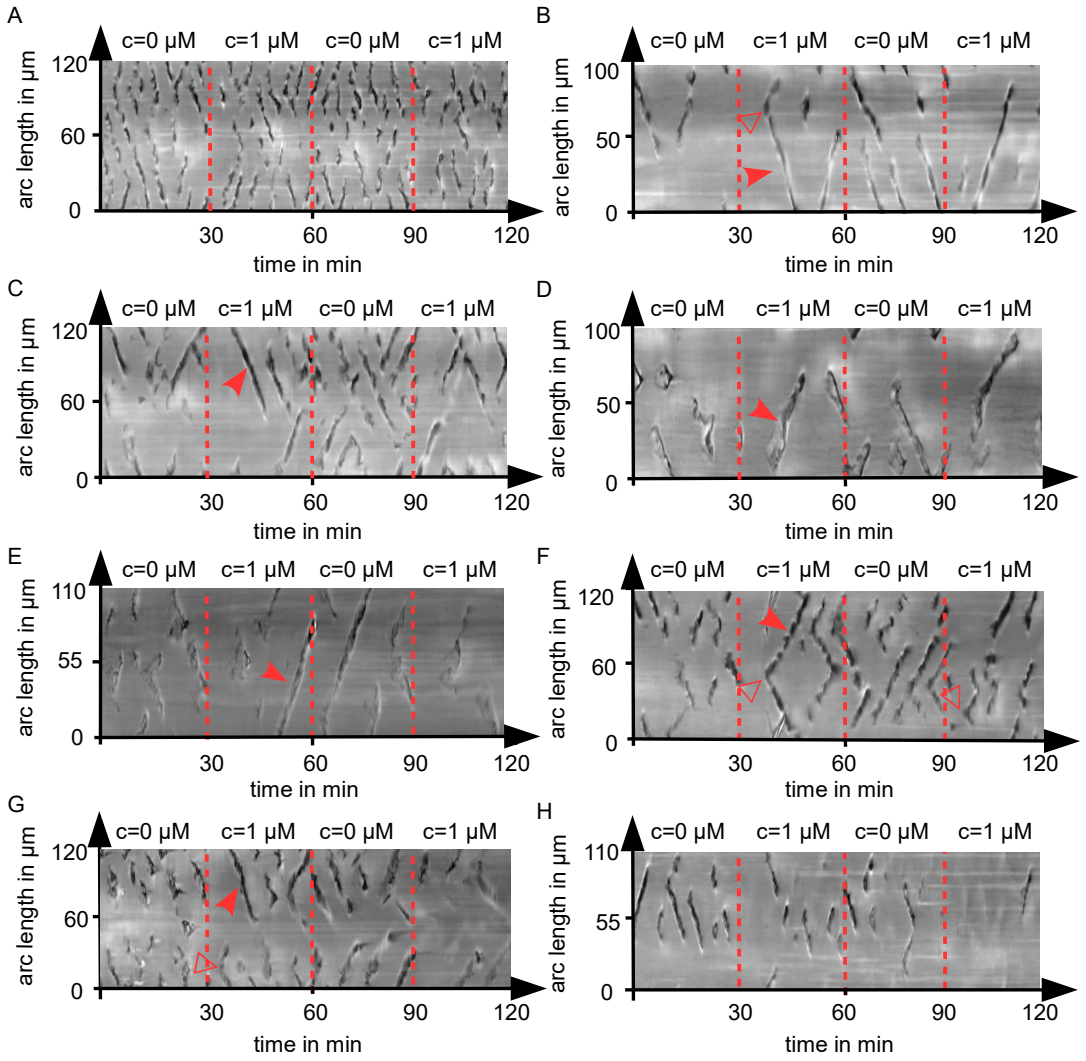

Figure 8.1: Examples of kymographs from fibroblasts treated with $1\,\mu M$ Wiskostatin. A-H show examples of kymographs from eight different fibroblasts underlying a change of their biochemical environment. Red dashed lines visualize the medium exchange between DMEM (concentration of Wiskostatin $c = 0\,\mu M$) and DMEM with added Wiskostatin ($c = 1\,\mu M$). Red filled arrowheads indicate longer lines in kymograph patterns, whereas unfilled red arrowheads highlight "<"-patterns in both cases after adding Wiskostatin.

is speculated to be due to a higher Wiskostatin concentration of $5\,\mu M$, utilized in their experiments with macrophages, in contrast to $1\,\mu M$ or $2\,\mu M$ in experiments with fibroblasts in this work and a much lower time period between addition and washout of Wiskostatin within two minutes (see also Section 8.4).

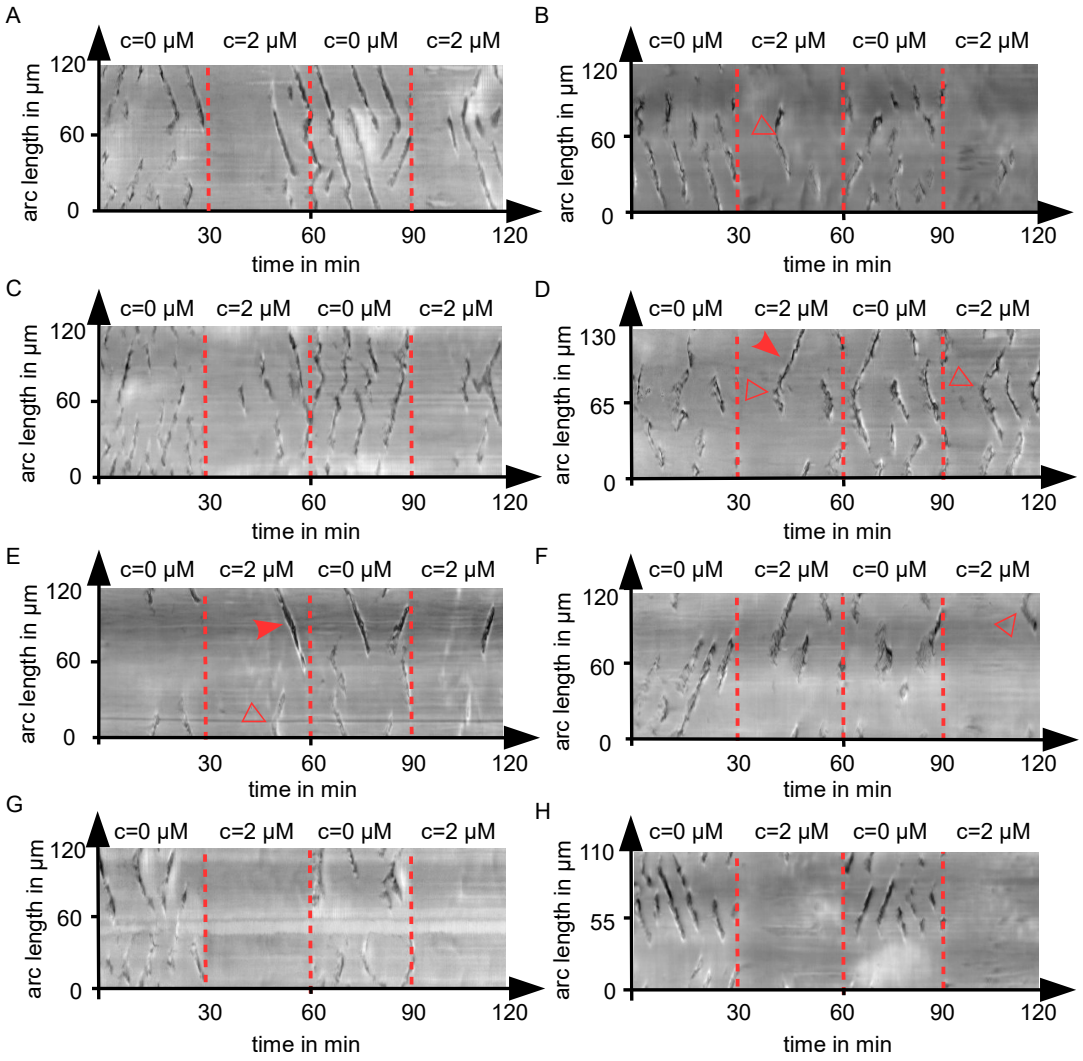

Figure 8.2: Examples of kymographs from fibroblasts treated with $2\,\mu M$ Wiskostatin. A-H show examples of kymographs from eight different fibroblasts underlying a change of their biochemical environment. Red dashed lines visualize the medium exchange between DMEM (named by the concentration of Wiskostatin $c = 0\,\mu M$) and DMEM with added Wiskostatin ($c = 2\,\mu M$). Red filled arrowheads indicate longer lines in kymograph patterns, whereas unfilled red arrowheads highlight "<"-patterns in both cases after adding Wiskostatin.

To quantify the observations from kymographs, the following sections will present an analysis of CDR lifetimes (Section 8.2), CDR velocities and periodicities (Section 8.3) as well as recovery times (Section 8.4).

8.2 Changes of CDR lifetimes after adding Wiskostatin

To analyze the influence of Wiskostatin and thus the influence of the inhibition of N-WASP on CDR lifetimes, average CDR lifetimes were calculated for all four time sections with different biochemical conditions (-Wisko: 0 to 30 minutes, +Wisko: 30 to 60 minutes, -Wisko: 60 to 90 minutes and +Wisko: 90 to 120 minutes) separately in several fibroblasts (Fig. 8.3 A). Comparing average CDR lifetimes in 16 fibroblasts between these four time sections of different biochemical conditions, an increase in CDR lifetimes after adding 1 µM Wiskostatin in both cases (after 30 minutes and after 90 minutes) was found, as well as a decrease of CDR lifetimes after a washout of 1 µM Wiskostatin (after 60 minutes). Mean values of average CDR lifetimes (± SE) were listed in Table 8.1. The differences in average CDR lifetimes in the same fibroblasts between two successive time sections also showed a predominant increase in CDR lifetimes after adding 1 µM Wiskostatin the first time (after 30 minutes) as well as a decrease in CDR lifetimes after a washout of 1 µM Wiskostatin (after 60 minutes) (Fig. 8.3 b1). In both cases, the differences in CDR lifetimes between the two successive time intervals are statistically significant (significance levels of 0.1 % and 0.5 %). In contrast, the slight increase of CDR lifetimes after adding 1 µM Wiskostatin the second time (after 90 minutes) is not statistically significant.

Table 8.1: Mean values of averaged CDR lifetimes (± SE) for four time sections with different biochemical conditions in 16 different fibroblasts in experiments with 1 µM Wiskostatin and 13 different fibroblasts in experiments with 2 µM Wiskostatin.

	-Wiskostatin (0 to 30 min)	+Wiskostatin (30 to 60 min)	-Wiskostatin (60 to 90 min)	+Wiskostatin (90 to 120 min)
1 µM	4.4 ± 0.6 min	6.4 ± 0.7 min	5.0 ± 0.6 min	5.5 ± 0.8 min
2 µM	4.1 ± 0.5 min	4.9 ± 0.6 min	4.3 ± 0.6 min	3.8 ± 0.8 min

However, comparing average CDR lifetimes of the four time sections with different biochemical conditions of 13 fibroblasts treated with 2 µM Wiskostatin, there was a smaller increase in averaged CDR lifetimes after adding 2 µM Wiskostatin the first time (after 30 minutes) compared to data from experiments with 1 µM Wiskostatin (see Table 8.1 and Fig. 8.3 a2). The differences between the average CDR lifetimes before and after adding Wiskostatin are predominantly positive (see Fig. 8.3 b2) and also tested out to be statistically significant (significance level of 2 %). In contrast, the slight decrease of averaged CDR lifetimes after a washout of 2 µM Wiskostatin is not statistically significant. Moreover, in comparison to the data of experiments with a Wiskostatin concentration of 1 µM, also a decrease instead of an expected increase in average CDR lifetimes after adding 2 µM Wiskostatin for the second time was observed (Fig. 8.3 b2).

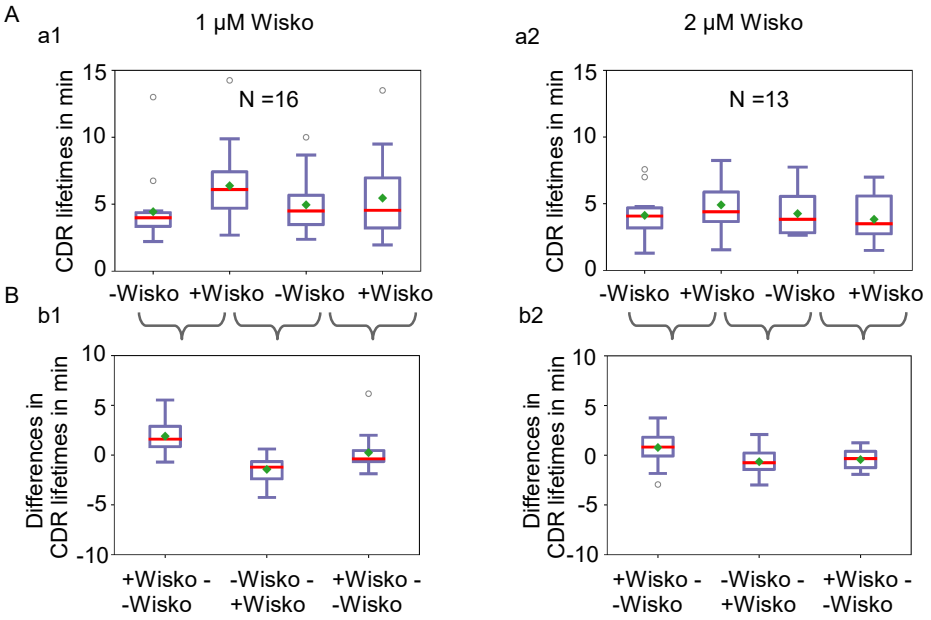

Figure 8.3: Boxplots of CDR lifetimes of fibroblasts treated with Wiskostatin. Boxplots in A show CDR lifetimes of fibroblasts treated with 1 µM (a1) and 2 µM (a2) Wiskostatin for all four time periods with alternating biochemical conditions of DMEM or DMEM with added Wiskostatin. In B differences in CDR lifetimes between two successive time periods from A are presented. N indicates the number of analyzed fibroblasts.

The measured average CDR lifetimes and their changes after adding Wiskostatin are in line with observations from kymographs described in Section 8.1. Kymographs transiently exhibited elongated line patterns resulting from CDRs which directly emerged after the recovery time after adding Wiskostatin for the first time (after 30 minutes). These elongated lifetimes, on the one hand, can be a result of the fact that CDRs cannot interact with existing ones due to collisions, or long-range interactions because of a limiting species like the total actin concentration, or a mechanical factor, like the membrane tension. On the other hand, they are speculated to be due to a recovery of the underlying substrate because it was observed that an inhomogenity of the underlying substrate encouraged CDR formation in distinct regions (see Chapter 5). This is in line with results of Masters et al. observing a recovery of the PIP_2 concentration and a recovery of the cell cortex, that is depleted in the interior of actin waves after a washout of Wiskostatin in macrophages [Masters et al., 2016].

However, this effect was observed more often in fibroblasts treated with 1 µM than with 2 µM Wiskostatin (Fig. 8.1 & 8.2) which leads to an increase in average CDR lifetimes, that is higher in fibroblasts treated with 1 µM than with 2 µM Wiskostatin.

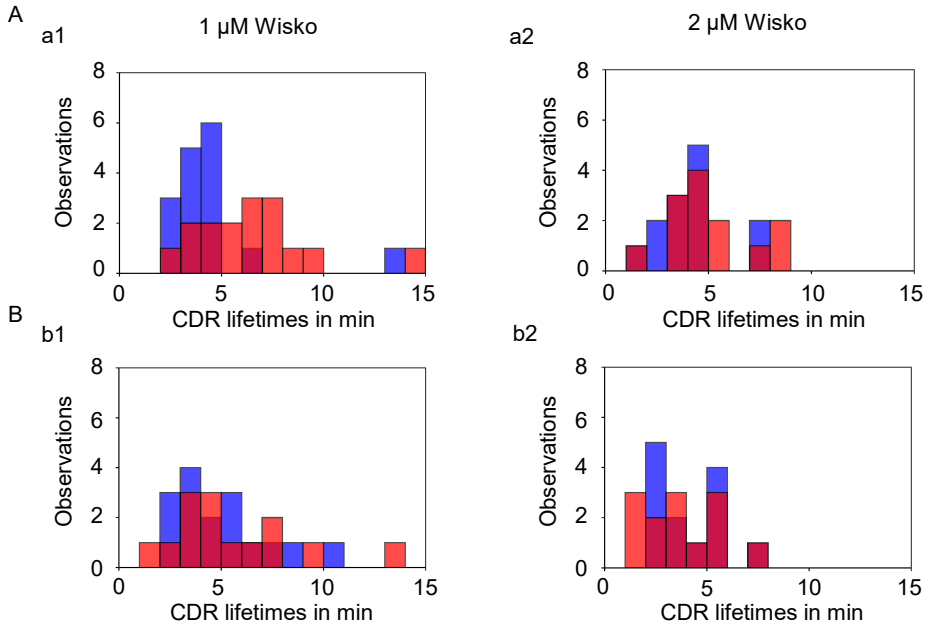

Figure 8.4: Histograms of CDR lifetimes before and after adding Wiskostatin. A shows a comparison between CDR lifetimes before (blue bars) and after (red bars) adding Wiskostatin with concentrations of 1 µM (a1) and 2 µM (a2) for the first time after 30 minutes. B demonstrates a comparison between CDR lifetimes, after a washout of Wiskostatin, before (blue bars) and after adding Wiskostatin with concentrations of 1 µM (b1) and 2 µM (b2) for the second time after 90 minutes.

This gives rise to the question why did this increase in CDR lifetimes occur more often for lower than for higher Wiskostatin concentrations and why it did not produce the same effect after adding Wiskostatin for the second time after a washout. A step towards answering these questions is to compare the distributions of average CDR lifetimes before and after adding Wiskostatin for both concentrations (1 µM and 2 µM). These distributions are believed to manifest the reaction of the system in response to the disturbance. Comparing the distributions before and after adding Wiskostatin the first time (after 30 minutes), a clear shift and a broadening of the distribution of average CDR lifetimes after adding 1 µM Wiskostatin was observed (Fig. 8.4 a1). In contrast, the distribution of average CDR lifetimes before and after adding 2 µM Wiskostatin for the first time were nearly similar (Fig. 8.4 a2). However, the distributions before and after adding Wiskostatin for the second time (after 90 minutes) were nearly similar for both Wiskostatin concentrations of 1 µM and 2 µM.

This leads to the presumption that after adding Wiskostatin in a concentration of 1 µM, the system overcompensated the inhibition of N-WASP as a response to a small disturbance. Afterwards, a washout of 1 µM Wiskostatin led to a slight return in the

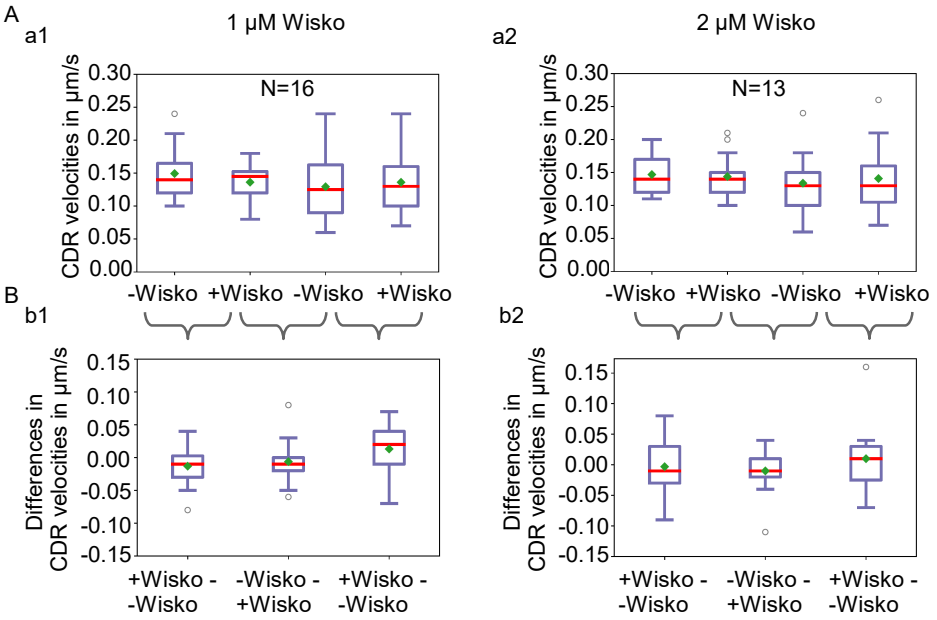

Figure 8.5: Boxplots of CDR velocities for fibroblasts treated with Wiskostatin. Boxplots in A show CDR velocities of fibroblasts treated with 1 µM (a1) and 2 µM (a2) Wiskostatin for all four time periods with alternating biochemical conditions of DMEM or DMEM with added Wiskostatin. In B differences in CDR velocities between two successive time periods from A are presented. N indicates the number of analyzed fibroblasts.

direction of its initial state and so a deviation in response to a second disturbance was only marginal. In contrast, for a Wiskostatin concentration of 2 µM, the disturbance due to an addition of Wiskostatin for the first time seemed to be too high for an overcompensation in form of a shift into a different state with longer CDR lifetimes.

8.3 No systematic change in CDR velocities and periodicities

To identify the influence of inhibiting N-WASP on CDR velocities, comparable to the analysis of CDR lifetimes, average CDR velocities were measured in several fibroblasts for all four time sections with different biochemical conditions separately. Fig. 8.5 A demonstrates that fibroblasts exhibited no systematic change in average CDR velocities between different biochemical conditions neither for a Wiskostatin concentration of 1 µM nor for 2 µM. This implied a potential increase or decrease in CDR velocities after adding Wiskostatin and a reversed effect after a washout of Wiskostatin. However, averaged CDR velocities differ between different time sections but this seems to be due to the normal fluctuations of CDR velocities within fibroblasts (see Chapter 5).

Table 8.2: Mean values of averaged CDR velocities (± SE) and averaged CDR periodicities (± SE) for four time sections with different biochemical conditions in 16 different fibroblasts in experiments with 1 µM Wiskostatin and 13 different fibroblasts in experiments with 2 µM Wiskostatin.

CDR velocities				
	-Wiskostatin (0 to 30 min)	+Wiskostatin (30 to 60 min)	-Wiskostatin (60 to 90 min)	+Wiskostatin (90 to 120 min)
1 µM	$0.15 \pm 0.01\,\mu m\,s^{-1}$	$0.13 \pm 0.01\,\mu m\,s^{-1}$	$0.13 \pm 0.01\,\mu m\,s^{-1}$	$0.14 \pm 0.01\,\mu m\,s^{-1}$
2 µM	$0.15 \pm 0.01\,\mu m\,s^{-1}$	$0.14 \pm 0.01\,\mu m\,s^{-1}$	$0.13 \pm 0.01\,\mu m\,s^{-1}$	$0.14 \pm 0.01\,\mu m\,s^{-1}$
CDR periodicities				
	-Wiskostatin (0 to 30 min)	+Wiskostatin (30 to 60 min)	-Wiskostatin (60 to 90 min)	+Wiskostatin (90 to 120 min)
1 µM	9.2 ± 1.4 min	7.9 ± 1.1 min	9.5 ± 1.6 min	10.4 ± 1.6 min
2 µM	6.6 ± 0.7 min	7.0 ± 0.8 min	7.5 ± 0.8 min	6.4 ± 0.7 min

Comparing only the first two sections, before and after adding Wiskostatin for the first time, one may observe that there is a slight decrease in CDR velocities after adding 1 µM Wiskostatin. A decrease in mean values of averaged CDR velocities of 16 fibroblasts of $0.15 \pm 0.01\,\mu m\,s^{-1}$ (± SE) before and $0.13 \pm 0.01\,\mu m\,s^{-1}$ (± SE) after adding 1 µM Wiskostatin was found. Moreover, the differences in CDR velocities between before and after adding Wiskostatin in the same fibroblasts are predominantly negative (Fig. 8.5 b1) and they were tested out to be statistically significant (significance level of 10 %). In contrast, at a higher Wiskostatin concentration of 2 µM mean values of average CDR velocities of 13 fibroblasts range from $0.15 \pm 0.01\,\mu m\,s^{-1}$ before adding Wiskostatin to $0.14 \pm 0.01\,\mu m\,s^{-1}$ after adding Wiskostatin. However, the differences in CDR velocities between before and after adding Wiskostatin show values in a wide reach in positive as well as negative directions (see Fig. 8.5 b2) and they were proven not to be statistically significant.

This decrease in CDR velocities for a lower Wiskostatin concentration of 1 µM may be provoked by the occurence of twin pulses in many cases, which increases the number of concurrently occuring CDRs for a short time period after reappearence of CDRs. The transient systematic increase of the number of concurrently occuring CDRs correlates with a decrease in CDR velocities and is in the same range as demonstrated in Chapter 5. However, this is contradictory to the fact that CDR velocities did not increase after a washout of Wiskostatin. It could be that the number of concurrently occuring CDRs remains higher than in the first time section, which is indicated in kymographs (see Fig. 8.1 & 8.2).

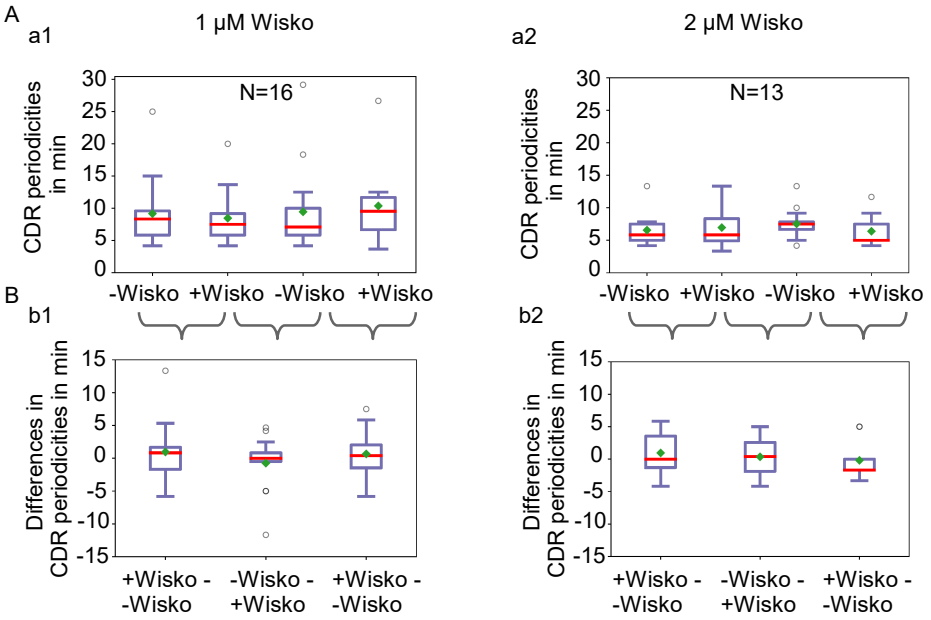

Figure 8.6: Boxplots of CDR periodicities. Boxplots in A show CDR periodicities of fibroblasts treated with 1 µM (a1) and 2 µM (a2) Wiskostatin for all four time periods with alternating biochemical conditions of DMEM or DMEM with added Wiskostatin. In B differences in CDR periodicities between two successive time periods from A are presented. N indicates the number of analyzed fibroblasts.

Average CDR periodicities were also measured for the four time intervals with different biochemical conditions. They seemed to be unaffected by changes in biochemical conditions. There is no systematic increase or decrease to identify after adding Wiskostatin for concentrations of 1 µM or 2 µM (see Fig. 8.6 A). Moreover, also the differences in average CDR periodicities in the same fibroblasts between successive time intervals show no evidence of a reaction of CDR periodicities to the influence of a N-WASP inhibition (Fig. 8.6 B).

To sum up, the suppression of N-WASP does not directly provoke changes in CDR velocities or periodicities, thus it does not directly affect the propagation of CDRs. This leads to the conclusion that the role of the actin nucleation promoting factor N-WASP differes from the role of actin itself, that directly influences CDR velocities and periodicities dependent on its concentration (see Chapter 6).

This seems to be contradictory to the outcome of the model of Peleg et al. They proposed a dependence of wave velocities on the activity of concave membrane protein complexes assumed to be consisting of N-WASP and Tuba [Peleg et al., 2011]. In this regard, an inhibition of N-WASP would lead to a decrease in the activity of the concave

membrane protein complex and hence a decrease in wave velocities. This was not the case in these experiments.

8.4 Recovery time of CDRs depends on the inhibitor concentration

To complete the picture of the response of fibroblasts regarding the formation of CDRs on the inhibition of N-WASP, recovery times of CDRs until a reappearence after adding Wiskostatin, visualized in Fig. 8.7 A, were investigated. For a Wiskostatin concentration of 1 µM, usually, with a few exceptions, fibroblasts exhibit CDRs after a recovery time of 2 to 12 minutes (Fig. 8.7 a1), which is in the range of normal CDR periodicities (see Fig. 8.6). After adding 1 µM Wiskostatin for the second time in the same fibroblasts the recovery times increase (Fig. 8.7 b2) compared to recovery times after adding Wiskostatin for the first time. In contrast, CDR recovery times after adding Wiskostatin with concentrations of 1.5 µM and 2 µM are similarly distributed comparing the first and the second time (Fig. 8.7 b3 & b4 and b5 & b6). However, for higher inhibitor concentrations the distributions of CDR recovery times appear broader and are shifted to larger recovery times.

Mean values of CDR recovery times after adding Wiskostatin were plotted against the inhibitor concentration split up into the first and second Wiskostatin treatment of the same fibroblasts. Fig. 8.7 C highlights that the recovery time increases with the inhibitor concentration, thus leading to the conclusion that the recovery time is a function of the inhibitor concentration. However, it has to be noted that the mean values of the recovery time for Wiskostatin concentrations of 1.5 µM and 2 µM were measured as slightly too low, because observed time intervals ended after 30 minutes. Measurement values of time intervals, in which no CDRs reappeared after 30 minutes, were set to 30 minutes as an upper limit. Despite this inaccuracy, of which the extent can be determined from the histograms (Fig. 8.7 B), a linear dependency of the recovery time on the inhibtitor concentration can be assumed.

In this regard, the question is raised whether a mechanical perturbation due to the medium exchange in the flow chamber may have led to the rapid collapse of CDRs after adding Wiskostatin and not the biochemical compound Wiskostatin itself. However, this hypothesis can be refuted with two arguments. First, the disappearence of CDRs only occured during a flow exchange while adding Wiskostatin and not while adding only cell culture medium (see Fig. 8.7 A, adding cell culture medium without Wiksostatin after 60 minutes) and second, the recovery time was dependent on the concentration of the inhibitor, as demonstrated in Fig. 8.7 C, while the flow rate was comparable in all medium exchanges. Still the question remains, whether there is a dependence of the recovery time until CDR reappearence on the inhibitor concentration.

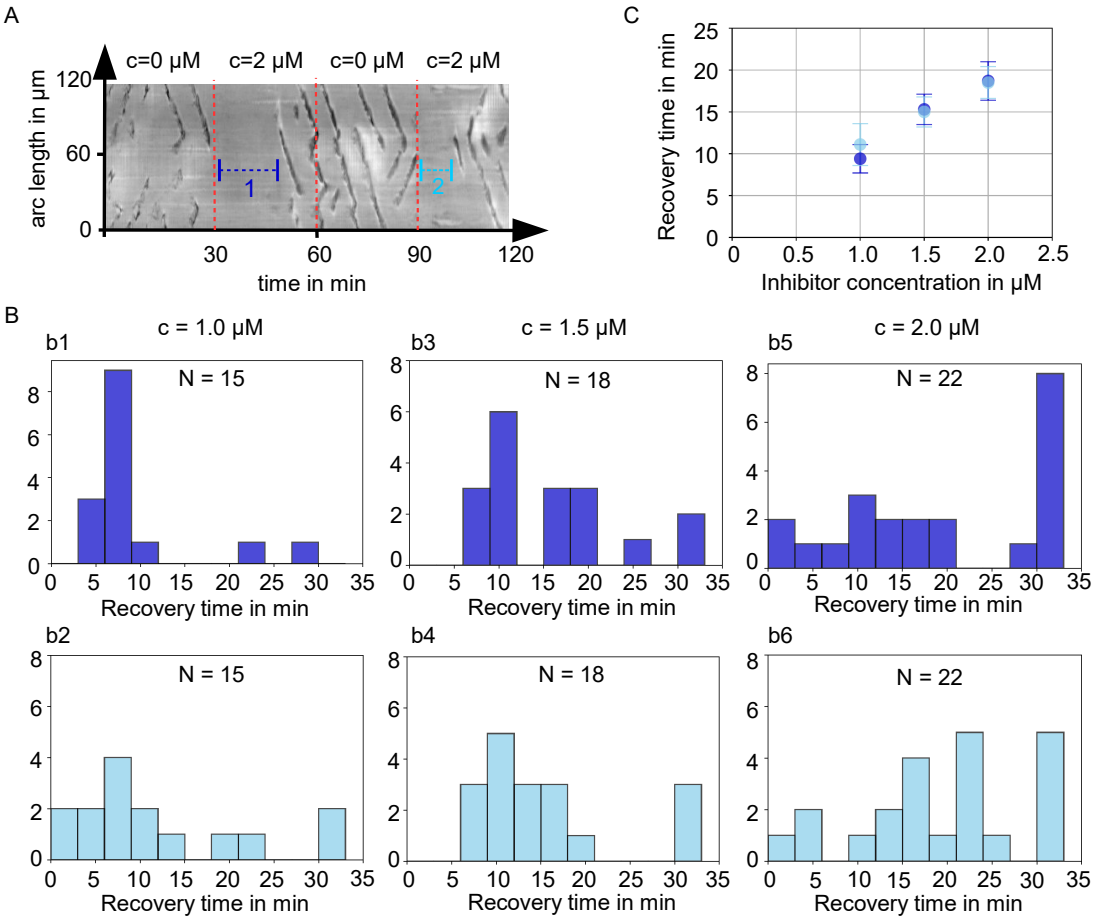

Figure 8.7: Recovery time until CDR reappearence after adding Wiskostatin. A shows a kymograph from a fibroblast treated with $2\,\mu M$ Wiskostatin, in which blue lines visualize recovery time until CDRs reappear after adding Wiskostatin for the first and second time. B shows histograms of recovery times until CDR reappearence after adding Wiskostatin for three different inhibitor concentrations, $1\,\mu M$ (b1 & b2), $1.5\,\mu M$ (b3 & b4) and $2\,\mu M$ (b5 & b6) splitted up into the first (b1, b3 & b5) and second time (b2, b4 & b6) Wiskostatin treatment of the same fibroblasts. C summarizes mean values of recovery times until CDR reappearence plotted against inhibitor concentrations, in which darker blue visualizes mean values of CDR recovery times after adding Wiskostatin for the first time and lighter blue mean values after the second time. Errorbars visualize the standard error. N indicates the number of analyzed fibroblasts.

8.5 Summary

The influence of N-WASP on CDR initiation and propagation was investigated. Therefore the biochemical compound Wiskostatin was utilized to inhibt N-WASP and studied

systematically the influence of the amount of N-WASP and thus the Arp2/3-mediated nucleation of actin filaments. It was observed that inhibiting N-WASP with different concentrations of Wiskostatin leads to a suppression of the formation of CDRs. This is in line with experiments by Masters et al. who observed a collapse of actin waves in macrophages after adding Wiskostatin [Masters et al., 2016]. This leads to the conclusion, that the protein N-WASP and therefore the Arp2/3-mediated actin nucleation play a crucial role in initiation of CDRs and also in other actin waves in various cell types.

Moreover, in contrast to former studies, this study focuses on the influence of N-WASP on the propagation of CDRs to examine the role of N-WASP in the underlying wave machinery. Therefore different and lower concentrations of Wiskostatin were used in order to affect the activity of N-WASP without inducing a complete suppression of CDR formation over a long time period. A collapse of CDRs for different inhibitor concentrations but also a reappearence of CDRs after a certain time period was found. It was detected that the recovery time of CDRs until CDRs reappeared depends on the inhibitor concentration. Furthermore, CDR lifetimes increased diretly after CDR reappearence. One explanation for this effect was the recovery of the substrates, like PIP_2 recovery and stress fiber reappearence observed in macrophages [Masters et al., 2016]. Alternatively it can be due to a neglection of CDR interaction like collisions or long-range interactions because of a complete suppression of CDRs after adding Wiskostatin. However, the effect of longer lifetimes was higher for smaller Wiskostatin concentrations, which primarily leads to the assumption of a reaction and overcompensation of the system due to small perturbation by the inhibitor.

Moreover, comparing CDR velocities and periodicities before and after Wiskostatin, no systematic change was observed. This leads to the conclusion that N-WASP plays a crucial role in formation of CDRs but does not affect their propagation. This seems to be contradictory to a previous CDR model. Peleg et al. proposed a dependence of wave velocities on the activity of concave membrane proteins, including N-WASP, in an underlying mechanisms of CDR propagation based on the interplay between curved membrane protein complexes [Peleg et al., 2011]. However, the crucial role of N-WASP in actin wave formation was also proposed by Bernitt et al. for actin waves in fibroblasts and Masters et al. for actin waves in macrophages [Bernitt et al., 2017, Masters et al., 2016]. Bernitt et al. proposed a positive feedback mechanism of actin polymerization, that includes N-WASP within its model of propagating wavefronts in a bistable regime of two stable actin states [Bernitt et al., 2017]. Furthermore, Masters et al. constructed a feedback mechanism of N-WASP regulating phospholipids in the context of a bistable regime of different actin states [Masters et al., 2016].

9 Conclusion and Outlook

This study focused on the mechanism underlying CDR formation and propagation in the context of actin waves. Therefore, experiments with fibroblasts of defined morphology attached on disk-like fibronection patches were performed. The disk-shaped fibroblasts were used to achieve comparable and reproducible boundary conditions. Moreover, the random impact of the cellular bundaries on CDR formation were further reduced by the geometry due to an even curvature. Furthermore, it confines CDRs to propagate on a one-dimensional trajectory between nucleus und cell boundary [Bernitt and Döbereiner, 2017].

In this study, it was observed that the long CDR propagation around the nucleus is caused by an interplay between an emerging, radially growing CDR and its collision with the curved cellular boundaries, that leads to a splitting into two twin pulses. Therefore, CDR velocities, periodicities and lifetimes are important observables to characterize and compare CDR dynamics in different biochemical environments. The question was raised, which factors influence these three parameters in order to characterize the wave machinery underyling CDR formation and propagation.

In contrast to former studies, a detailed quantitative study of CDR dynamics, which revealed fundamental insights into the underlying wave machinery was presented. For the first time, a dependence of CDR velocities on the number of concurrently occuring CDRs was found. In contrast, the lifetimes of CDRs were shown to be independent of a rising number of concurrently occuring CDRs, but they seem to be restricted by long-range interactions between different CDRs. Further main results of this study are the observed dependence of CDR velocities, periodicities and lifetimes on the total amount of actin. Moreover, a suppression of PIP_3 via an inhibition of PI3K have been found to correlate with a decrease in lifetimes and a slight decrease of CDR velocities. However, CDR periodicities were unaffected by inhibition of PI3K, and moreover N-WASP, the nucleator of actin polymerization, did not affect CDR velocities, periodicities or lifetimes, but led to a rapid collapse of CDRs.

Numerical solutions of a prototype model of a system within a bistable regime on an annulus domain resemble coherently propagating wavefronts similar to CDRs in disk-shaped fibroblasts. Compared to experimental results, a decrease in wavefront velocities with a rising number of waves fronts or a reduction in the total available actin was found. Furthermore, a reduced perturbation threshold by an increased concentration of total available actin was discovered, so that smaller perturbations are necessary to

induce propagating wavefronts.

9.1 CDR dynamics and the role of membrane tension

In contrast to former studies in random shaped cells, disk-shaped fibroblasts exhibit CDR propagation around the nucleus over minutes. That allows a systematic study of CDR dynamics without strong dependences of the CDR movement on the cell shape. To date, it is still debated, which factors influence CDR lifetimes, velocities or even peridocities. Furthermore, in this regard, the influences of different macromolecules on CDR formation were often explored but the role of mechanical properties on CDR dynamics are widely unknown. It seems to be evident, that membrane tension has a great impact on the formation of CDRs, but it was not tested in detail yet. However, the role of membrane tension was incorporated in different theoretical models of CDR formation, in which, inter alia, it was hypothesized, that CDR velocities depend on the membrane tension [Peleg et al., 2011].

In this thesis a dependence of CDR velocities on the number of concurrently occuring CDRs was found (see Chapter 5). A decrease in CDR velocities with a rising number of CDRs indicate a dependence of CDR propagation on a limiting species, like the concentration of the total amount of actin. However, it can also hint to a long-range interaction between different CDRs due to the membrane tension, as proposed by Peleg et al. [Peleg et al., 2011]. In this regard, a dependence of CDR velocities on the total amount of actin was found (see Chapter 6), which supported the guiding role of the total amount of actin. Simulations with a prototype model within a bistable regime of two stable actin states underpin these experimental findings (see Chapter 6).

Furthermore, long-range interactions between different CDRs were observed, where a CDR rapidly collapsed at the moment when another CDR appeared at a different position on the dorsal cell side (see Chapter 5). Thus, it seems obvious, that the membrane tension plays a crucial role in CDR formation and propagation. Furthermore, these long-range interactions demonstrate that CDR periodicities restrict their lifetimes. This leads to the conclusion, that stochastic processes of perturbations in the underlying wave machinery, as proposed by Bernitt and Döbereiner [Bernitt and Döbereiner, 2017], govern CDR periodicities and therefore also CDR lifetimes. However, the experimental results in this work partly differ from theoretical findings of Bernitt and Döbereiner, who assumed a restriction of CDR lifetimes due to their collision and annihilation [Bernitt and Döbereiner, 2017]. Therefore, they concluded a dependence of CDR lifetimes on the number of concurrently occuring CDRs, which could not be confirmed with the experimental data of this study. These data lead to the conclusion, that an upper limit of CDR lifetimes is governed by CDR collisions, but the interactions between the stochastic processes of perturbations and the membrane tension have a regulating role in CDR lifetimes.

These conclusions are further strengthened by experiments with changed biochemical conditions. Longer CDR lifetimes and larger CDR periodicities were discovered by a decrease in the total available actin. In this regard, it was speculated that a higher perturbation threshold due to a decrease in the total available actin leads to larger CDR periodicities. This was corroborated by theoretical results, in which larger perturbations were required to stimulate propagating wavefronts at a decreased concentration in the total available actin within the bistable regime of the prototype model (see Chapter 6).

9.2 The role of actin, PIP3 and N-WASP in CDR formation and propagation

To date, the influence of a large number of macromolecules on CDR formation was explored, that included, inter alia, actin itself, different actin associated proteins, membrane deforming proteins, Rho GTPases and phospholipids [Buccione et al., 2004, Itoh and Hasegawa, 2012]. However, the impact of individual macromolecules on CDR propagation in that quantitative manner as presented in this work has not been investigated before. This work focused on the role of actin itself, the phosphoinositide PIP_3 and the actin nucleation promoting factor N-WASP on CDR dynamics, that were assumed to have a big impact on CDR formation and propagation in the context of a bistable regime between two stable actin states.

As a main point in this thesis, a governing role of actin in CDR dynamics was figured out. It can be traced back to experimental results, in which a strong dependence of CDR velocities, periodicities and lifetimes on the total amount of actin was found (see Chapter 6). This leads to the conjecture that actin itself directly regulates CDR formation and propagation. A decrease in the total amount of actin leads to a reduction in CDR velocities. Furthermore, larger CDR periodicities and longer CDR lifetimes were found after reducing the total amount of actin. Therefore, a decreased perturbation threshold due to a reduction of the total available actin is proposed. Furthermore, a reduction of the concentration of the total available actin leads to a loss of wave stability.

These characteristics are, inter alia, in line with the findings of Bernitt et al. that CDRs are propagating wavefronts in a bistable regime between two stable actin states [Bernitt et al., 2017]. Moreover, a similar mechanism was also proposed for actin waves in macrophages by Masters et al. [Masters et al., 2016]. However, it is in contrast to the assumption of Zeng et al. who proposed that CDR formation and propagation are affected by an interplay between the regulatory proteins Rac and Rho upstream to actin [Zeng et al., 2011].

Furthermore, phosphoinositides are proposed to play a fundamental role in actin wave formation, in particular in *Dictyostelium*, but also within macrophages [Gerisch et al.,

2009, Masters et al., 2016]. It was also found that PIP_3 is localized to the CDR interior and thus it is proposed to play a crucial role within the bistable model of CDR propagation [Hoeller et al., 2013, Bernitt et al., 2017]. An inhibition of PI3K and thus a reduction of PIP_3 was investigated and a reduction of CDR lifetimes and CDR ring sizes was observed. However, CDR velocities were only slightly affected by PI3K (see Chapter 7). It leads to the conclusion that PIP_3 plays a fundamental role in CDR formation and moreover, also in regulating CDR ring sizes by activating the Arf GAP ARAP1 [Hasegawa et al., 2012, Campa et al., 2009]. This seems to be in line with its localization to the CDR interior and is also in line with the hypothesis that CDRs are wavefronts in a bistable regime with two stable actin states between the interior and exterior of CDRs, whereas there is a depletion of cortical actin and stress fibers in the CDR interior [Bernitt et al., 2017]. However, it is conjectured that PIP_3, in contrast to actin itself, is not directly involved in regulating CDR propagation due to its weak influence on CDR velocities and that it does not affect CDR periodicities.

Moreover, it was observed that N-WASP plays a crucial role in CDR formation because an inhibition of N-WASP leads to a disappearence of CDRs (see Chapter 8). This is in line with investigations of the role of N-WASP in CDRs within fibroblasts by Bernitt et al. and also with the role of N-WASP, that interacts with phosphoinositides in actin waves within macrophages by Masters et al. [Bernitt et al., 2017, Masters et al., 2016]. However, N-WASP does not systematically affect CDR velocities, periodicities or lifetimes. Thus, there is no influence of N-WASP on the propagation of CDRs. This contrasts the statement of Peleg et al.. They modeled CDR dynamics via an interplay between the membrane shape and curved membrane protein complexes, that incorporated actin nucleation promoting factors like N-WASP [Peleg et al., 2011]. They postulated a dependence of wave velocities on the activity of concave membrane protein complexes that includes N-WASP.

To sum up, actin directly regulates CDR formation and propagation, whereas N-WASP is strongly involved in the formation of CDRs, but it does not regulate their propagation. Moreover, PIP_3 seems to be involved in CDR formation and has a big influence on their ring sizes. The role of PIP_3 in CDR propgation is not entirely clear and should be further investigated. In this regard, this experimental system would be helpful, but it should be combined with life cell stainings of the examined macromolecules. Further, it can be extended with optogenetic tools, that would be more controllable and diminish side effects, that are not clear so far.

9.3 The mechanism underlying CDR formation and propagation

Different kinds of actin waves were observed in various cell types, for examples *Dictyostelium*, macrophages or neutrophiles [Vicker, 2000, Masters et al., 2016, Weiner

et al., 2007]. The crucial question was whether these different types of actin waves have the same underlying wave machinery. CDR velocities in fibroblasts were found in the same range as wave velocities in *Dictyostelium*, neutrophiles or macrophages [Gerisch et al., 2012, Weiner et al., 2007, Masters et al., 2016], which leads to the conclusion of similarities in the wave propagation mechanism. In this context, most studies that focused on actin waves considered them as waves in an excitable system with different molecular players [Vicker, 2000, Gerisch et al., 2012, Whitelam et al., 2009]. However, there is also the hypothesis that actin waves behave as wavefronts in a bistable regime between two stable actin states [Masters et al., 2016].

In the context of actin waves, four fundamental models of underlying CDR formation and propagation were presented at the beginning of this work (Chapter 3). They differ in their concepts; three of them are reaction-diffusion models that distinguish between excitable or bistable regimes based on a different molecular nature, in which a perturbation leads to wave propagation [Zeng et al., 2011, Bernitt and Döbereiner, 2017, Bernitt et al., 2017]. However, other studies focused on the mechanical interactions between actin polymerization and the membrane, inter alia, a potential interplay between concave and convex membrane protein complexes that interrelate with the membrane shape [Peleg et al., 2011].

This thesis mainly focused on the examination of the models in an experimental and quantitative manner as well as with theoretical simulations. The main hypothesis of this work is that CDRs can be considered as wavefronts in a bistable regime. This is based on the observations of two different actin states in the interior and exterior of CDRs [Bernitt, 2015, Bernitt et al., 2017]. In this regard, a direct regulating role of actin in CDR formation and propagation was discoverd in this work (see Section 9.2). Moreover, due to a reduction of the total amount of available actin, a wave instability was observed. CDRs did not collapse directly but lost their clear ring shape by splitting up into small waves with chaotic dynamics. This was comparable with the behavior of wavefronts near a Hopf bifurcation in a bistable regime at a transition from a stable to an unstable regime within the prototype model of Bernitt et al. [Bernitt et al., 2017]. Moreover, simulations of propagating wavefronts in a bistable regime of this model were carried out. It was found that features like coherently propagating wavefronts that annihilate each other by colliding with each other or a reappearence after a defined time period, were also observed after perturbations in a bistable regime. These features were previously only known from excitable systems [Bernitt and Döbereiner, 2017, Zeng et al., 2011]. Furthermore, similar to experimental results, a decrease in wave veocities by reducing the total available actin was observed. These results underpin the model of Bernitt et al [Bernitt et al., 2017]. Moreover, a regulating role of PIP_3 in CDR ring sizes was found. It is known that PIP_3 is localized in the interior of CDRs and disfavors actin assembly [Hoeller et al., 2013, DiPaolo and Camilli, 2006]. In this regard, PIP_3 favors a polarity between the CDR interior and exterior that leads to different states of

actin. This fact underline the idea, that CDRs propagate as wavefronts in a bistable regime between two stable actin states and exclude the idea of an excitable regime with one steady state, in which perturbations leads to traveling waves.

The oberserved governing role of actin contrasts with the proposed model of Zeng et al. [Zeng et al., 2011]. They formulated a regulation of CDR dynamics through the Rho GTPases Rac and Rho, which act upstream of actin itself. Moreover, the results of this study also contradicts the model of Peleg et al., which focused on an interaction of concave and convex membrane protein complexes and the membrane shape, that leads to propagating wavefronts [Peleg et al., 2011]. That model predicts a dependence of wave velocities on concave membrane protein complexes that include the activity of N-WASP. The results of this study did not show a dependence of wave velocities on the N-WASP activity.

In conclusion, the results of this study confirm the hypothesis that CDRs behave as propagating wavefronts in a bistable regime between two stable states of actin. In this regard, actin plays a governing role in CDR formation and propagation, whereas PIP_3 restricts CDR ring sizes. The prototype model of Bernitt et al. captures the formation and propagation of CDRs very well, whereas the results of this study disagree with the model of Zeng et al. and Peleg et al. [Zeng et al., 2011,Peleg et al., 2011]. Moreover, the model of Bernitt et al. should be extended with stochastic perturbations similar to the study of actin waves in a noise driven excitable system [Bernitt and Döbereiner, 2017]. Furthermore, also the role of membrane tension has to be further investigated and ideally should be incorporated in such a model system. Such a proposed extended model would help to further increase the understanding of the underlying wave machinery and to prove the interactions of CDR periodicities and lifetimes (see Section 9.2).

10 Bibliography

[Abercrombie and Ambrose, 1958] Abercrombie, M. and Ambrose, E. J. (1958). Interference microscope studies of cell contacts in tissue culture. *Experimental Cell Research*, 15(2):332–345.

[Alberts et al., 2015] Alberts, B., Johnson, A., Lewis, J., Morgan, D., Raff, M., Roberts, K., and Walter, P. (2015). *Molecular Biology of the Cell*. Garland Science, Taylor & Francis Group, LLC, 6 edition.

[Allard and Mogilner, 2013] Allard, J. and Mogilner, A. (2013). Traveling waves in actin dynamics and cell motility. *Current Opinion in Cell Biology*.

[Azimifar et al., 2012] Azimifar, S. B., Böttcher, R. T., Zanivan, S., Grashoff, C., Krüger, M., Legate, K. R., Mann, M., and Fässle, R. (2012). Induction of membrane circular dorsal ruffles require co-signalling of integrin-ilk-complex and egf receptor. *Journal of Cell Science*, 125:435–448.

[Balla, 2013] Balla, T. (2013). Phosphoinositides: Tiny lipids with giant impact on cell reguation. *Physiological Reviews*, 93:1019–1137.

[Bernitt, 2015] Bernitt, E. (2015). *The dynamics of dorsal actin waves*. PhD thesis, Universität Bremen.

[Bernitt and Döbereiner, 2017] Bernitt, E. and Döbereiner, H.-G. (2017). Spatiotemporal patterns of noise-driven confined actin waves in living cells. *Physical Review Letters*, 118:048102.

[Bernitt et al., 2017] Bernitt, E., Döbereiner, H.-G., Gov, N. S., and Yochelis, A. (2017). Fronts and waves of actin polymerization in a bistability-based mechanism of circular dorsal ruffles. *Nature Communications*, 8:15863.

[Bernitt et al., 2015] Bernitt, E., Koh, C. G., Gov, N., and Döbereiner, H.-G. (2015). Dynamics of actin waves on patterned substrate: A quantitative analysis of circular dorsal ruffles. *PLoS One*, 10.

[Beta, 2010] Beta, C. (2010). Bistability in the actin cortex. *PMC Biophysics*, 3(12).

[Bishop and Hall, 2000] Bishop, A. L. and Hall, A. (2000). Rho gtpases and their effector proteins. *Biochemical Journal*, 348:241–255.

[Blanchoin et al., 2014] Blanchoin, L., Boujemaa-Paterski, R., Sykes, C., and Plastino, J. (2014). Actin dynamics, architecture and mechanics in cell motility. *Physiological Reviews*, 94:235–263.

[Bloomfield and Kay, 2016] Bloomfield, G. and Kay, R. R. (2016). Uses and abuses of maropinocytosis. *Journal of Cell Science*, 129:2697–2705.

[Boguski and McCormick, 1993] Boguski, M. S. and McCormick, F. (1993). Proteins regulating ras and its relatives. *Nature*, 366:643–654.

[Bretschneider et al., 2009] Bretschneider, T., Anderson, K., Ecke, M., Müller-Taubenberger, A., Schroth-Diez, B., Ishikawa-Ankerholf, H. C., and Gerisch, G. (2009). The three-dimensional dynamics of actin waves, a model of cytoskeletal self-organization. *Biophysical Journal*, 96:2888–2900.

[Bretschneider et al., 2004] Bretschneider, T., Diez, S., Anderson, K., Heuser, J., Clarke, M., Müller-Taubenberger, A., Köhler, J., and Gerisch, G. (2004). Dynamic actin patterns and arp2/3 assembly at the substrate-attached surface of motile cells. *Current Biology*, 14:1–10.

[Bubb et al., 1994] Bubb, M. R., Senderowicz, A. M. J., Sausville, E. A., Duncan, K. L. K., and Korn, E. D. (1994). Jasplakinolide, a cytotoxic natural product, induces actin polymerization and competitively inhibits the binding of phalloidin to f-actin. *The Journal of Biological Chemistry*, 269(21):14869–14871.

[Bubb et al., 2000] Bubb, M. R., Spector, I., Beyer, B. B., and Fosen, K. M. (2000). Effects of jasplakinolide on the kinetics of actin polymerization. *The Journal of Biological Chemistry*, 275(7):5163–5170.

[Buccione et al., 2004] Buccione, R., Orth, J. D., and McNiven, M. A. (2004). Foot and mouth: Podosomes, invadopodia and circular dorsal ruffles. *Nature Reviews Molecular Cell Biology*, 5:647–657.

[Campa et al., 2009] Campa, F., Yoon, H.-Y., Ha, V. L., Szentpetery, Z., Balla, T., and Randazzo, P. A. (2009). A ph domain in the arf gap arap1 binds ptdins(3,4,5)p3 and regulates arf gap activity independently of recruitment to the plasma membranes. *Journal of Biological Chemistry*.

[Chesarone and Goode, 2009] Chesarone, M. A. and Goode, B. L. (2009). Actin nucleation and elongation factors: Mechanism and interplay. *Current Opinion in Cell Biology*, 21:28–37.

[Chhabra and Higgs, 2007] Chhabra, E. S. and Higgs, H. N. (2007). The many faces of actin: mathching asembly factors with cellular structures. *Nature Cell Biology*, 9(10):1110–1121.

[Chinkers et al., 1979] Chinkers, M., McKanna, J. A., and Cohen, S. (1979). Rapid induction of morphological changes in human carcinoma cells a-431 by epidermal growth factors. *Journal of Cell Bio*, pages 260–265.

[Clainche and Carlier, 2008] Clainche, C. L. and Carlier, M.-F. (2008). Regulation of actin assembly associated with potrusion and adhesion in cell migration. *Physiological Reviews*, 88:489–513.

[Dalby et al., 2004] Dalby, B., Cates, S., Ohki, A. H. E. C., Tilkins, M. L., Price, P. J., and Ciccarone, V. C. (2004). Advanced transfection with lipofectamine 2000 reagent: Primary neurons, sirna, and high-throughput applications. *Methods*, pages 95–103.

[Deneke and Di Talia, 2018] Deneke, V. E. and Di Talia, S. (2018). Chemical waves in cell and development biology. *Journal of Cell Biology*, 217.

[Deuel and Chang, 2014] Deuel, T. F. and Chang, Y. (2014). Chapter 16 - growth factors. In Lanza, R., Langer, R., and Vacanti, J., editors, *Principles of Tissue Engineering (Fourth Edition)*, pages 291 – 308. Academic Press, Boston, fourth edition edition.

[DiPaolo and Camilli, 2006] DiPaolo, G. and Camilli, P. D. (2006). Phosphoinositides in cell regulation and membrane dynamics. *Nature*, 443:651–657.

[Dowrick et al., 1993] Dowrick, P., Kenworthy, P., McCann, B., and Warn, R. (1993). Circular ruffle formation and closure lead to macropinocytosis in hepatocyte growth factor/scatter factor-treated cells. *European Journal of Cell Biology*, 61(1):44–53.

[FitzHugh, 1968] FitzHugh, R. (1968). Motion picture of nerve impulse propagation using computer animation. *Journal of Applied Physiology*, 25(5).

[Gerhardt et al., 2014] Gerhardt, M., Ecke, M., Walz, M., Stengl, A., Beta, C., and Gerisch, G. (2014). Actin and pip3 waves in giant cells reveal the inherent scale of an excited state. *Journal of Cell Science*, 127:5407–4517.

[Gerisch et al., 2009] Gerisch, G., Ecke, M., Schroth-Diez, B., Gerwig, S., Engel, U., Maddera, L., and Clarke, M. (2009). Self-organizing actin waves as planar phygocytotic cup structures. *Cell Adhesion and Migration*, pages 373–382.

[Gerisch et al., 2011] Gerisch, G., Ecke, M., Wischnewski, D., and Schroth-Diez, B. (2011). Different modes of state transition determine pattern in the phosphatidylinositide-actin system. *BMC Cell Biology*, 12:1–15.

[Gerisch et al., 2012] Gerisch, G., Schroth-Diez, B., Müller-Taubenberger, A., and Ecke, M. (2012). Pip3 waves and pten dynamics in the emergence of cell polarity. *Biophysical Journal*, 103:1170–1178.

[Gov and Gopinathan, 2006] Gov, N. and Gopinathan, A. (2006). Dynamics of membranes driven by actin polymerization. *Biophysical Journal*, 90:454–469.

[Ha et al., 2016] Ha, K. D., Bidlingmaier, S. M., and Liu, B. (2016). Macropinocytosis exploitation by cancer and cancer therapeutics. *frontiers in Physiology*, 7(381).

[Hall, 1998] Hall, A. (1998). Rho gtpases and the actin cytoskeleton. *Frontiers in Cell Biology*, 279:509–514.

[Hasegawa et al., 2012] Hasegawa, J., Tsujita, K., Takenawa, T., and Itoh, T. (2012). Arap1 regulates the ring size of circular dorsal ruffles through arf1 and arf5. *Molecular Biology of the Cell*, 23:2481–2489.

[Higgs and Pollard, 1999] Higgs, H. N. and Pollard, T. D. (1999). Regulation of actin polymerization by arp2/3 complex and wasp/scar proteins. *The Journal of Biological Chemistry*, 274(46):32531–32534.

[Hoeller et al., 2013] Hoeller, O., Bolourani, P., Clark, J., Stephens, L. R., Hawkins, P. T., Weiner, O. D., Weeks, G., and Kay, R. R. (2013). Two distinct functions of pi3-kinases in macropinocytosis. *Journal of Cell Science*, 126:4296–4307.

[Holmes et al., 1990] Holmes, K. C., Popp, D., Gebhard, W., and Kabsch, W. (1990). Atomic model of the actin filament. *Nature*, 347.

[Hoon et al., 2012] Hoon, J.-L., Wong, W.-K., and Koh, C.-G. (2012). Functions and regulation of circular dorsal ruffles. *Molecular and Cellular Biology*, 32(21):4246–4257.

[Itoh and Hasegawa, 2012] Itoh, T. and Hasegawa, J. (2012). Mechanistic insights into the regulation of circular dorsal ruffle formation. *Journal of Biochemistry*, 153(1):21–29.

[Jaffe and Hall, 2005] Jaffe, A. B. and Hall, A. (2005). Rho gtpases: Biochemistry and biology. *Annual Review of Cell Biology*, 21:247–269.

[Kazlauskas, 1994] Kazlauskas, A. (1994). Receptor tyrosine kinases and their targets. *Current Biology*, 4:5–14.

[Kiuchi et al., 2011] Kiuchi, T., Nagai, T., Ohashi, K., and Mizuno, K. (2011). Measurements of spatiotemporal changes in g-actin concentration reveal its effect on stimulus-induced actin assembly and lamellipodium extension. *Journal of Cell Biology*, 193(2):365–380.

[Koestler et al., 2009] Koestler, S. A., Rottner, K., Lai, F., Block, J., Vinzenz, M., and Small, J. V. (2009). F- and g-actin concentrations in lamellipodia of moving cells. *PLoS One*, 4:e4810.

[Kovacs et al., 2006] Kovacs, E. M., Makar, R. S., and Gertler, F. B. (2006). Tuba stimulates intracellular n-wasp dependent actin assembly. *Journal of Cell Science*, 119:2715–26.

[Lee et al., 1998] Lee, E., Shelden, E. A., and Knecht, D. A. (1998). Formation of f-actin aggregates in cells treated with actin stabilizing drugs. *Cell Motility and the Cytoskeleton*, 39:122–133.

[Legg et al., 2007] Legg, J. A., Bompard, G., Dawson, J., Morris, H. L., Andrew, N., Cooper, L., Johnston, S. A., Tramountanis, G., and Machesky, L. M. (2007). N-wasp involvement in dorsal ruffle formation in mouse embryonic fibroblasts. *Molecular Biology of the Cell*, 18:678–687.

[Masters et al., 2016] Masters, T. A., Sheetz, M. P., and Gauthier, N. C. (2016). F-actin waves, actin cortex dissessembly and focal exocytosis driven by actin-phospoinositide positive feedback. *Cytoskeleton*, 73:180–196.

[Mattila et al., 2007] Mattila, P. K., Pykäläinen, A., Saarikangas, J., Paavilainen, V. O., and Vihinen, H. e. a. (2007). Missing-in-metastasis and irsp53 deform pi(4,5)p2-rich membranes by an inverse bar domain-like mechanism. *Journal of Cell Biology*, 176:953–64.

[Mellström et al., 1988] Mellström, K., Heldin, C.-H., and Westermark, B. (1988). Induction of circular membrane ruffling on human fibroblasts by platelet-derived growth factor. *Experimental Cell Research*, 177:347–359.

[Mellström et al., 1983] Mellström, K., Höglund, A. S., Nistér, M., H., H. C., Westermark, B., and Lindberg, U. (1983). The effect of platelet-derived growth factor on morphology and motility of human glial cells. *Journal of Muscle Research and Cell Motility*, 4(5):589–609.

[Mercer and Helenius, 2009] Mercer, J. and Helenius, A. (2009). Virus entry by macropinocytosis. *Nature Cell Biology*, 11(5):510–520.

[Mim and Unger, 2012] Mim, C. and Unger, V. M. (2012). Membrane curvature and its generation by bar proteins. *Trends in Biochemical Sciences*, 37(12):526–533.

[Mullins et al., 1998] Mullins, R. D., Hauser, J. A., and Pollard, T. D. (1998). The interaction of the arp2/3 complex with actin: Nucleation, high affinity pointed end capping, and formation of branching networks of filaments. *Proceedings of the National Academy of Sciences of the United States of America*, 95:6181–6186.

[Ohmstede, 2016] Ohmstede, M. (2016). Development of an experimental setup for high precision cell stimulation. Master's thesis, Universität Bremen.

[Orth and McNiven, 2006] Orth, J. D. and McNiven, M. A. (2006). Get off my back! rapid receptor internalization through circular dorsal ruffles. *Cancer Re*, 66(23):11094–11096.

[Peleg et al., 2011] Peleg, B., Disanza, A., Scita, G., and Gov, N. (2011). Propagating cell-membrane waves driven by curved activators of actin polymerization. *PLoS ONE*, 6(4):e18635.

[Peter et al., 2004] Peter, B. J., Kent, H. M., G, M. I., Vallis, Y., and Butler, P. J. G. e. a. (2004). Bar domains as sensors of membrane curvature: the amphiphysin bar structure. *Science*, 303.

[Peterson et al., 2004] Peterson, J. R., Bickford, L. C., Morgan, D., Kim, A. S., Ouerfelli, O., Kirschner, M. W., and Rosen, M. K. (2004). Chemical inhibition of n-wasp by stabilization of a native autoinhibited conformation. *Nature Structural & Molecular Biology*, 11(8):747–755.

[Pollard and Borisy, 2003] Pollard, T. D. and Borisy, G. G. (2003). Cellular motility driven by assembly and disassembly of actin filaments. *Cell*, 112:453–465.

[Prinz and Hinshaw, 2009] Prinz, W. and Hinshaw, J. E. (2009). Membrane bending proteins. *Critical Reviews in Biochemistry and Molecular Biology*, 44(5):278–291.

[Reyes-Reyes et al., 2010] Reyes-Reyes, E. M., Teng, Y., and Bates, P. J. (2010). A new paradigm for aptamer therapeutic as1411 action: Uptake by macropinocytosis and its stimulation by a nucleolin-dependent mechanism. *Cancer Research*, 70(21):8617–8629.

[Ridley, 2006] Ridley, A. J. (2006). Rho gtpases and actin dynamics in membrane protrusion and vesicle trafficking. *Trends in Cell Biology*, 16(10):522–529.

[Ridley and Hall, 1992] Ridley, A. J. and Hall, A. (1992). The small gtp-binding protein rho regulates the assembly of focal adhesions and actin stress fibers in response to growth factors. *Cell*, 70:389–399.

[Ridley et al., 1992] Ridley, A. J., Paterson, H. F., Johnston, C. L., Diekmann, D., and Hall, A. (1992). The small gtp-binding protein rac regulates growth factor-induced membrane ruffling. *Cell*, 70:401–410.

[Rottner et al., 2017] Rottner, K., Faix, J., Bogdan, S., Linder, S., and Kerkhoff, E. (2017). Actin assembly mechanism at a glance. *Journal of Cell Science*, 130:3427–3435.

[Sackmann and Merkel, 2010] Sackmann, E. and Merkel, R. (2010). *Lehrbuch der Biophysik*. WILEY-VCH Verlag.

[Sawicka et al., 2015] Sawicka, K. M., Seeliger, M., Musaev, T., Macri, L. K., and Clark, R. A. F. (2015). Fibronectin interaction and enhancement of growth factors: Importance of wound healing. *Advances in Wound Care*, 4(8):469–478.

[Schindelin et al., 2012] Schindelin, J., Arganda-Carreras, I., Frise, E., Kaynig, V., Longair, M., Pietzsch, T., Preibisch, S., Rueden, C., Saalfeld, S., Schmid, B., Tinevez, J.-Y., White, D. J., Hartenstein, V., Eliceiri, K., Tomancak, P., and Cardona, A. (2012). Fiji: An open-source platform for biological-image analysis. *Nature Methods*, 9:676–682.

[Shlomovitz and Gov, 2007] Shlomovitz, R. and Gov, N. (2007). Membrane waves driven by actin and myosin. *Physical Review Letters*, 98:168103.

[Stanishneva-Konovalova et al., 2016] Stanishneva-Konovalova, T. B., Derkacheva, N. I., Polevova, S. V., and Sokolova, O. S. (2016). The role of bar domain proteins in the regulation of membrane dyanamics. *Acta Naturae*, 8(4):60–69.

[Stow and Condon, 2016] Stow, J. L. and Condon, N. D. (2016). The cell surface environment for pathogen recognition and entry. *Clinical and Translational Immunology*, 5.

[Swanson, 2008] Swanson, J. A. (2008). Shaping cups into phagosomes and macropinocomes. *Molecular Cell Biology*, 9:639–649.

[Takenawa and Miki, 2001] Takenawa, T. and Miki, H. (2001). Wasp and wave family proteins: key molecules for rapid rearrangement of cortical actin filaments and cell movement. *Journal of Cell Science*, 114:1801–1809.

[Tallquist and Kazlauskas, 2004] Tallquist, M. and Kazlauskas, A. (2004). Pdgf signaling in cells and mice. *Cytokine and Growth Factor Reviews*, 15:205–213.

[Théry and Piel, 2009] Théry, M. and Piel, M. (2009). Adhesive micropatterns for cells: A microcontact printing protocol. *Cold Spring Harbor Protocols*, 4.

[van Aelst and D'Souza-Schorey, 1997] van Aelst, L. and D'Souza-Schorey, C. (1997). Rho gtpases and signaling networks. *Cold Spring Harbor Laboratory Press*, 11:2295–2322.

[Vicker, 2000] Vicker, M. G. (2000). Reaction-diffusion waves of actin filament polymerization / depolymerization in dictyostelium pseudopodium extension and cell locomotion. *Biophysical Chemistry*, 84:87–98.

[Vicker, 2002] Vicker, M. G. (2002). Eukaryotic cell locomotion depends on the propagation of self-organized reaction-diffusion waves and oscillations of actin filament assembly. *Experimental Cell Research*, 275:54–66.

[Weeds and Maciver, 1993] Weeds, A. and Maciver, S. (1993). F-actin capping proteins. *Current Opinion in Cell Biology*, 5:63–69.

[Weiner et al., 2007] Weiner, O. D., Marganski, W. A., Wu, L. F., Altschuler, S. J., and Kirschner, M. W. (2007). An actin-based wave generator organizes cell motili. *PLoS Bio*, 5(9):e221.

[Wennström et al., 1994] Wennström, S., Hawkins, P., Cooke, F., Hara, K., Yonezawa, K., Kasuga, M., Jackson, T., Claesson-Welsh, L., and Stephens, L. (1994). Activation of phosphoinositide 3-kinase is required for pdgf-stimulated membrane ruffling. *Current Biology*, 4(5):385–393.

[Whitelam et al., 2009] Whitelam, S., Bretschneider, T., and Burroughs, N. (2009). Transformation from spots to waves in a model of actin pattern formation. *Physical Review Letters*.

[Yin and Janmey, 2003] Yin, H. L. and Janmey, P. A. (2003). Phosphoinositide regulation of the actin cytoskeleton. *Annual Review of Physiology*, 65:761–89.

[Zeng et al., 2011] Zeng, Y., Lai, T., Koh, C. G., LeDuc, P. R., and Chiam, K.-H. (2011). Investigating circular dorsal ruffles through varying substrate stiffness and mathematical modeling. *Biophysical Journal*, 101:2122–2130.